MODELING GROUNDWATER RECHARGE IN THE BRAZOS RIVER ALLUVIUM AQUIFER (BRAA) USING CLM 4.5

A Thesis

by

EFRAIN EDUARDO OLIVARES RAMOS

Submitted to the Office of Graduate and Professional Studies of
Texas A&M University
in partial fulfillment of the requirements for the degree of

MASTER OF SCIENCE

Chair of Committee,	Gretchen R. Miller
Committee Members,	Huilin Gao
	Hongbin Zhan
Head of Department,	Robin Autenrieth

December 2020

Major Subject: Civil Engineering

ABSTRACT

Traditional hydrologic modeling has partitioned water cycle into its different component (i.e. rainfall, run-off, or groundwater models). An alternative approach will be described in this research project. Over most of the river alluvium aquifers around the world, those processes are vastly interconnected; therefore, representing them by separated models would not be adequately accurate and, as a consequence, an integrated model (such as a Land Surface Model) would be a solution to assess more than one component simultaneously and reduce the error likelihood associated with estimated boundary conditions. One of these codes is the Community Land Model (CLM) which represents several components related to land biogeophysics, hydrologic cycle, and biogeochemistry; provides the advantage of parallel computing; and examines how these processes affect climate across the world at any temporal scale.

A regional scale simulation in the Brazos River Alluvium Aquifer (BRAA) will be performed to compare results over this area with the Groundwater Availability Model (GAM) report made by the Texas Water Development Board (TWDB) for a 40-year period (1965 to 2004). Previous studies carried on in some parts of the BRAA suggested large variability of recharge rates depending either on the area scientist made their test or the method they selected to obtain their results. Ultimately, USGS estimated a range from 2 to 5 inches per year which could be more reliable. After simulating the BRAA for 40 years, the spatially and historically annual average is close to 3 inches per year which strongly suggest that a LSM such as CLM4.5 could be applied to study hydrologic process in at least a minor aquifer.

Several factors affect recharge rates such as irrigation, weather conditions (severe precipitations and drought seasons), soil type, vegetation, or interaction with other aquifers. After

running the simulation over the BRAA, we conclude that recharge rates are higher in the south portion of the BRAA than in the norther portion of it. Moreover, results of the remaining parameters we obtained from the CLM4.5 over the BRAA which include net radiation and its components, infiltration, interception and evapotranspiration suggests that there is more solar energy and hydrologic fluxes in the southern portion as well.

AKNOWLEDGEMENTS

I would like to thank my committee chair, Dr. Gretchen Miller, and my committee members, Dr. Huilin Gao and Dr. Hongbin Zhan, for their guidance, support and motivation throughout the course of this research project.

I also wish to extend thanks to my friends and peers in the Miller Geoecohydrology Research Group for their encouragement throughout my graduate studies.

Finally, to my parents, Vicky Ramos and Efrain Olivares, my sister, Karina Olivares, my aunt Sonia Phillips, my grandmother in heaven, Victoria Aparicio, and all my relatives, thank you for your advice, support, prayers, and patient encouragement throughout the last two years.

CONTRIBUTORS AND FUNDING SOURCES

Contributors

This work was supervised by a thesis committee consisting of Professor Gretchen R. Miller (advisor and chair) of the Department of Civil Engineering, Professor Huilin Gao of the Department of Civil Engineering, and Professor Hongbin Zhan of the Department of Geology and Geophysics.

All work of this thesis was completed independently by the student.

Funding Sources

There are not outside funding contributions to acknowledge related to the research and compilation of this document.

TABLE OF CONTENTS

Page

LIST OF FIGURES

Page

LIST OF TABLES

Page

1. INTRODUCTION

1.1 Background

Over the last two decades interest in groundwater (GW) - surface water (SW) interaction has grown steadily. New interdisciplinary research on GW and SW systems that addresses the linkages between hydrology, biogeochemistry and ecology at nested scales and precisely accounts for small/regional scale spatial and temporal patterns of GW-SW exchange is required (Fleckenstein et al., 2010). Consequently, governments and water managers should develop an efficient management plan of groundwater and surface-water resources as a single unit to face some critical problems such as decreasing of freshwater supplies. In this context, it is being more important to explicitly characterize the water exchange between surface water and aquifers (Bartsch et al., 2014). To face these challenges, this process requires not only an enhanced basic and applied research but also a large variety of tools ranging from field techniques to advanced technology for water control and regulation such as models (land, climate, hydrology, etc.), remote sensing, geographic information systems (GIS), decision support systems and spatial analysis procedures (Wang et al, 2016). However, numerical modeling in hydrology has been rapidly evolving and proved it is one of the most reliable and efficient ways to understand and predict the potential impacts of population, land use, and climate change on water resources field (Paniconi, C. and Putti, M., 2015).

In Texas, the Texas Water Development Board (TWDB) supports the development of regional water plans and incorporates them into a state water plan for the orderly and responsible development, management, and conservation of the state's water resources (TWDB, 1957). Currently, the TWDB follows the 2017 State Water Plan, which has a 2050 planning horizon.

Therefore, in order to achieve the requirements of the Water Plan, the TWDB commissioned the creation or updating of a series of computer models of the major and minor aquifers along the state (Bruun et al., 2017). The model covers entire extent of those aquifer and accounts for hydrological processes occurring within aquifer and between aquifer and its surroundings as well (Ewing, 2017).

The Brazos River Alluvium Aquifer (BRAA), one of the minor aquifers in Texas, consists of the alluvial floodplain and connected terrace deposits of the Brazos River from Whitney Dam to Fort Bend County (Ashworth, 1995). The sediments comprising this typically unconfined aquifer range from clay to large cobbles up to 85 feet or even more depending on the area. It is up to 7 miles wide (ranges from 0.25 to 10 miles depending on the area as well) and covers an area of roughly 1,050 square miles (*TWDB*, 2017), traversing portions of Bosque, Hill, McLennan, Falls, Milam, Robertson, Burleson, Brazos, Washington, Grimes, Austin, Waller, and Fort Bend counties (Shah, 2007). Approximately, 21% of the aquifer production is used for irrigation, 15% for livestock and 21% for domestic and small municipalities use (TWDB, 2017). The aquifer is assumed to be hydraulically connected to Brazos River along 365 river-km length (Cronin & Wilson, 1967). Alluvial aquifers regularly have a high degree of heterogeneity, with hydraulic conductivity values ranging several orders of magnitude (Miall, 1996). Several challenges associated with alluvial aquifers becomes more complex when large systems must be modeled under stressed conditions with different hydrological processes occurring simultaneously to understand and project multiple scenarios for water management.

Traditional land surface models (LSMs) use quantitative methods to simulate the exchange of water and energy fluxes at the Earth surface–atmosphere interface. For instance, some traditional land surface models (LSMs), like Soil Vegetation Atmosphere Transfer Schemes

(SVATS) or the Canadian Land Surface Scheme (CLASS), were used for numerical weather simulation, climate projection, and as inputs to water management decision support systems (NASA, 1998). They have been widely applied in fields such as numerical weather and hydrologic cycle simulations, climate projection, and as inputs to water management decision support systems (Maxwell and Miller, 2005). Initially, development of these models included vegetation, surface resistance, and snow schemes that calculate time- and space-varying momentum, heat, and moisture fluxes to the lower atmosphere (e.g., Dickinson et al. 1986; Sellers et al. 1986). Next, LSMs developed improved representations of subsurface hydrology, lateral soil moisture movement, evapotranspiration (Abromopoulos et al. 1988), and continental-scale river routing (Russell and Miller, 1990). Moreover, regional climate modeling with similar LSMs began to provide higher spatial resolution – about 1-degree resolution or even finer. More recently, detailed descriptions of surface infiltration and lateral baseflow have been developed (Famiglieti and Wood, 1991).

LSMs have evolved from a leaky-bucket approximation to more sophisticated land surface water, groundwater, and energy budget models that typically have a specified bottom layer flux to depict the lowest model layer exchange with deeper aquifers. In addition, they have evolved into complex models that can be used alone or as part of general circulation models to investigate the biogeochemical, hydrological, and energy cycles at the earth's surface. However, the water balance computed by most of the land surface models can be much improved by inclusion of groundwater processes and the interactive flux between the water table (WT) and the LSM lower layer (Lawrence et al, 2011). Suffering from similar, yet reversed issues, traditional groundwater models have a simplified upper boundary condition that is externally specified and intended to represent fluxes of water related to processes such as infiltration and evapotranspiration. These fluxes are

often simplified, uncoupled, and may be averaged in time and space, possibly missing key dynamics of important land surface processes.

It is important to quantify the influence of many small-scale processes that have not been taken into consideration in previous large-scale models and to model representative processes that significantly impact the exchange under different modes of aquifer and river conditions; such that these can be effectively incorporated in large-scale regional-level models. In this research project, the Community Land Model which is one of the land models carried out by the National Center for Atmospheric Research (NCAR) for the Community Earth System Model (CESM) will be used to reach the objectives of this thesis (section 1.2). The Brazos River Alluvium Aquifer will be simulated by this model to estimate groundwater recharge rates in this region.

1.2 Research Objectives

Land surface models may also be useful in estimating rates of an important, yet understudied, process in hydrology: groundwater recharge. Here, CLM4.5 will be applied in the Brazos River Alluvium Aquifer (BRAA) in order to find spatially and historically distributed recharges rates. The aquifer is currently represented in a groundwater availability model (GAM) developed by the Texas Water Development Board and Intera, Inc. In this loosely coupled approach, we will generate recharge rates generated using CLM4.5, compare them to the simplified values currently in the GAM and previous studies developed in this area Analysis will be geared towards identifying areas with statistically significant anomalies (southern and northern portion of the BRAA) and correlating them to influential environmental and/or infrastructural factors such as topography, vegetation, hydraulic conductivity, soil type, or location. The overarching objective is to get the recharge rates along the Brazos River Alluvium Aquifer using

the CLM4.5, do the sensitivity analysis, and compare the results with those ones obtained by the Texas Water Development Board which have realized their analysis using the GMS software. Additionally, we will test other parameters and analyze their behavior over the BRAA.

1.3 Literature Review

1.3.1 Groundwater Availability Models

The TWDB began creating the Texas Groundwater Availability Models, or GAMs, in 1999 in order to facilitate development of the state's water resources across the urban, agricultural, and industrial sectors (Bruun et al, 2017). Groundwater availability models include comprehensive information on each aquifer along the state such as geology and how that conveys into the framework of the model; rivers, lakes, and springs; water levels; aquifer properties; and pumping. It was intended as a tool to determine the variability in availability of groundwater across the BRAA extension. At its core, GAM complies parameter sets (hydraulic conductivity, specific yield, specific storage) based on data from its aquifer section and solves the governing groundwater flow equation (GFE) for all the specified cells in the model using an iterative process. Since the model need to predict long-term changes which are transient in nature, GAM also solves the GFE for a user-determined timeframe and a set number of time steps in said timeframe. Finally, the iterative process repeats the solving of the whole array of equations at each timestep until convergence is reached; this means, until the solutions encountered satisfy the whole array of equations for a given timestep and then, moves to the next timestep and solves the whole array again taking the previous solution as the new starting point. For a solution to be encountered, an initial state has to be provided to the model and, based on that initial state, the model continues solving the array.

1.3.2 CLM

The Community Land Model (CLM) is the distributed land model for the Community Earth System Model (CESM), a fully-coupled, global, climate model that provides state-of-art computer simulations of the Earth's past, present, and future climate states (Lawrenceet al., 2018). The model formalizes and quantifies concepts of ecological climatology. It is a collaborative project between scientists in the Terrestrial Sciences Section (TSS) and the Climate and Global Dynamics Division (CGD) at the National Center for Atmospheric Research (NCAR). One of the latest versions (CLM4.5) was developed for three main reasons: (1) incorporate several recent scientific advances in the understanding and representation of land surface processes, (2) expand model capabilities, and (3) improve surface and atmospheric forcing datasets (Oleson et al., 2013). In this particular model version, several parameterizations were revised to reflect new scientific understanding and in an attempt to reduce biases identified in CLM4 simulations including low soil carbon stocks especially in the Arctic, excessive tropical GPP and unrealistically low Arctic GPP, a dry soil bias in Arctic soils, unrealistically high LAI in the tropics, a transient 20th century carbon response that was inconsistent with observational estimates, and several other more minor problems or biases (Oleson et al., 2013). NCAR released a user's guide for CLM4.5 in CESM1.2.0 in 2013 and a technical description document for CLM4.5 which instruct both the novice and experienced user on running CLM, and describe the biogeophysical and biogeochemical parameterizations and numerical implementation of version 4.5 of the Community Land Model (CLM4.5).

Predominantly, CLM4.5 represents several aspects of the land surface including spatial heterogeneity (Oleson et al., 2013). It consists of components or sub models related to land biogeophysics, the hydrologic cycle, biogeochemistry, human dimensions, and ecosystem

dynamics. In addition, some of the specific processes that are represented includes: vegetation composition, structure and phenology, absorption, heat transfer in soil, canopy hydrology, soil hydrology, plant hydrodynamics, lake temperatures and fluxes, urban energy balance and climate, and dynamic landcover change (Bonan, 2002). CLM is typically run within the broader CESM framework, a set of models that can be run independently or together to simulate various facets of the Earth system (Figure 1).

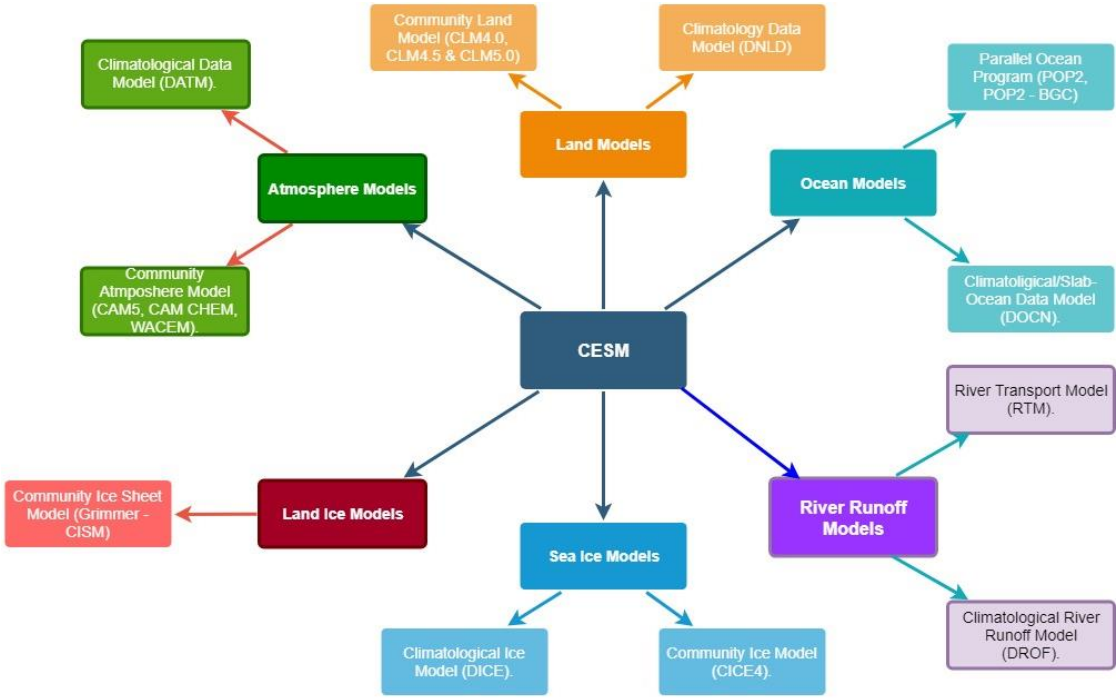

Figure 1: CESM interface description (adapted from Oleson et al., 2013)

CLM has been developed to aid in a variety of interdisciplinary scientific goals, including to: ascertain vulnerability of water resources under climate change; establish role of land surface processes in droughts and floods; quantify land forcing and feedbacks to climate change, e.g. permafrost-carbon, snow- and vegetation-albedo, land-cover and land-use change, and soil

moisture-ET feedbacks; evaluate utility of ecosystem management as mechanism to mitigate climate change; assess response and vulnerability of ecosystems to climate change and disturbances (human and natural); and improve understanding of carbon and nitrogen cycle interactions and their impact on long term trajectory of terrestrial carbon sink (Oleson et al., 2013). Attributes such as hourly time step and dynamic vegetation make these types of studies possible (Table 1).

Table 1: CLM processes

Attribute	CLM4.5
Energy Balance	Yes (rural and urban included)
Water Balance	Yes (over oceans included)
Model Time Step (minimum)	30 min
Lateral flow	No
Tile drains, crops	Yes
Soil Temperature Profile	Yes
Soil Water	Drainage and Vertical diffusion
Top model for surface runoff	Yes
Canopy resistance	Ball-Berry algorithm
No. of model soil layers	10
Soil thermodynamics	Heat conduction equation
No. of canopy layers	1
Hydrology	Dry surf, layer, var. soil depth up to 8.5 m Revised GW and canopy interaction
Carbon	Revision to carbon allocation and decomposition
Vegetation	Plant hydraulics and hydraulic redistribution, deep rooted tropical trees.
Crops	Global crop model with transient irrigation and fertilization (8 crop types)
Land cover/user	Dynamic land units, revised PFT-distribution, shifting cultivation
Isotopes	Carbon and water isotope enabled
Fire	Trace gas and aerosol emissions

1.3.3 The Brazos River and Its Alluvial Aquifer

1.3.3.1. Brazos River – Aquifer Interaction

Water exchange between river and aquifer is a temporarily dynamic and spatially process. Traditionally, modeling studies that include river aquifer interactions have been focused on questions of regional-scale water management and conjunctive use (Wang et al. 1995). In this context, interaction between the aquifer and rivers is motivated mainly by interest in the regional water balance. Mean monthly flows and long river reaches with simplified geometries are typically used to estimate the long-term exchange with the aquifer. Riverbed conductivities are determined by calibration, and aquifers are often represented as laterally extensive layers with relatively uniform parameters. Those parameters and factors affect flux exchange under different conditions and therefore should be well incorporated into numerical models to quantify the amount of water for any hydrology process we are simulating (Woessner, 2000).

1.3.3.2 General Characteristics

Sediment deposition related to the Brazos River includes both floodplain and terrace alluvial deposits. The Quaternary deposits basically consist of typical alluvial sediments, including gravel, fine to coarse sand, silt, and clay (Figure 2), in lenses that pinch out or grade both laterally and vertically. In general, the deposits are coarser at the base and fine upward according US Department of Agriculture soil survey (USDA, 2017). The sequence of finer upper deposits transitioning to coarser lower deposits is consistent throughout the aquifer. However, due to pinching out and interfingering, the grain size and relative position of individual constituents in the sequence vary highly from place to place. The transition from one type of material to another, both laterally and vertically, can be either sharp and distinct or gradual (*TWDB*, 2016). Groundwater in the Brazos River Alluvium Aquifer is predominately under unconfined conditions.

However, in some areas where clay lenses overlie lenses of sand or gravel, locally confined conditions may sporadically exist. Aquifer thickness ranges between a few feet at its edges to a maximum of 127 feet in the central and southern parts of the aquifer (i.e. Grimes County). Average thickness of the alluvium is typically modeled as 51 feet (*TWDB*, 2016).

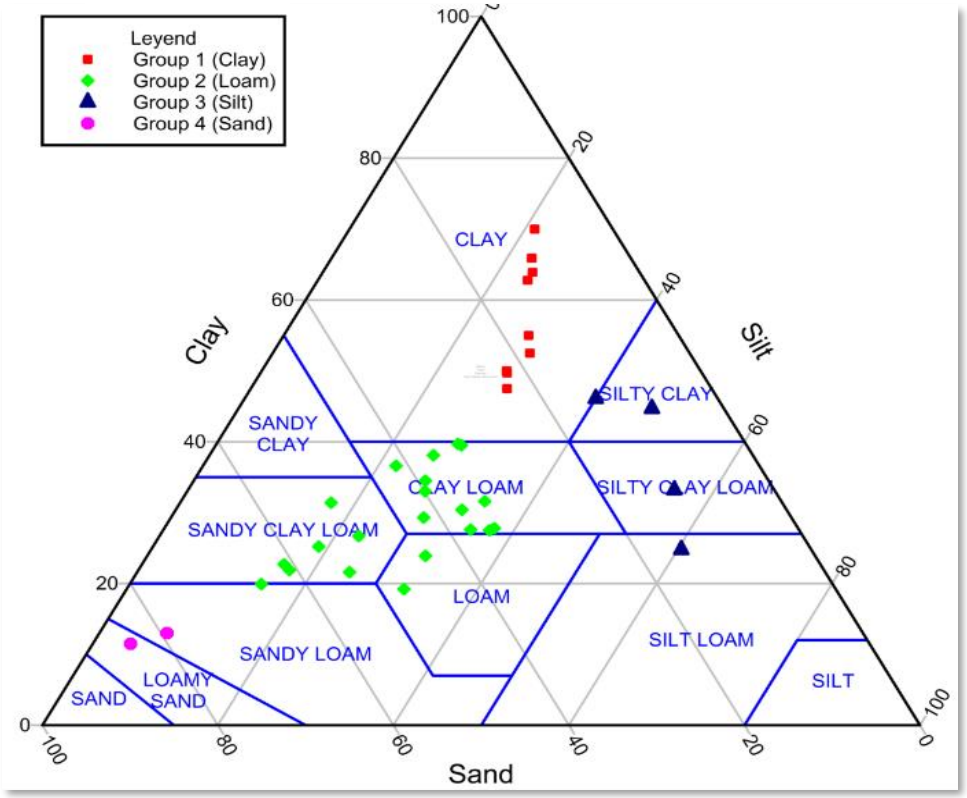

Figure 2: Soil texture triangle for the BRAA

Major aquifers that underlie the BRAA are the Carrizo-Wilcox and Gulf Coast aquifers. Minor aquifers that underlie the BRAA are the Queen City, Sparta, and Yegua-Jackson aquifers (Table 2). These aquifers interact not only with the BRAA aquifer, but also with the Brazos River which tends to gain water from these underlying aquifers. This interaction mostly happens in the southern portion of the BRAA because of the location of these aquifers.

Table 2: Major and minor aquifers

Aquifer Name	Type	Location	Interaction with BRAA
Carrizo-Wilcox	Major	Southern Portion	Yes
Trinity	Major	Northern Portion	No
Gulf Coast	Major	Southern Portion	Yes
Edwards Balcones	Minor	Northern Portion	No
Queen City	Minor	Northern Portion	Yes
Sparta	Minor	Northern Portion	Yes
Yegua-Jackson	Minor	Southern Portion	Yes
Woodbine	Minor	Northern Portion	No

According to historical data, water levels had remained generally stable since 1950, with small fluctuations. No significant water level declines have occurred in the aquifer (Furnans, 2017). Water levels generally dip toward the Brazos River locally and follow the regional downward trend in topography from the northwest towards the Gulf of Mexico (Figure 3). Target water levels and hydrographs have been identified and were used in the calibration of the numerical model of the Brazos River Alluvium Aquifer (Ashworth and Hopkins, 1995) carried out by TWDB. Moreover, groundwater flow in the Brazos River Alluvium Aquifer is affected by surface topography, the Brazos River and its tributaries, and the configuration of underlying confining beds (Cronin and Wilson, 1967; Harlan, 1990). Typically, groundwater flows toward the Brazos River and slightly down valley, but terraces and tributaries may locally direct flow toward tributary channels (Harlan, 1990). The alluvial sediments occur immediately adjacent to the Brazos River channel, resulting in a hydrologic connection between surface water and groundwater. Groundwater levels are known to fluctuate in response to river levels, indicating a fairly direct connection (Cronin and Wilson, 1967).

Recharge rates to both the BRAA and the outcrops of the formations underlying it have been estimated based on previous studies and base flow analyses (TWDB, 2017). Within the study area, pre-development recharge is estimated to be approximately 40,000 acre-feet per year in the Brazos River Alluvium Aquifer and approximately 710,000 acre-feet per year in the outcrops of the underlying formations (Figure 3). Post-development recharge was estimated to be approximately 50,000 acre-feet per year in the Brazos Alluvium Aquifer in 2012 (*Texas Water Development Board, 2017*). Furthermore, recharge rates are spatially distributed and temporally variable. In other words, they change at all from north or south, east to west (Figure 4) and the recharge rates change from year to year (Table 3).

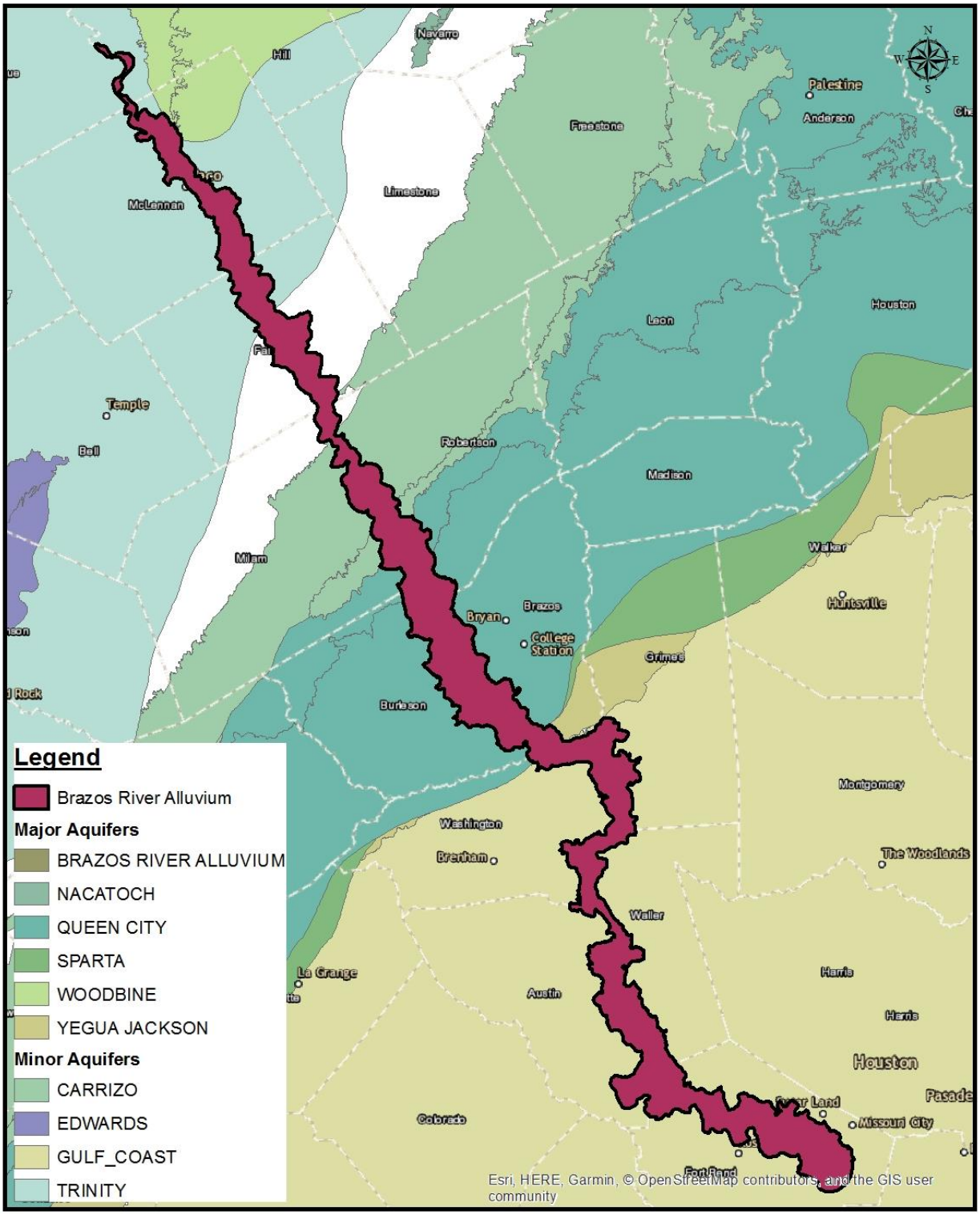

Figure 3: BRAA and underlaying formations

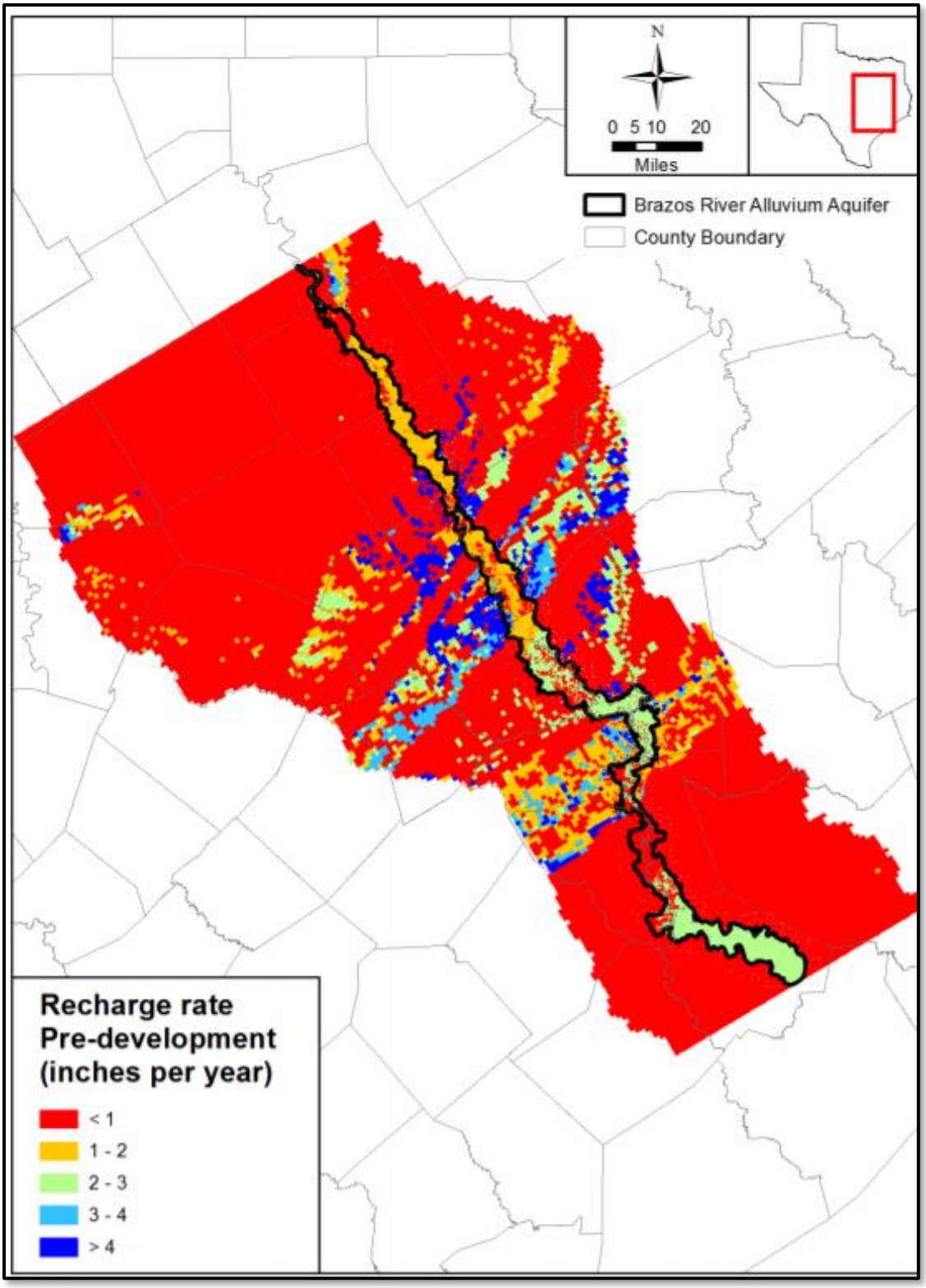

Figure 4: Pre-development recharge rates, (reprinted from Ewing et al, 2016)

Table 3: Recharge rates variations (adapted from Xia et al, 2017)

Year	Recharge (inches per year)			Method	Source
	Minimum	Maximum	Average		
1957 – 1961	1.8	5.3	3.5	Flow between flow lines (Keech and Dreesen, 1959)	Cronin and Wilson (1967)
1994 – 2004	0.06	5.57	0.74	Digital base flow separation	Chowdbury and others (2010)
1934 – 1998	0.02	9.7	0.95	Digital base flow separation	Chowdbury and others (2010)
1934 – 1998	0.11	3.39	0.33	Chloride Mass Balance	Chowdbury and others (2010)

The interaction between the Brazos River Alluvium Aquifer and surface water bodies, including the Brazos River, its tributaries, reservoirs, and oxbow lakes have been evaluated by previous studies developed by the Texas Water Development Board (*TWDB*, 2017). Gain/loss studies have been evaluated to describe the gains and losses between the Brazos River and its tributaries and the groundwater system at snap-shots in time. Long-term estimates of the contribution of the groundwater system to the base flow in the Brazos River and its tributaries has also been evaluated through hydrograph separation analyses (*Intera*, 2017). These novel approaches to studying subsurface discharge to a major river revealed significant findings that will have important implications for future hydrologic studies (Rhodes et al., 2017)

1.3.4 Modeling Recharge in MODFLOW and LSMs

1.3.4.1 Recharge Estimations

Recharge has been defined as the process of addition of water to the saturated zone. However, it is surely almost impossible to measure recharge directly. Therefore, it is usually estimated by indirect means (Table 4 and 5). According USGS, it is a good practice to estimate

recharge rates using multiple methods and compare those results as a mechanism to test the accuracy of the indirect estimation.

Table 4: Summary of methods for estimating GW recharge

Methods for Estimating Groundwater Recharge				
Water Budget	**Unsaturated Zone Methods**	**Groundwater Methods**	**Streamflow Methods**	**Tracer Methods**
• Deep Percolation Model • HELP3 Model	• Darcian Method • Zero-Tension Lysimeters • Zero-Flux Plane	• Groundwater Modeling • Water-Table Fluctuations	• Seepage Meters • Streamflow Gain/Loss Measurements (Seepage Run) • Recession-Curve Displacement Method • Watershed Methods	• Chloride • Chloro-fluoro-carbons • Temperature • Tritium

Table 5: Description of methods for estimating GW recharge (adapted from USGS, 2020)

Description of Methods for Estimating Groundwater Recharge
Deep Percolation Model
The Deep Percolation Model estimates, on a daily-basis, the long-term average groundwater recharge from precipitation. It was developed by USGS to simulate the recharge in large areas with variable weather, soils, and land uses.
HELP3 Model
The Hydrologic Evaluation of Landfill Performance (HELP3) model was developed by the U.S. Army Waterways Experiment Station to compute the water balance of landfills on a daily time scale. It estimates potential recharge at a point in the watershed.
Darcian Method
The Darcian unit-gradient method can produce point estimates of potential recharge from measurements of hydraulic conductivity and water content in the unsaturated zone.
Zero-Tension Lysimeters
Gravity lysimeters are a method of estimating recharge by directly measuring the vertical flow of water through a large undisturbed section of the unsaturated zone.
Zero-Flux Plane
The zero-flux plane (ZFP) method provides a point estimate of potential recharge based on the premise that recharge is equal to changes in soil-moisture storage below the ZFP.

Table 5: Continued

Description of Methods for Estimating Groundwater Recharge
Groundwater Modeling
Ground-water models such as MODFLOW can be used to estimate groundwater recharge by calibration of the model to "known" values of aquifer transmissivity, hydraulic head, and discharge (base flow).
Water Table Fluctuations
The water-table fluctuation method provides a point value of recharge computed from the water-level rise in a well multiplied by the specific yield of the aquifer. It assumes that a water-level rise is caused by recharge arriving at the water table and that the specific yield is constant.
Seepage Meters
Seepage meters directly measure stream infiltration at a point beneath the streambed, providing an estimate of potential recharge that could reach the water table from that point on the stream.
Streamflow Gain/Loss Measurements
Measurements of streamflow losses along a reach provide an estimate of potential recharge that could arrive at the water table.
Recession-Curve Displacement Method
The computer program RORA provides estimates of groundwater recharge from the displacement of the streamflow-recession curve from equations developed by Rorabaugh (1964) and Glover (1964).
Watershed Method
Watershed-based rainfall-runoff models, such as PRMS can be used to estimate recharge for various temporal and spatial scales.
Chloride
The chloride-tracer method provides an estimate of recharge by use of a mass-balance equation. The premise of the method is that the chloride concentration of wet and dry deposition times the quantity of precipitation equals the chloride concentration of recharge times the quantity of recharge.
Chlorofluorocarbons
Chlorofluorocarbons (CFCs) are man-made compounds introduced into the atmosphere that can be used to estimate the date at which groundwater was recharged during about the past 50 years.
Temperature
Measurement of temperature beneath a stream or lake can be used to infer the rate of infiltration at a point location for periods of days to years. Estimates of potential recharge can be made from by comparing measurements of temperature to values modeled for sediments of assumed thermal diffusivity with infiltration of various rates.
Tritium
Tritium is a naturally occurring radioactive isotope of hydrogen with a half-life of 12.3 years introduced to the atmosphere in large quantities from atmospheric nuclear testing, with peak concentrations occurring about 1962. The tritium method is conducted by measuring tritium concentrations in groundwater at various depths and locating the depth of peak tritium concentration.

Recharge rates vary temporally and spatially by season, storm water intensity, stream stage, soil type, vegetation type and cover, elevation, slope, temperature, solar radiation and other factors, including the presence of buildings, paved surfaces and drainage culverts. For instance, spatial variations in soil types may be related to lithologic differences in the rocks intersecting the ground surface or variations in mineralization. Soil type not only directly affects infiltration, it influences the vegetation type, which affects the rate of evapotranspiration. After simulate the BRAA these factors will be analyzed to understand the influence they have in recharge rates.

1.3.4.2 MODFLOW

The U.S. Geological Survey (USGS) developed a computer program for simulating common features in ground-water systems called modular finite-difference groundwater flow model (MODFLOW). Since it was constructed by 1980, it has regularly evolved with the inclusion of several new packages and related programs for groundwater studies (McDonald and Harbaugh, 1988; Harbaugh and McDonald, 1996). Nowadays, MODFLOW is the most widely used program in the world for simulating ground-water flow and there are several research studies which applied it to make simulations and projection of aquifers because it has attributes that makes it popular Substantially, MODFLOW is a finite-difference groundwater flow modeling program, written by the USGS, which allows users to develop a numerical representation (i.e. a groundwater model) of the hydrogeologic environment at any field site they are investigating. It uses the finite-difference method to divide the groundwater flow model domain into a series of rows, columns and layers, which defines a unique set of grid blocks (i.e. model cells) to represent the distribution of hydrogeologic properties and hydrologic boundaries within the model domain (USGS, 2017).

Table 6: MODFLOW applications (adapted from USGS, 2017)

MODFLOW APPLICATIONS (and academical paper examples)		
Unconfined and confined aquifers	Groundwater flow and storage changes.	Steady State Analytical and Numerical Solutions of Confined and Unconfined Flows in Aquifers with Discontinuous Aquiclude, *Korkmaz, S.*, 2019
Faults and other barriers	Resistance to horizontal ground-water flow.	Numerical Simulation of Ground Water Flow in Dual Porous Media of the Karun 4 Dam (Iran) Foundation and Abutments, *Hosseiny, S.*, 2018
Confining units	Groundwater flow and storage changes. Grained confining units and interbeds	Enhancing SWAT+ simulation of groundwater flow and groundwater-surface water interactions using MODFLOW routines, Bailey, R. et al, 2020.
Rivers	Exchange of water with aquifers	A modified approach for modeling river-aquifer interaction of gaining rivers in MODFLOW, including riverbed heterogeneity and river bank seepage, *Ghysels, G. et al*, 2019.
Drains and springs	Discharge of water from aquifers	Modeling Barton Springs Segment of the Edwards Aquifer Using MODFLOW-DCM, *Sun, A. et al*, 2005.
Ephemeral streams	Exchange of water with aquifers	A new streamflow-routing (SFR1) package to simulate stream-aquifer interaction with MODFLOW-2000, *Prudic, E.*, 2004.
Reservoirs	Exchange of water with aquifers	Application of MODFLOW for Oil Reservoir Simulation During the Deepwater Horizon Crisis, *Hsieh, P.*, 2011
Recharge/Evapotranspiration	From precipitation and irrigation	Using MODFLOW 2000 to Model ET and Recharge for Shallow Ground Water Problems, *Doble, R.*, 2009
Wells	Withdrawal or recharge at specified rates	Modeling Multiaquifer Wells with MODFLOW, *Neville, C.*, 2004

MODFLOW has been designed to simulate aquifer systems in which saturated flow conditions exist, Darcy's Law applies, the density of ground water is constant, and the principal directions of horizontal hydraulic conductivity or transmissivity do not vary within the system. These conditions are met for many aquifer systems and MODFLOW can simulate a variety of hydrologic processes for these systems. A variety of features and processes such as rivers, streams, drains, springs, reservoirs, wells, evapotranspiration, and recharge from precipitation and irrigation also can be simulated (Table 6). Moreover, at least four different solution methods have been implemented for solving the finite-difference equations that MODFLOW constructs.

MODFLOW – USG was the code selected for the groundwater model in the GAMs. This is a three – dimensional control volume that solves the groundwater flow equation (Harbaugh, 2005). The program is used by hydrogeologists to simulate the flow of groundwater through aquifers. Some of the advantages of using MODFLOW-USG are: (1) Groundwater flow physics is included in MODFLOW; (2) The most extensively accepted groundwater flow code is MODFLOW; (3) It is a public domain and was written and supported by the United States Geological Survey; (4) MODFLOW-USG allows for refinement in areas of interest in a computationally efficient manner (TWDB, 2017). A MODFLOW model consists basically of grouping of input text files, also called packages, that describe various components of the groundwater flow system (Table 7). The output files written by MODFLOW contain water levels (HDS), drawdown (DDN), water budget information (CBB), adjusted flow rate (AFR), stream-routing information (FLO), and a listing of the characteristics of the run (LST). Essentially, the model consists of three layers having uniform hydrogeological properties and the model grid has square grid cells with a size ranging from 1/8 mile to 1-mile size.

Table 7: Summary of model input packages and filenames

File Type Abbreviation	File Type	Input File Name
BAS6	Basic Package	braa.bas
DISU	Discretization File	braa.dis
DRN	Drain Package	braa.drn
EVT	Evapotranspiration Package	braa.evt
SMS	Sparse Matrix Solver Package	braa.sms
OC	Output Control Option	braa.oc
RCH	Recharge Package	braa.rch
SFR	Streamflow-Routing Package	braa.sfr
RIV	River Package	braa.riv
LPF	Layer Property Flow Package	braa.lpf
GNC	Ghost Node Correction	braa.gnc
WEL	Well Package	braa.wel

The groundwater model of the Brazos River Alluvium Aquifer represents the minor BRAA itself as well as the surficial portions of the major Carrizo – Wilcox and Gulf Coast aquifers and the minor Queen City, Sparta, and Yegua-Jackson aquifers within the Brazos River Basin. The model has three layers: with layers 1 and 2 representing the Brazos River Alluvium Aquifer and layer 3 representing the surficial portions of the formations underlying the Brazos River Alluvium Aquifer (Figure 5). This conceptual model was followed by David O'Rourke (2006) who prepared a groundwater model for Brazos G Regional Water Planning Group (portion of the BRAA corresponding to Milan, Burleson, Robertson, and Brazos counties). The main purpose of this model report was to assess the potential for conjunctive use of surface water from the Brazos River and groundwater from the alluvial aquifer. The results of this model were useful to examine the response of the aquifer system to enhanced recharge, to monitor the movement of this recharge

water through the system, to evaluate potential water losses from the system, and to determine an appropriate operational cycle for recharge and recovery (O'Rourke, 2006).

1.3.4.3 LSMs

Land surface models (LSMs) used in numerical and weather prediction and climate projections and as inputs for water management decision support systems have seen considerable development since 1969. From the pioneering work by Deardorff (1978), the development of globally applicable LSMs by Dickinson et al. (1986) and Sellers et al. (1986) and the building of the first models that represent vegetation dynamics (e.g., Foley et al. 1996), LSMs now represent heterogeneity, complex vegetation responses to environmental conditions, detailed surface and subsurface hydrology, dynamic evolution of snowpacks, and even representations of urban, lake, and biogeochemical processes. They are key component of climate models. Two decades ago, they were just oversimplified schemes, which described the surface boundary conditions for general circulation models (GCMs); however, these days they represent complex models that can be used alone or as part of GCMs to investigate the biogeochemical, hydrological, and energy cycles at the earth's surface. Most of the time, LSMs have a higher emphasis given to the formulation of one-dimensional, vertical physics relative to the treatment of horizontal heterogeneity in surface properties, particularly sub grid soil moisture variability and its effects on runoff generation. There a huge number of LSMs (about 100 of them); however, many of them are just research models, local-state oriented with a specific process emphasis. A list of some LSM model software is shown in Table 8.

Table 8: List of LSMs

LSM
Canadian Land Surface Scheme (CLASS)
Interaction soil-biosphere-atmosphere (ISBA)
Joint UK Land Environment Simulator (JULES)
Community Land Model (CLM)
Unified NOAH LSM

Traditionally, he LSM lower boundary is often assumed zero flux or the soil moisture content is set to a constant value; an approach that while mass conservative, ignores processes that can alter surface fluxes, runoff, and water quantity and quality (Maxwell, 2005). By contrast, groundwater models (GWMs) for saturated and unsaturated water flow, while addressing important features such as subsurface heterogeneity and three-dimensional flow, often have overly simplified upper boundary conditions that ignore soil heating, runoff, snow, and root-zone uptake. However, several studies made simulations using any LSM tried to demonstrate the temporal dynamics of their coupled modeling system. Maxwell and Miller (2005) demonstrated that groundwater representation in land surface schemes should be improved using CLM-PF in Valdai, Russia for a period time of 18 years. The simulations of evapotranspiration they made were very similar between the coupled and uncoupled models, but simulations of runoff and soil moisture are improved in CLM.PF. Moreover, the coupled model reproduces the averaged observations for the Valdai wells, and some discrepancies in WT during periods of freeze/thaw have been demonstrated. Finally, there were also divergences in simulation between the coupled model and the Valdai data that warranted the need to investigate the effects of representing some processes and parameters of the area (such as topography, subsurface heterogeneity, runoff, infiltration, and snow) in a distributed manner (Maxwell and Miller, 2005).

More recently, potential recharge estimates from three LSMs across the Western US were compared by R. Niraula (2018). In his study, simulations of three LSMs (Noah, Mosaic and VIC) obtained from the North American Land Data Assimilation System (NLDAS-2) were used to estimate potential recharge in the western US. Modeled recharge was compared with published recharge estimates for several aquifers in the region. For the most part, his results stated that LSMs had the potential to capture the spatial and temporal patterns and the seasonality of recharge at large scales more precisely (Niraula et al., 2018). As a consequence, he suggested that LSMs could be used as a tool for estimating future recharge rates in regions with limited data access or small areas as well.

2. METHODOLOGY

2.1 CLM Modeling Overview

Regarding CLM4.5 code itself, land surface parameterization used with the community climate model (CCM3) and the climate earth system model (CESM1), the National Center for Atmospheric Research land surface model (NCAR LSM1), has been modified as part of the development of the climate models. In CESM2 (the new model), which now include CLM4.0, 4.5, and 5.0, the surface is represented at least by five primary sub grid land cover types (glacier, lake, wetland, urban, vegetated) in each grid cell (Oleson et al., 2013). The Community Land Model (CLM4.5 in CESM1.2.0) is the latest in a series of global land models developed by the CESM Land Model Working Group (LMWG) and maintained at the National Center for Atmospheric Research (NCAR). The relative area of each sub grid unit, the plant functional type, and leaf area index are obtained from 1-km satellite data. The soil texture dataset allows vertical profiles of sand and clay (Bonan et al, 2002).

Biogeophysical processes simulated by CLM include solar and longwave radiation interactions with vegetation canopy and soil, momentum and turbulent fluxes from canopy and soil, heat transfer into soil and snow, hydrology of canopy, soil, and snow, and stomatal physiology and photosynthesis. In the latest versions (CLM4.5 and CLM5.0) there are many improvements and differences from other land models that include many updates to soil hydrology, soil thermodynamics, snow model, albedo parameters, land surface types dataset, river transport model, and some other minor modifications (Lawrence et al, 2011).

The model parameterizes interception, throughfall, canopy drip, snow accumulation and melt, water transfer between snow layers, infiltration, evaporation, surface runoff, sub-surface

drainage, redistribution within the soil column, and groundwater discharge and recharge (ΔW) to simulate changes in canopy water ΔW_{CAN}, surface water ΔW_{SFC}, snow water ΔW_{SNW}, and soil ΔW_{soil}, and water in the unconfined aquifer ΔW_a (all in kg m^{-2} or mm of H2O) (Figure 5).

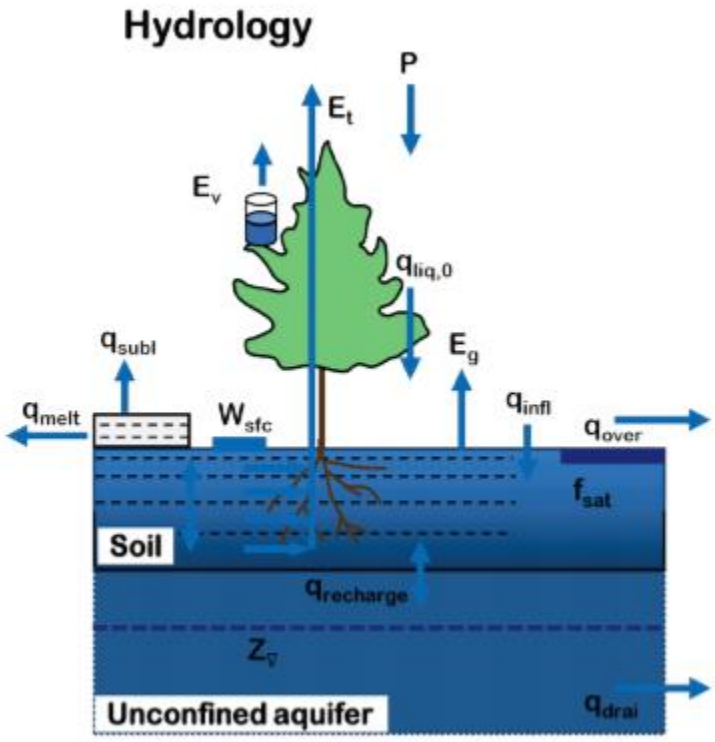

Figure 5**:** Hydrologic processes represented in CLM 4.5 (reprinted from Oleson, 2013)

$$\Delta W = \left(q_{rain} + q_{snow} - E_V - E_g - q_{over} - q_{h2osfc} - q_{drai} - q_{rgwl} - q_{snwcp,ice}\right)\Delta t \qquad (1)$$

where:

q_{rain} is liquid part of precipitation.

q_{snow} is the solid part of precipitation.

E_v is ET from vegetation.

E_g is ground evaporation.

q_{over} is surface runoff.

q_{h2sfc} is runoff from surface water storage.

q_{drai} is surface drainage.

q_{rgwl} and $q_{snwcp,ice}$ are liquid and solid runoff from glaciers, wetland, and lakes, and runoff from other surface types due to snow capping if any.

Drainage or sub-surface runoff is based on the SIMTOP scheme (Niu et al. 2005) with a modification to account for reduced drainage in frozen soils. In the work of Niu et al. (2005), the drainage q_{drai}(kg m^{-2} s^{-1}) was formulated as

$$q_{drai} = q_{drai,max} \exp(-f_{drai} z_{\nabla}) \tag{2}$$

Here, the water table depth z_{∇} has units of meters. Determination of water table depth z_{∇} is based on work by Niu et al. (2007). In this approach, a groundwater component is added in the form of an unconfined aquifer lying below the soil column (Figure 7). When the water table is within the soil column, W_a is constant because there is no water exchange between the soil column and the underlying aquifer. In this case, recharge to the water table is diagnosed by applying Darcy's law across the water table:

$$q_{recharge} = -k_{aq} \frac{(\Psi_{\nabla} - \Psi_{jwt})}{(z_{\nabla} - z_{jwt})} \tag{3}$$

Where $\Psi_{\nabla} = 0$ is the matric potential at the water table and k_{aq} is the hydraulic conductivity of the layer containing the water table. In addition, for the case when the water table is below the soil column, the change in water stored in the unconfined aquifer W_a (mm) is updated as:

$$\Delta W_a = (q_{recharge} - q_{drai}) \Delta t \tag{4}$$

In addition, we will use the net radiation equation as well as follows:

$$R_n = LE + H + G \tag{5}$$

Where:

R_n: Net Radiation

Le: Latent Heat Flux (Energy used to change state of water)

H: Sensible Heat Flux (Energy used to change temperature of atmosphere)

G: Ground Heat Flux (Energy used to change temperature of the subsurface)

Another governing equation is Richard's Equation. Some researchers figured out that the mass-conservative numerical scheme is deficient, especially when the water table is within the soil column, and these deficiencies cannot be resolved by increasing the vertical resolution of the soil column (L*awrence et al*, 2011). The solution is to explicitly subtract the hydrostatic equilibrium soil moisture distribution, resulting in a modified Richards equation (*Zeng and Decker*, 2009):

$$\frac{\partial \theta}{\partial t} = \frac{\partial}{\partial z}\left[k\left(\frac{\partial(\varphi - \varphi_E}{\partial z}\right)\right] - Q \tag{6}$$

Where θ is the volumetric soil water content (mm^3 of water mm^{-3} of soil), k is the hydraulic conductivity (mm/s), Ψ is the soil matric potential (mm), Ψ_E is the equilibrium soil matric potential (mm), and Q is a soil moisture sink term representing soil water losses due to transpiration. This equilibrium distribution can be derived at each time step from a constant hydraulic potential above the water table, representing a steady-state solution of the Richards equation. Then, the equilibrium soil matric potential is:

$$\varphi_E = \varphi_{sat}\left(\frac{\theta_E(z)}{\theta_{sat}}\right)^{-B} \tag{7}$$

Where Ψ_{sat} is the saturated soil matric potential (mm), the exponent B is a function of soil texture, θ_{sat} is the saturated volumetric water content ($mm^3\ mm^{-3}$), and the equilibrium volumetric water content $\theta_E(z)$ ($mm^3\ mm^{-3}$) at depth z. (*Brooks and Corey*, 1964).

In previous CLM versions, the partitioning of evapotranspiration into its components was extremely poor. It was developed further and improved in CLM 4.0 and 4.5 by incorporating a soil resistance term in the calculation of soil evaporation (Stockli et al, 2008). They demonstrate that the relationship between the bare soil evaporation and soil water content is more realistic by replacing the soil resistance with an empirical factor β_{soi} which ranges from 0 to 1 and is intended to represent the molecular diffusion process from the soil pore to the surface within the unsaturated part of the soil (Lee & Pielke, 1992):

$$\beta = \begin{cases} 1 & \theta_1 \geq \theta_{fc,1}\ or\ q_{atm} - q_g > 0 \\ 0.25(1 - f_{sno}) & \\ \left[1 - \cos\left(\pi \frac{\theta_1}{\theta_{fc,1}}\right)\right]^2 & \theta_1 < \theta_{fc,1} + f_{sno} \end{cases} \quad (8)$$

Where θ_1 and $\theta_{fc,1}$ are the volumetric liquid water content and field capacity of the top soil layer ($m^3\ m^{-3}$) and f_{sno} is the fraction of ground covered by snow.

Organic matter alters the thermal and hydraulic properties of soil. In CLM4.5, soil physical properties are assumed to be a weighted combination of values for mineral soil and values for pure organic soil (Lawrence and Slater, 2008). For example, the volumetric water content at saturation (porosity) is now defined as:

$$\Theta_{sat,i} = (1 - f_{om,i})\Theta_{sat,min,i} + f_{om,i}\Theta_{sat,om} \quad (9)$$

Where $f_{om,i}=\rho_{om,i}/\rho_{om,\ max}$, $\rho_{om,i}$ is the organic matter density for layer i obtained from the CLM organic matter dataset, $\Theta_{sat,\ min\ ,i}$ is the porosity of mineral soil, and $\Theta_{sat,om}=0.9$ is the porosity

of organic matter. Parameters for thermal conductivity, heat capacity, saturated hydraulic conductivity, and soil water retention are similarly treated.

Nicolsky et al. (2007) and Alexeev et al. (2007) demonstrated that soil temperature dynamics cannot be accurately modeled with a shallow soil column and that a ground depth of at least 30 m is required for century-scale integrations. Therefore, in order to account for the thermal inertia of deep ground, the number of ground layers is extended in CLM4 from 10 to 15 layers.

Surface and runoff: The saturation excess term is a function of the saturated fraction f_{sat} of the soil column, which includes a dependence on the surface layer frozen soil impermeable area fraction $f_{frz,l}$ (Niu and Yang, 2006):

$$f_{sat} = \left(1 - f_{frz,1}\right) f_{max} \exp(-0.5 f_{over} z\nabla) + f_{frz,1} \quad (10)$$

Where f_{max} is the maximum saturated fraction, $z\nabla$ is the water table depth, and f_{over} is a decay factor.

Furthermore, CLM4.5 calculates infiltration rates which has a different approach from recharge rates. The surface moisture flux remaining after surface runoff has been removed:

$$q_{in,surface} = (1 - f_{sat}) q_{liq,0} \quad (11)$$

Therefore, it is divided into inputs to surface water ($q_{in,h2osfc}$) and the soil $q_{in,soil}$. If $q_{in,soil}$ exceeds the maximum soil infiltration capacity (kg m^{-2} s^{-1})

$$q_{infl,max} = (1 - f_{sat}) \Theta_{ice} \mathrm{k}_{sat} \quad (12)$$

where Θ_{ice} is an impedance factor. Afterwards, infiltration excess runoff is calculated using Hortonian theory:

$$q_{infl,excess} = max\left(q_{in,soil} - \left(1 - f_{h2sofc}\right) q_{infl,max}, 0\right) \quad (13)$$

d transferred from $q_{in,soil}$ to $q_{in,h2osfc}$. Therefore, the balance of surface water is then calculated as:

$$\Delta W_{sfc} = \left(q_{in,h2sofc} - q_{out,h2osfc} - q_{drain,h2osfc}\right)\Delta t \quad (14)$$

Then, bottom drainage from the surface water store is added to $q_{in,soil}$ giving the total infiltration into the surface soil layer:

$$q_{infl} = q_{in,soil} + q_{drain,h2osfcl} \quad (15)$$

2.1.1 Technical Description

CLM4.5 is one of the five separate models simultaneously simulating the Earth's atmosphere, ocean, land, land-ice, and sea-ice in CESM1.2.0 which allows researchers to conduct fundamental research into the Earth's past, present, and future climate states after running and installing some software and operating system prerequisites (Table 9).

Table 9: CESM software/operating system prerequisites

CESM Software/Operating System Prerequisites	
Operating System	UNIX, LINUX, AIX, OSX.
Scripting Languages	csh, sh, perl, xml.
Subversion Client version	1.6.11 or greater
Compilers	Fortran 90, pgi, intel, xfl.
Fortran 90 Directory (optional)	MPI (Message Passing Interface)
Software libraries	netCDF 3.6.2 or greater, pnetcdf 1.1.1 or greater (optional)
Open Source Software	ESMF (Earth System Modeling Framework)

CESM basically consists of five geophysical models: atmosphere (atm), sea-ice (ice), land (lnd), ocean (ocn), and land-ice (glc), plus a coupler (cpl) that coordinates the models and passes

information between them (Oleson et al., 2013). Each model may have "active," "data," "dead," or "stub" component version allowing for a variety of "plug and play" combinations.

During the course of a CESM run, the model components integrate forward in time, periodically stopping to exchange information with the coupler. The coupler meanwhile receives fields from the component models, computes, maps, and merges this information, then sends the fields back to the component models. Model components are written primarily in Fortran 90.

The active (dynamical) components are generally fully prognostic, and they are state-of-the-art climate prediction and analysis tools (Oleson et al., 2013). Data models that cycle input data are included for testing, spin-up, and model parameterization development due to time-consuming run simulation. The dead components generate scientifically invalid data and exist only to support technical system testing.

The CESM system can be configured a number of different ways from both a science and technical perspective. CLM4.5 in CESM 1.2.0 supports several different resolutions and component configurations. In addition, each model component has input options to configure specific model physics and parameterizations. CESM can be run on a number of different hardware platforms and has a relatively flexible design with respect to processor layout of components.

The CESM components can be combined in numerous ways to carry out various scientific or software experiments. A particular mix of components, along with component-specific configuration and/or namelist settings is called a component set or "compset". For purposes of this investigation, we will use the land component which implies that CLM will be active combined with atmospheric, and stub ice, ocean, and glacier data.

The grids are specified in CLM4.5 by setting an overall model resolution. Once the overall model resolution in set, components will read in appropriate grids files and the coupler will read in appropriate mapping weights files as well. The components will send the grid data to the coupler at initialization, and the coupler will check that the component grids are consistent with each other and with the mapping weights files (Oleson et al., 2013).

CLM4.5 in CESM 1.2.0 supports several types of grids out-of-the-box including single point, finite volume, spectral, cubed sphere, displaced pole, and tripole. Usually, input datasets are on the same grid. However, in some particular cases, they can be interpolated from regular lon/lat grids in the data models. The finite volume and spectral grids are generally associated with atmosphere and land models but the data ocean and data ice models are also supported on those grids.

Scripts for supported machines, prototype machines and generic machines are provided with the CESM release. Supported machines have machine specific files and settings added to the CESM1 scripts and are machines that should run CESM cases out-of-the-box (i.e. Yellowstone, Bluefire, Titan). In order to get a machine ported and functionally supported in CLM4.5 in CESM 1.2.0 (i.e. Ada, Terra, or Curie clusters which are the supercomputers provided by Texas A&M University), local batch, run, environment, and compiler information must be configured in the CESM scripts.

2.2 Data Collection

In order to obtain better represent the study area, physical properties specific to the Brazos River Alluvium Aquifer (BRAA) were used in CLM in place of default parameterization (NCAR, 2013). These parameters included: hydraulic conductivity, soil texture and type, hydrologic soil

group, depth to bedrock, groundwater well classification, and vegetation PFT. This information was collected using two data bases: SSURGO and STATSGO, from the United States Department of Agriculture (USDA). After visualized this data in ArcGIS, we exported it to Excel and, afterwards, we created input files in a netCDF format for the CLM4.5 simulation.

At the same time, the atmospheric forcing data required by CLM4.5 in CESM 1.2.0 is supplied by observed datasets. The standard forcing provided with the model is a 110-year (1901-2010) dataset called CRUNCEP (Viovy, 2011). An alternative atmospheric forcing dataset for land model development and, especially, for long-term simulations of historical land surface is also provided by CLM4.5 which was used to do this research project. This is a global 3-hourly forcing data set for driving CLM4.5 (or even CLM5.0) from 1948 to 2004 except for the 6-hourly precipitation and solar data. The forcing dataset covers the global land areas at T62 (~ 1.875°) resolution. It includes precipitation, surface air temperatures, downward solar radiation, specific humidity, wind speed, and air pressure. The QUIAN dataset has been used to force CLM for studies of vegetation growth, evapotranspiration, and gross primary production (Mao et al. 2012, Mao et al. 2013, Shi et al. 2013) and for the TRENDY (trends in net land-atmosphere carbon exchange over the period 1980-2010) project (Piao et al. 2012). Version 4 is used here (Viovy, 2011). It also reproduced many aspects of the long-term mean, annual cycle, interannual and decadal variations, and trends of streamflow for the Brazos River.

The dataset is divided into those three data streams: solar, precipitation, and everything else (temperature, pressure, humidity and wind). The time-stamps of the data were also adjusted so that they are the beginning of the interval for solar, and the middle for the other two.

GAM conceptual model took precipitation and temperature datasets from the Parameter-elevation Regressions on Independent Slopes Model (PRISM) developed by the PRISM Climate

Group at Oregon State University which provides a distribution of average annual temperature and precipitation based on the period from 1981 to 2010 (PRISM Climate Group, 2013). According this information, the average annual precipitation ranges from a low of about 35 inches in the northwest to a high of 50 inches in the southeast roughly. According this data, a potential extreme event could produce a rainfall of more than 45 inches per year. CLM4.5 takes precipitation, temperature, and solar fluxes input parameters from Quian et al dataset included in the model. Monthly precipitation (Figure 6) ranges from 2 to 6 inches with low precipitation during summer season (June, July, and August) and high peaks during the first months of the year (from January to April especially).

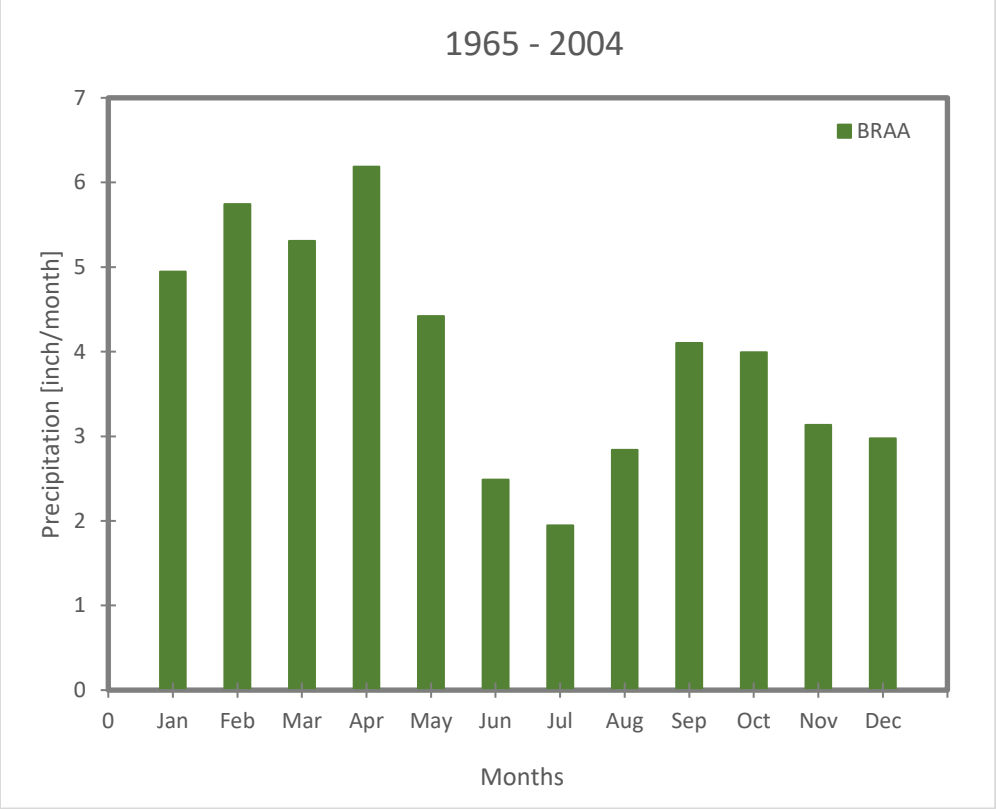

Figure 6: Precipitation – input data

Additionally, yearly precipitation datasets imply that precipitation is not constant over this area and that some extreme events happened in certain years. First, precipitation ranges from 26 to 53 inches per year and it has a standard deviation which ranges from 2 to almost 7 inch/month (Figure 7). Peak of this plot (more than 45 inches per year) occurred during the following years: 1968, 1973, 1979, 1991, 1997, 2001, and 2004. Since one of the biggest sources of larger recharge rates are precipitation rates, these values during these years will be important at the time we analyze final results. Moreover, it is importance to notice that precipitation using this dataset increase from the northwest to the southeast as the GAM reported as well (Figure 8).

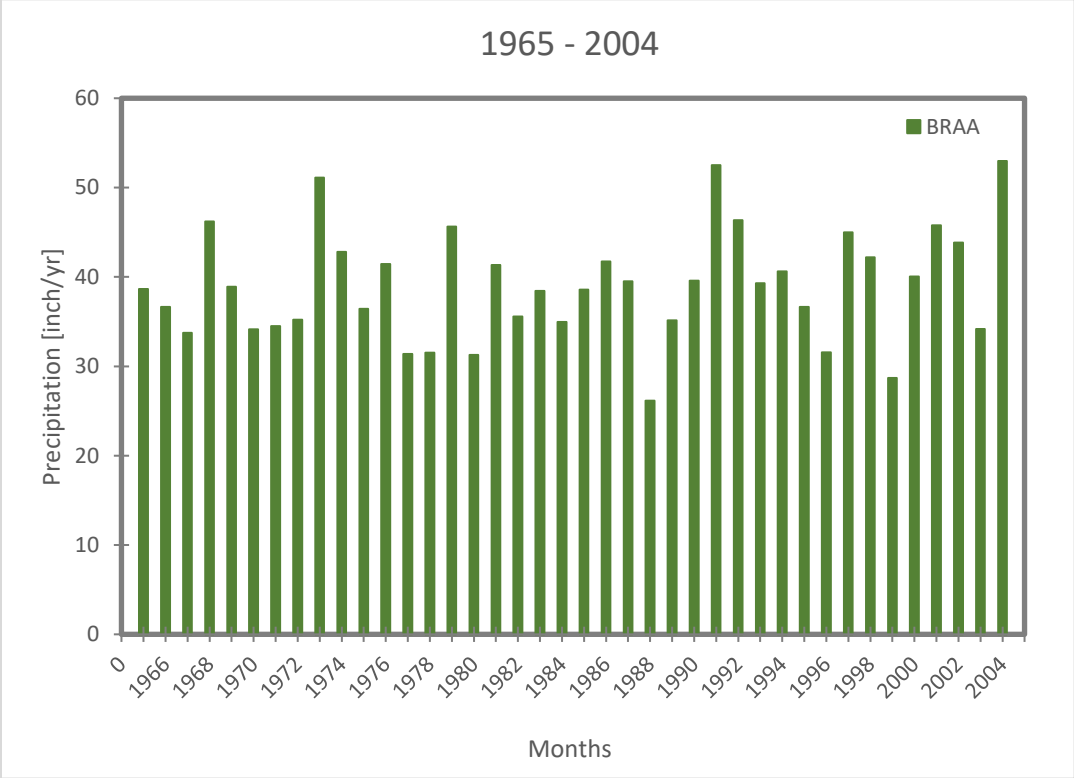

Figure 7: Yearly precipitation rates

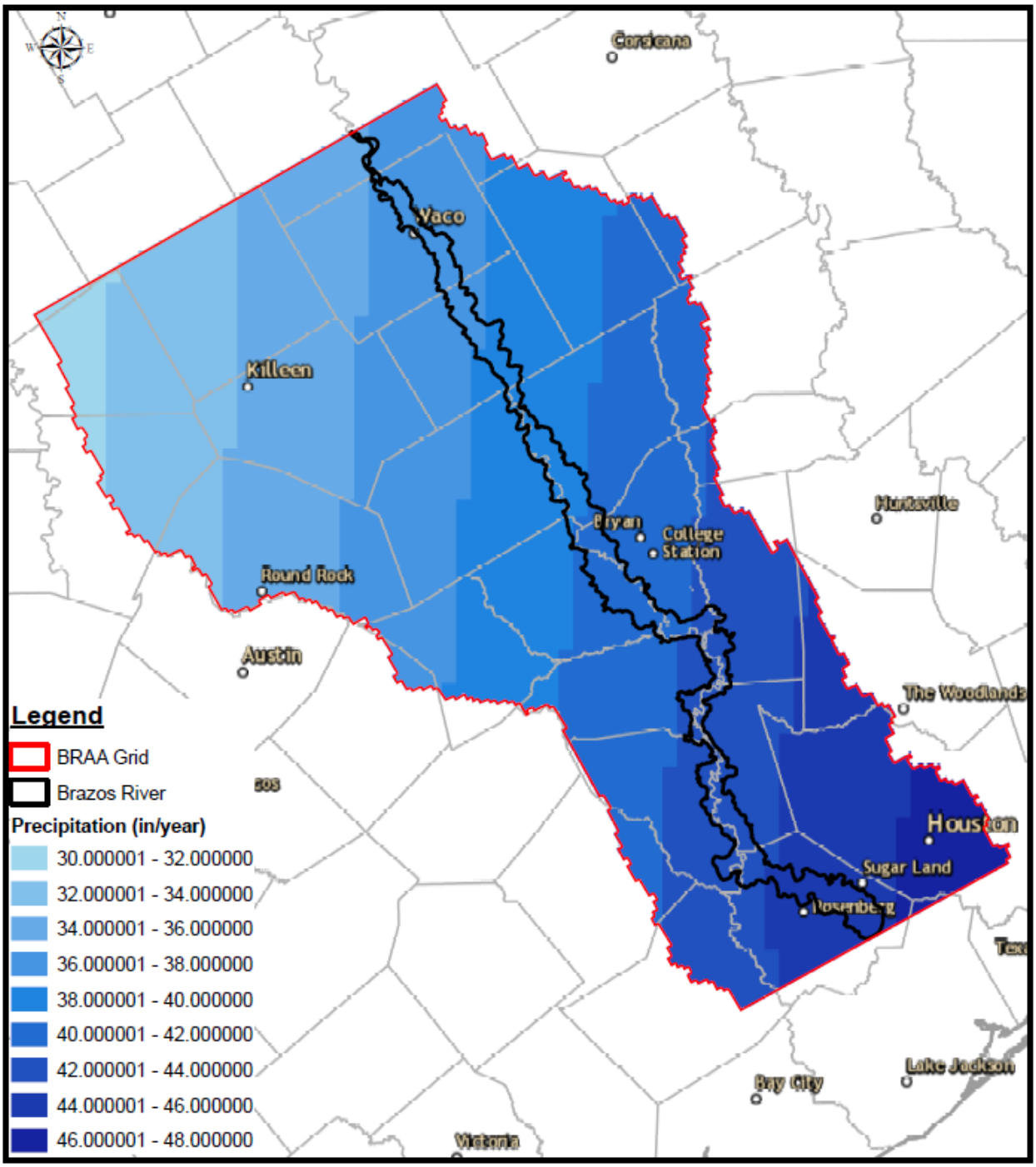

Figure 8: Precipitation in the BRAA

2.3 Modeling Approach

Overall, in order to get the recharge rate of this alluvium aquifer, the code we used to implement the numerical model is the Community Land Model (CLM4.5 and CLM – SP), as described above. We set up several characteristics of the alluvium aquifer (i.e. soil type, hydraulic conductivity, percentage silt, sand and clay) to modify the code in FORTRAN (if needed) and then run the case in CLM4.5. In order to get the results, we read all the output files by using MATLAB R2020a and then used Excel to do our sensible test and create some plots to show in the final report.

One of the biggest sources of discrepancy were the soil properties measurements due to the usage of two sources of information: SSURGO and STATSGO. Properties and physics parameters of the aquifers were reviewed and validated using these sources. If any parameter were not consistent with the ones from the model, a file with the correct values of those parameters was generated (i.e. hydraulic conductivity, percentage of silt, sand and clay, geology, soil type, soil texture, and vegetation).

In the particular case of the BRAA, the numerical model is based on the conceptual model (Erwing et al, 2016). Figure 9 shows a schematic of the cross section through the study area which is the same that will be use in this research project, along with a conceptual block diagram showing the aquifer layers.

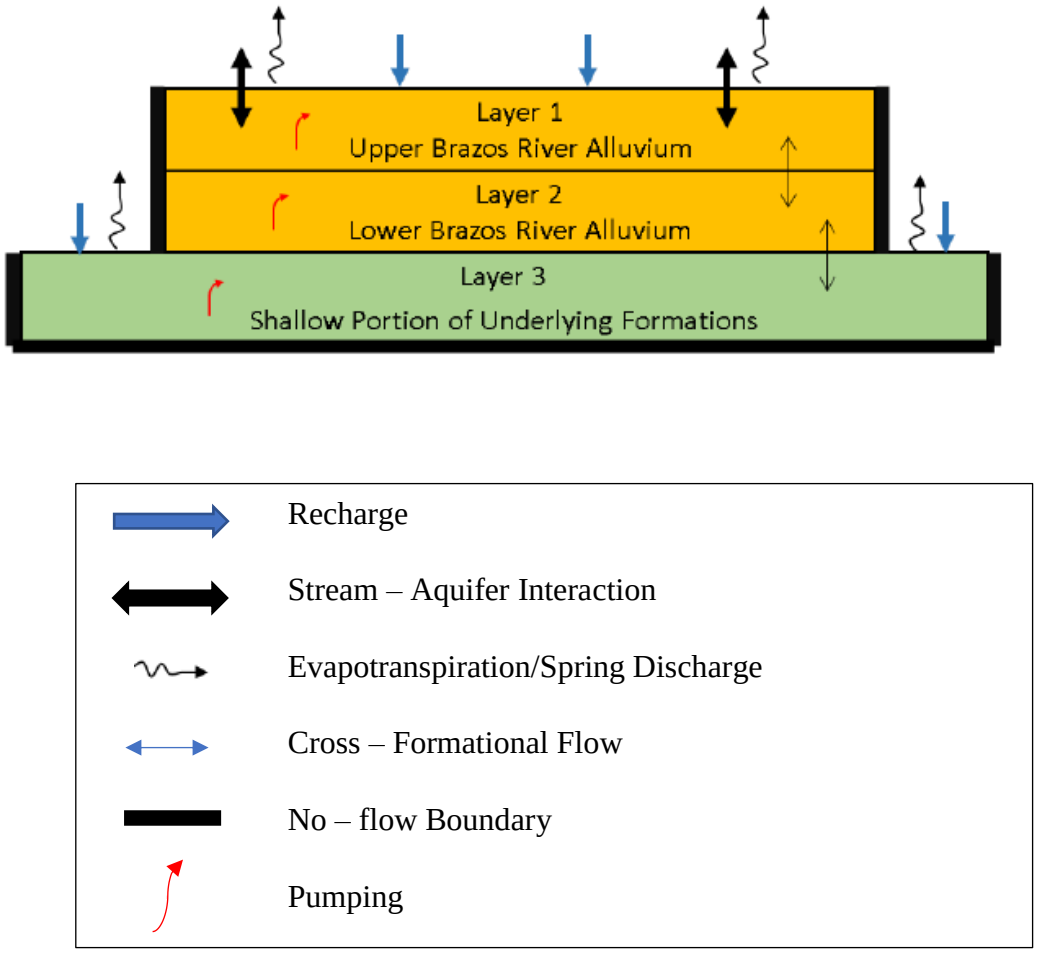

Figure 9: Groundwater flow model for the BRAA (reprinted from Ewing & Jigmond, 2016)

2.4 Method

CLM4.5 in CESM 1.2.0 was run through a set of scripts provided with the model. Basically, after collecting and review all the information from one of the sources, we needed to create a model in CLM. As we discussed before, this software uses a FORTRAN compilation to simulate different scenarios according our purposes. Therefore, a CLM4.5 code was modified for a particular variable with the information collected (i.e. hydraulic conductivity, vegetation, soil

types). After code modification, a case in CLM4.5 was created, calibrated, run, and validated. Predominantly, the basic steps we performed to create a case and run it in CLM were the following:

- Created input files with a refined grid of 1.0 x 1.0 km.
- Matched the information collected before with the one in CLM4.5
- Modified the CLM4.5 code or any parameter needed (hydraulic conductivity and soil texture)
- Created a new case: This sets up a new simulation. It was the most complicated of these four steps due to the several making choices to set up the model configuration.
- Invoked case.setup: This step configured the model so that it can compile.
- Built the executable: This step compiled the model.
- Spun up the model before starting the modeling run to stabilize it.
- Submitted the run to the batch queue: This step submitted the model simulation to the supercomputer queue.
- Validated the simulation

2.4.1 Simulation Setup

CLM4.5 was tested in a regional-scale mode and the satellite phenology (SP) with some exception noted below. Some extension modes such as dynamic global vegetation, biogeochemical cycles (BGC), or even carbon-nitrogen cycling (CNC) were in general not considered since they do not affect this study.

Regular resolutions in CESM1.2 are high because this code is vastly used to do simulation in the whole world (i.e. 10x10, 5x5, 1x1, 0.9x0.6, 0.3x0.5 degrees). For a regional simulation, it

wouldn't be accurate to use any of these resolutions, therefore, a small grid cell size was created using the 'mknocnmap.pl' utility provided in Community System Earth Community (CESM). This utility creates a new SCRIP grid data file. For this research project a 1 km x 1 km resolution over the south-central portion of Texas for the BRAA area was created (Table 10). Grid cell file is described by 1 and 0 values where 1 represents activated cells (which represents the BRAA) and 0 deactivated cells.

Table 10: CESM system and software prerequisites

Grid Latitude and Longitude (degrees)	
Top Right	(-95.03, 32.22)
Top Left	(-98.55, 32.22)
Bottom Right	(-95.03,28.80)
Bottom Left	(-98.55, 28.80)

Subsequently, surface input datasets and domain files were determined using the 'mksurfdata_map' utility provided in CLM4.5. The utility derives its values from satellite-based global datasets of phenology, soils, and topography, provided by University Corporation for Atmospheric Research (UCAR) (Oleson et al., 210 2013). Base on previous studies, it was decided to use default parameters from the global dataset, except for soil texture (percent of sand, clay, and silt respectively), and hydraulic conductivity in certain areas according STATSGO and SSURGO information. In this step, these parameters were modified in FORTRAN (i.e. soil texture and hydraulic conductivity) using the 'SourceMods' utility provided by CLM4.5. These mapping files and scripts (.nc files) will be used as input files to make the simulation in the BRAA.

Moreover, a spin up simulation was done using the input files described above to stabilize the model. To initialize simulation, CLM4.5 was first executed with a cold start (i.e. randomly produced initial conditions) and a hybrid run type simulation over 30 years (1935 - 1964). Since it would require a huge computational cost (which are limited for students), a startup simulation of more than 30 years was not conducted. As input, Quian meteorological forcing data (3-hourly precipitation and 6-hourly solar fluxes) were set up for these 40 years simulation over the BRAA. Once solar fluxes and recharge rates were stabilized, 'interpinic' utility provided by CLM4.5 was used to interpolate initial conditions file from a standard resolution to the one created before.

Afterwards, a case in CLM4.5 was set up. Input files previously created were used. In addition, CLM4.5 code required some parameters to create and then run the case (Table 11). A supercomputer called ADA provided by the Texas A&M High Performance Research Computing (HPRC) was used to run all the simulation in CLM4.5. ADA is an Intel x86-64 Linux cluster with 852 compute nodes (17,340 total cores) and 8 login nodes. Most (792) of the compute nodes are IBM NeXtScale nx360 M4 dual socket servers based on the Intel Xeon 2.5GHz E5-2670 v2 10-core processor, commonly known as the Ivy Bridge. These are housed in 11 19-inch racks (*HPRC User Guide*, 2019). The other nodes are configured with distinct hardware so as to enable special functional capabilities: GPGPU processing; very fast data transfers to external hosts; login access; etc. The speed in this ADA cluster is about 59.7 GB/s to read and write data. A summary of compute nodes equipped in ADA supercomputer could be viewed in Table 12.

Once the BRAA case was created and compiled in the supercomputer, the job was submitted in the queue to get ready for last step: run the job. A simulation year lasted roughly from 7 to 8 hours to run. Therefore, as this project consists of a period of 40 years, in total it was consumed 300 hours Service Units (SU) or hours used by the supercomputer.

Output frequency for both solar and hydrologic fluxes parameters were daily and monthly to get a better spatial and historical perspective. Outcomes were written in netCDF format. Consequently, a code in MATLAB was generated to read the variables needed for this project and export them to excel in order to develop our sensible analysis. Using Microsoft Excel, a statistics analysis was done. Therefore, we created our own plots using all the information and result gotten in the aquifer simulation.

Table 11: BRAA case specifications

Case specifications	
Case Name	BRAZOS_1965_2004
Machine	ADA
Resolution	CLM_USRDAT (created by the user)
Component Set (Compset)	ICLM45 (Includes Quian atmospheric forcing data, clm4.5 physics, and clm4.5 satellite phenology)
Run Type	Branch
Run Start Date	01-01-1965
Run End Date	12-31-2004
Time Step	30 min (1800 seg)

For some variables, linear regressions were performed to compare southern and northern portion of the BRAA trends. Goodness-of-fit of the regression analysis was determined based on coefficient of determination (R-squared) where appropriate. This analysis was focused on two main groups of variables such as Radiative and Hydrology (i.e. net radiation, latent heat flux, sensible heat, soil-related variables, and recharge and runoff rates).

Table 12: Compute nodes description (adapted from Texas A&M HPRC, 2019)

	General 64GB Compute	PHI 64GB Compute	GPU 64GB Compute	GPU 256GB Compute	256GB Compute	1 TB Compute	2 TB Compute	V100 GPU 192 GB Compute
Total Nodes	792	9	10	20	6	11	4	4
Processor Types	Intel Xeon E5-2670 v2, 10 core, 2.5 GHz					Intel Xeon E7-4860, 10-core, 2.26 GHz		Intel Xeon Gold 5118, 12-core,
Sockets/Node	2					4		2
Cores/Node	20					40		24
Memory//Node	64 GB, 1886 MHz			256 GB, 1866 MHz		1 TB, 1066 MHz	2 TB, 1066 MHz	192 GB, 2400 MHz
Accelerator(s)	N/A	2 Intel Xeon Phi 5110P	2 NVIDIA k20 GPUs		N/A			2 NVIDIA 32 GBV100 GPUs
Interconnect	FDR-10 Infiniband							
Local Disk Space	834GB 10K rpm SAS drives: 4 drives in 26 of the 256GB-memory nodes; 1 drive in all other							300GB

3. RESULTS AND DISCUSSION

The data sets used in the 40-years simulation over the BRAA (from 1965 to 2004) were divided in two sets. First, hydrology variables such as canopy evaporation and transpiration, infiltration, runoff, interception, recharge and ground evaporation; and radiative fluxes variables such as total latent heat, heat flux into soil, sensible heat, net radiation, and solar radiation, were estimated in a monthly basis. Second, hydrology variables such as recharge and runoff; and radiative fluxes variables latent heat, net radiation, solar radiation, photosynthesis, sensible heat, and net radiation were estimated in an hourly basis. For hourly data it has been taken more than 350,000 observations and for monthly data sets almost 500 observations either spatially and historically over the BRAA.

3.1 Solar Radiation

Daily net radiation and its components (latent heat, ground heat, and sensible heat) for a 40-years period over the Brazos River Alluvium Aquifer are normally distributed in time with peaks between 12 and 2 pm roughly (Figure 10). Simulated latent heat values in the Brazos River Alluvium Aquifer range from 6.34 to 177.83 W/m^2 with a standard deviation of 2.18 to 13.78 W/m^2 (Figure 10a). Latent heat in the south BRAA is around 8.50% higher than in the north BRAA. Simulated sensible heat values range from -9.02 to 148.85 W/m^2. In this particular case, we obtained an average negative sensible heat flux from 6 to 9 pm. One of the reasons why this flux is negative during that time period is because the ground is cooling and water vapor is condensing, leading to a positive gradient in temperature. In other words, subsurface ground of the BRAA is warmer than the surface; therefore, there is an upward energy flux from the subsurface

to the surface. This behavior is scientifically accepted because during nighttime there is no solar shortwave and radiation is all infrared and it is less than during the day (most of the cases 0 or close to it and negative values). Sensible Heat is about 5.10% higher in the south than in the north BRAA (Figure 10b). The standard deviation varies from 5.62 to 7.13. Ground heat Flux in the Brazos River Alluvium Aquifer is negative during nighttime and reach a its peak at 1:30 pm roughly (Figure 10c). It ranges from -62.72 to 134.98 W/m^2. Standard deviation is relative higher than the other parameters. It ranges from 2.87 to 19.00. Ground Heat Flux is positive when it is directed away from the surface into ground.

Therefore, it is negative when it is directed away from the ground to the surface which only occurs at nights. Ground heat flux in the south BRAA is about 3% higher than in the north BRAA. Finally, net radiation, which represents the gain of energy by the surface from radiation, is normally distributed and has a positive value during daytime. It ranges from -49.22 to 433.24 W/m^2 (Figure 10d). Net radiation in north BRAA is about 17.8% smaller than net radiation in south BRAA. When it is positive, gain of energy is towards the surface (during daytime), and when it is negative, gain of energy is into the ground (nighttime).

(a) Latent heat (LH)

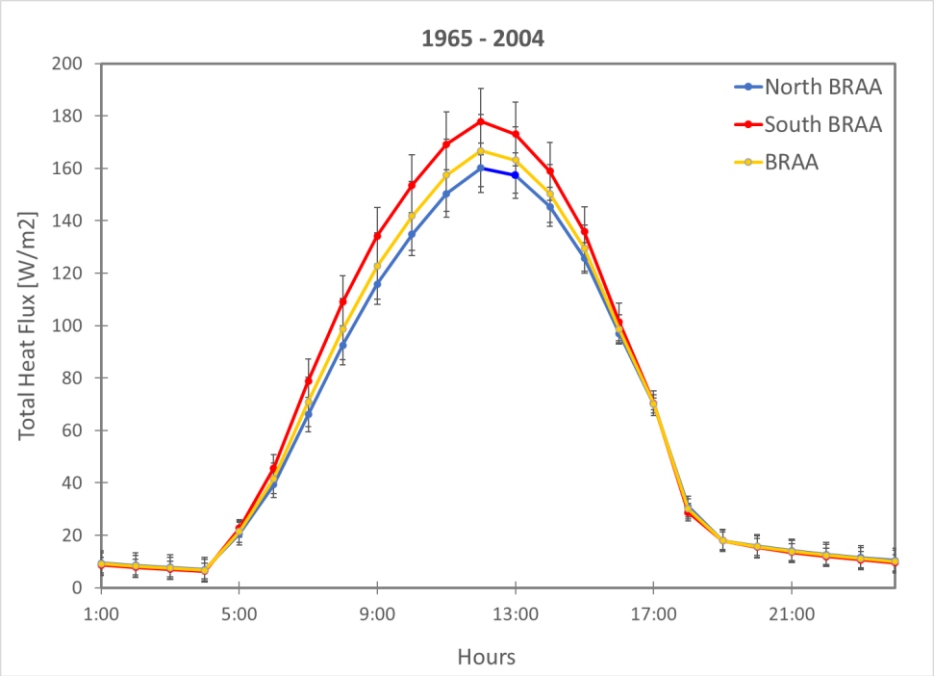

(b) Sensible heat (SH)

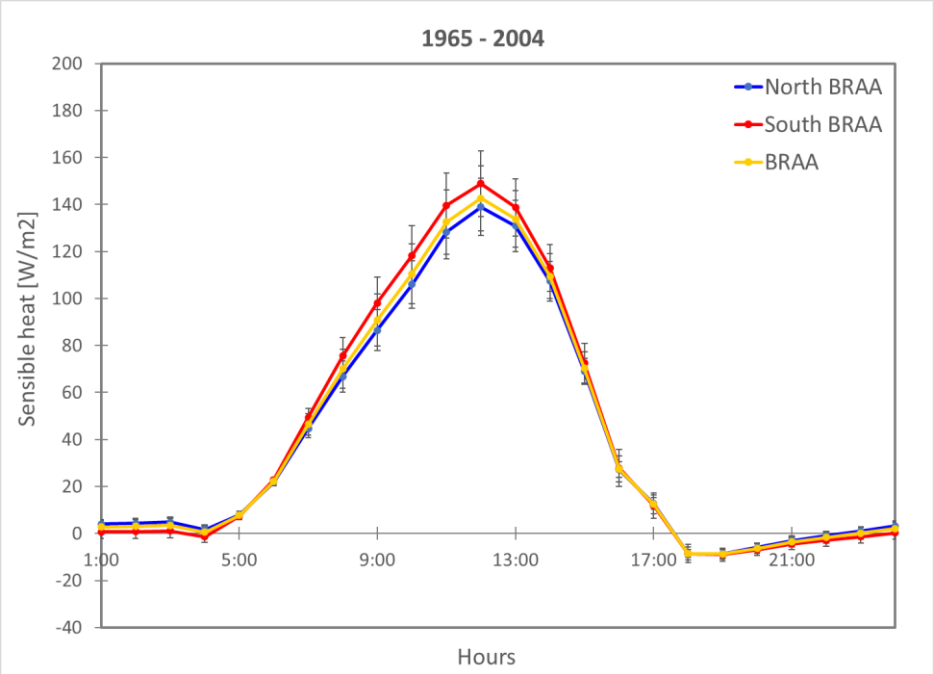

Figure 10: Daily radiative fluxes

(c) Ground heat flux (G)

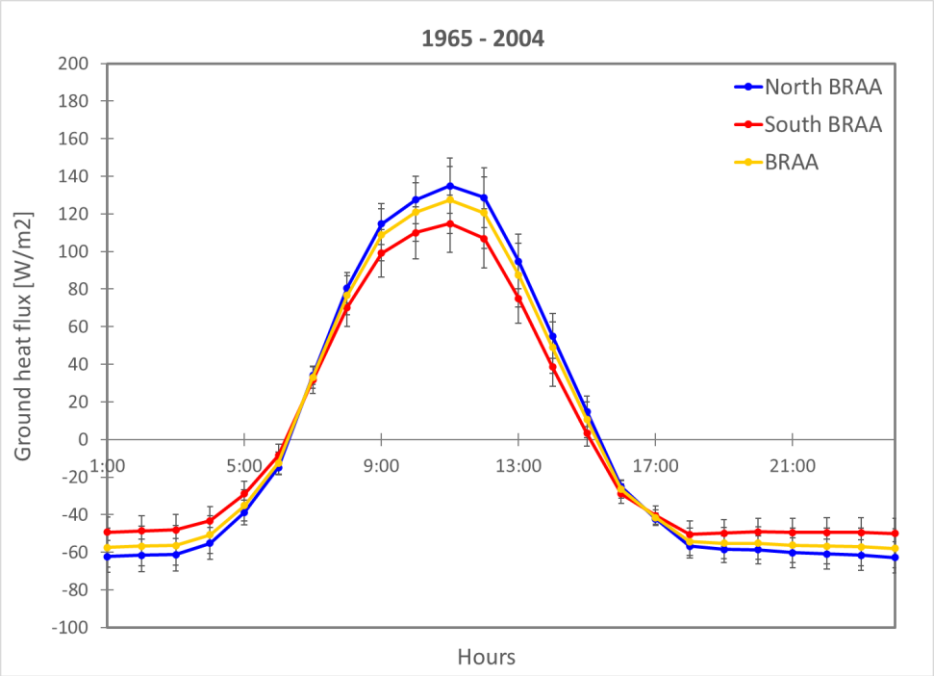

(d) Net radiation (NR) = LH + SH + G

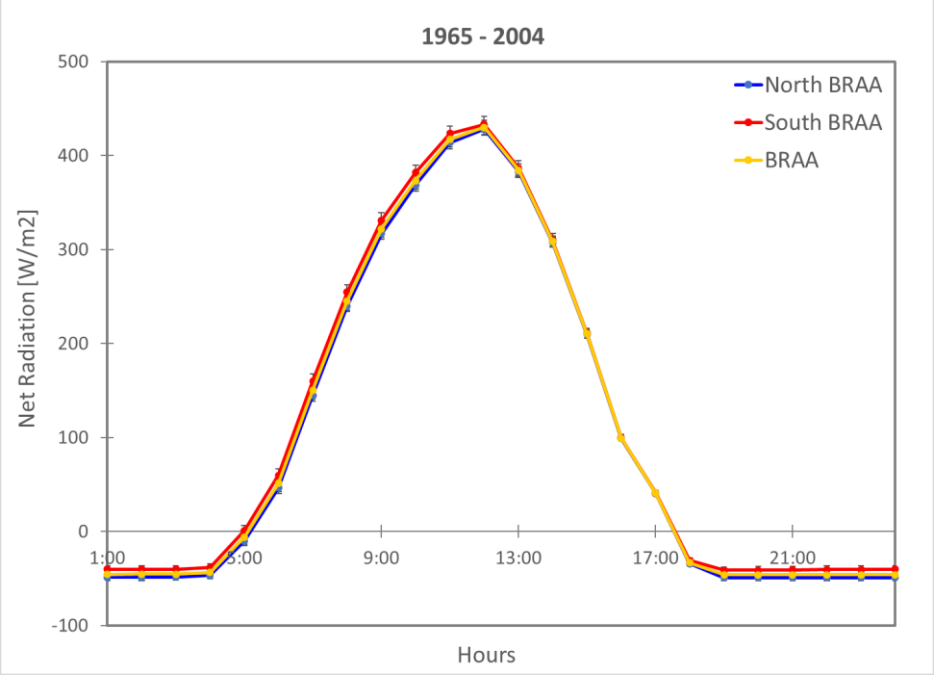

Figure 10: Continued

Peaks of monthly net radiation plot and its components over the BRAA for a time period of 40 years from 1965 to 2004 occurred during the summer, as expected, when solar energy is higher than any other season of the year (Figure 11).

Monthly latent heat flux over the BRAA varies from 19.5 to 115.1 W/m^2 and standard deviation ranges from 1.71 to 12.0 W/m^2 (Figure 11a). Over summer season there is about 57% more variability in the BRAA than in another season. Additionally, there is a drop in August (5% smaller than September) caused by a smaller gradient in temperature and a specific humidity in August than in September in average for this time period. Moreover, we have to take into account that there is less variability in September than in August (8 versus 10.5). Additionally, this historical drop was clearly affected by crops timeline since latent heat is ordinarily the largest consumer of available solar energy consuming between 60 and 70% of net radiation in a crop growing season. Usually, over this region there are virtually no tall crops from December to March (Texas Fil Commission, 2020). During summer season (especially in June and July) wheat is at its peak, while corn, cotton, rice, peanuts, and soybeans are harvested moderately later (starting in mid-August and finishing in December at most) and are at their peak in September and October. Furthermore, some weeds start growing during the beginning of the fall such as dandelion, bermudagrass, and johnsongrass (perennial weeds); common chickweed, purslane, bluegrass, and smooth crabgrass (annual weeds). A comparison of this variable over the northern and southern portion of the BRAA indicated that the latter were about 9% higher than the former.

Monthly Ground flux were negative for winter season and positive for the rest of the year, with a peak in June, at the middle of the summer season. It ranges from -12.6 to 11.30 W/m^2 (Figure 11b). These number are significantly smaller than Latent Heat values. However, standard

deviation ranges from 1.03 to 3.31 W/m^2, which implies there is less variability of the data for this parameter over the 40 years simulation.

Sensible Heat flux is always positive and it is normally distributed (Figure 11c). It ranges from 6.0 to 77.0 W/m^2 and the standard deviation varies from 1.91 to 14.72 W/m^2 (higher than Ground Heat flux standard deviation). However, it cannot be considered an anomaly, because it is known that July and August are the warmest months along the year.

Net radiation flux is always positive for this time period (Figure 11d). It ranges from 9.82 to 193 W/m^2 and variability is relatively small (standard deviation goes from 1.83 to 22.21 W/m^2). Peaks of this plot occurs between June and July with a highest value of 193 W/m^2 roughly in mid-June.

(a) Monthly latent heat flux

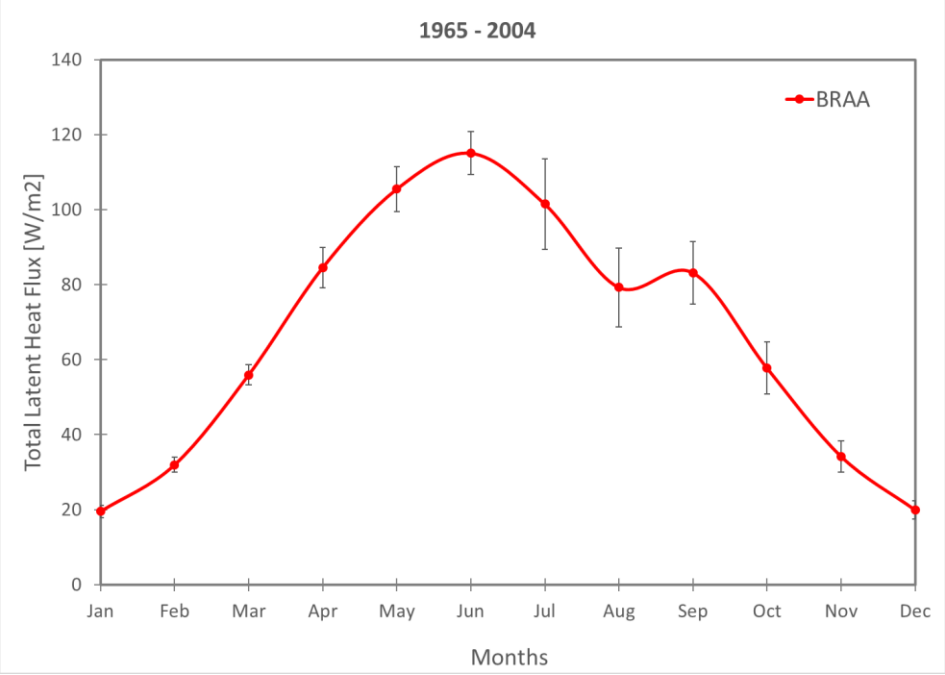

Figure 11: Monthly radiative fluxes

(b) Monthly ground flux

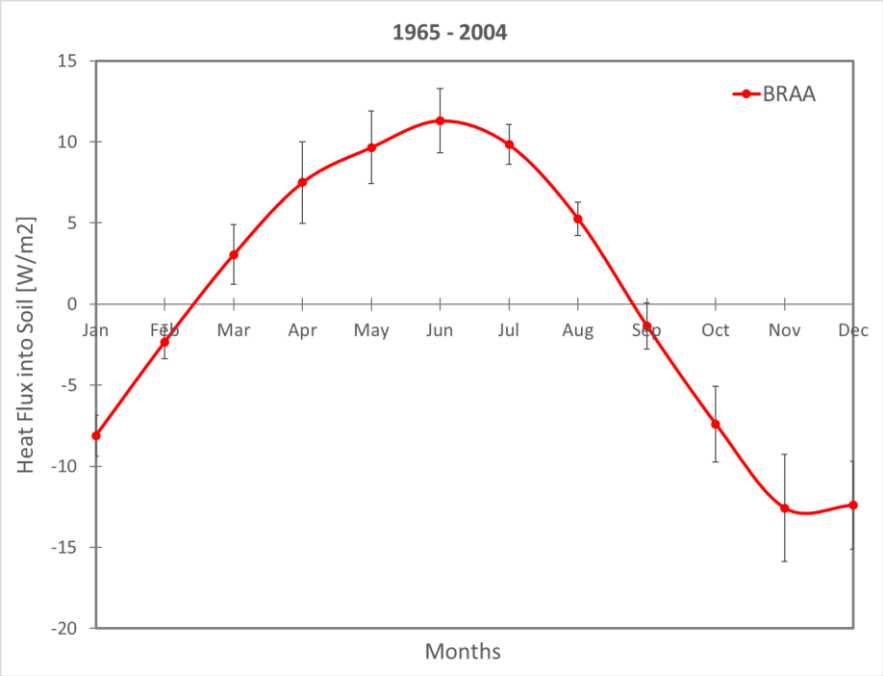

(c) Monthly sensible heat

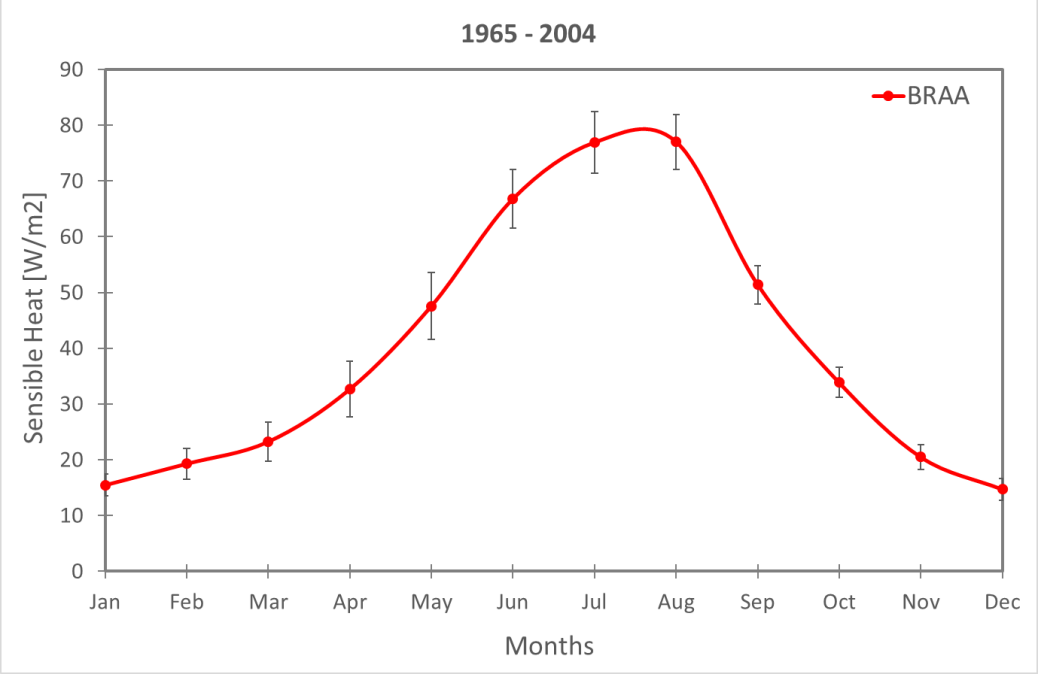

Figure 11: Continued

(d) Monthly net radiation

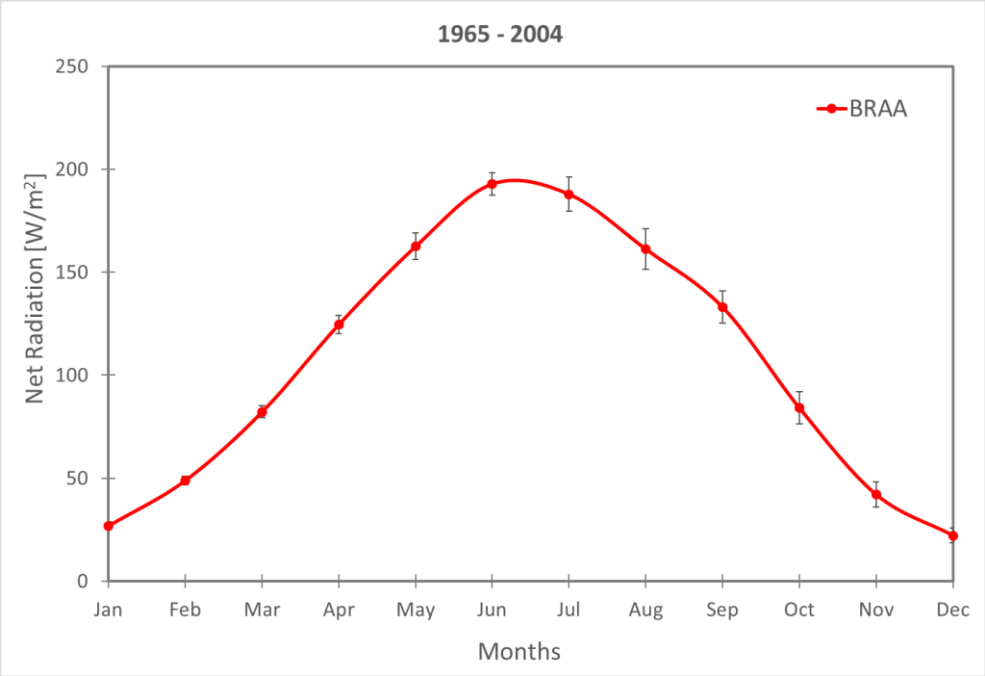

Figure 11: Continued

3.2 Evapotranspiration Fluxes

CLM4.5 partitioned Evapotranspiration (ET) into monthly canopy transpiration, soil or ground evaporation, and canopy evaporation which better represents the interaction between land and atmosphere (Figure 12) along the 40-years' time period of simulation.

Monthly canopy evaporation varied from 0.26 to 13.03 mm/month with a standard deviation between 0.61 and 3.46 mm/month (Figure 12a). It had a drop during July and August and a small peak in September. Monthly canopy transpiration seems to be normally distributed and had one peak (Figure 12b). It ranged from 5.40 to 69.06 mm/month and standard deviation which ranges from 1.27 to 11.42 mm/month, was relative higher than in canopy evaporation. Peak fluxes took place in June and July (summer season). Monthly ground evaporation plot had two

peaks and one drop and all the values are positives (Figure 12c). It ranged from 14.24 to 34.16 mm/month and standard deviation varied from 2.09 to 9.10 mm/month (smaller variability than canopy transpiration). Finally, monthly evapotranspiration (ET) had two peaks (in June and September) and a drop in August (Figure 12d). It ranged from 21.36 to 119.20 mm/month and standard deviation ranged from 1.96 to 13.37 mm/month. There were higher values during summer because temperatures are warmer and driest and there is a limited supply of soil moisture which leads evaporation flux rates to increase over this season. On the contrary, during winter and fall time, evaporation flux tends to be smaller because temperature gradient is colder.

3.3 Soil Hydrology Fluxes

Runoff was parametrized in CLM4.5 based on the TOPMODEL runoff model and SIMTOP developed in 2005 by Niu et al. Overall, the mean runoff over this time period simulation was 0.34 in/year (8.55 mm/year) and standard deviation fluctuates between 0.11 and 0.21 in/year which represents a low variability of this parameter during this time (Figure 13a). The lowest value for runoff happens in July and the highest in May. These results could be explained by the fact that rainfall rates are higher over the first semester of the year and the driest month of the year is July. Moreover, runoff rates were about 35% higher in the northern portion of the BRAA than in the southern portion.

Theoretically, runoff calculations should be calculated explicitly from a discrete cumulative distribution function (CDF) at each grid cell at the resolution the model was running such as 0.01 x 0.01 degrees for this particular case (Oleson, 2013). Unfortunately, because this is a computationally intensive and time-consuming task even for regional applications in CLM4.5, results are calculated at 0.125° resolution using HYDRO1K dataset from USGS following the

(a) Monthly Canopy Evaporation

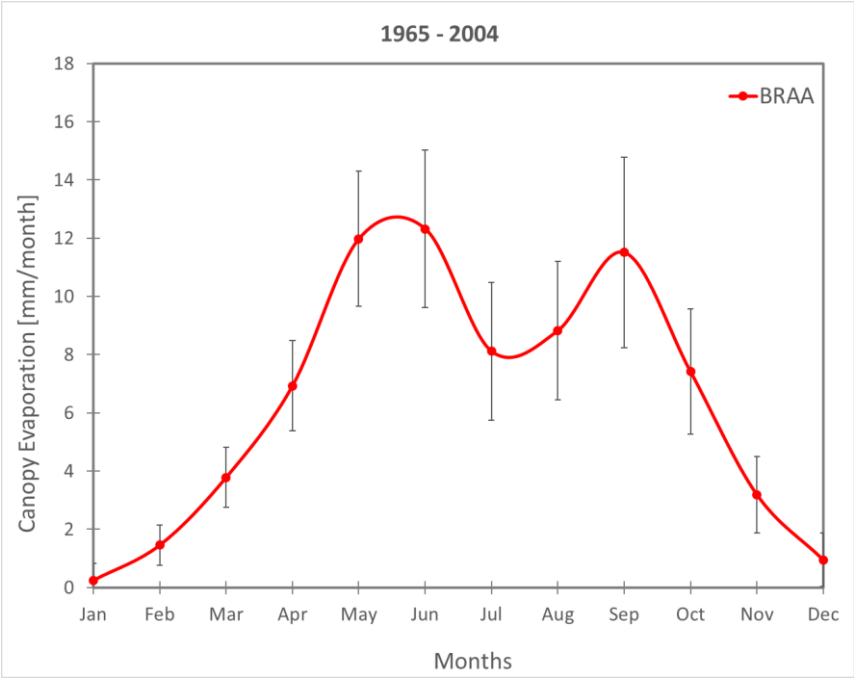

(b) Monthly Canopy Transpiration

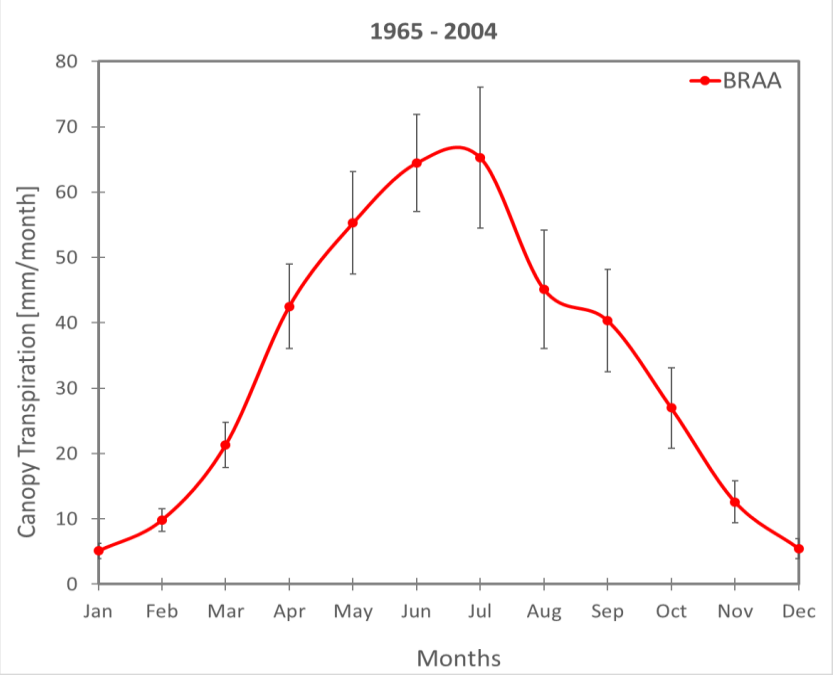

Figure 12: Monthly ET fluxes

(c) Monthly Ground Evaporation

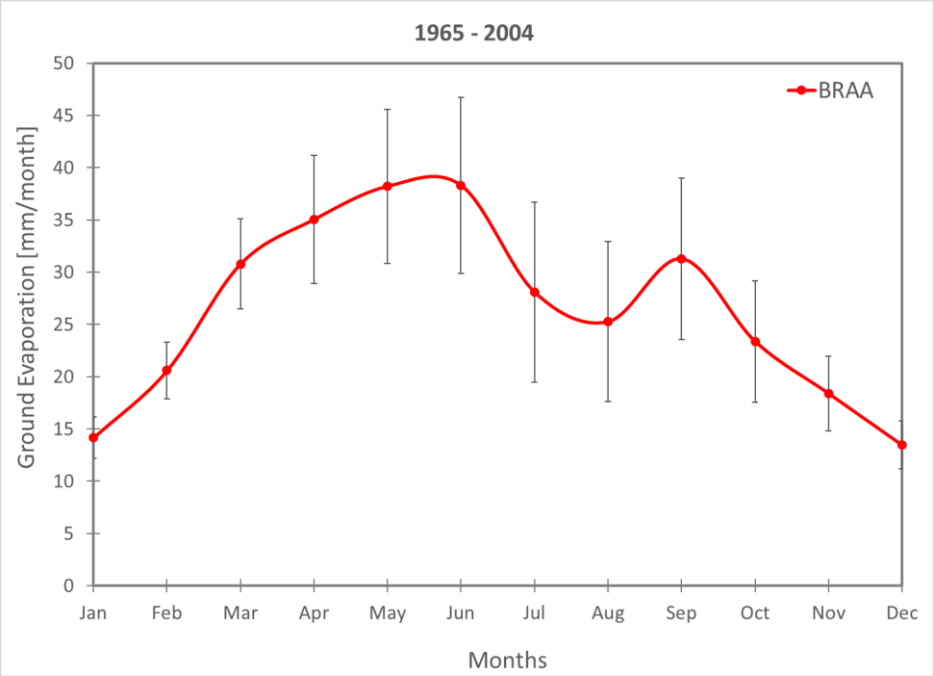

(d) Monthly Evapotranspiration (ET)

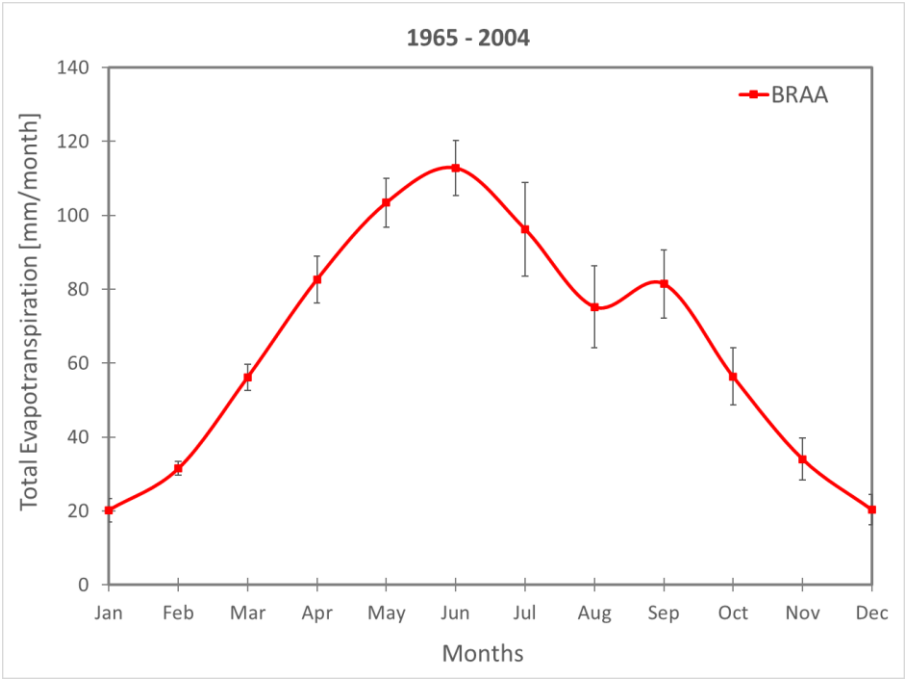

Figure 12: Continued

algorithm in Niu et al which is more than 12 times higher than the desired resolution. Some grid cells with topographic indices exceeding the 95-percentile threshold at this resolution are excluded from the calculation to eliminate biased estimation of statistics because of large CTI values at pixels on stream networks (Oleson, 2013). As a consequence, an error associated with this parametrization was expected and, therefore, results obtained were not 100% accurate.

The lowest monthly infiltration rate over this period time happens in July (summer time) and it has a peak in October (Figure 13b). Annual infiltration rate is 18.8 in/year with a relatively low standard deviation, which fluctuates between 3.1 to 5.2 in/year. Lower infiltration rates occurred during summer season (especially in July and August), and the rest of the year it seemed to be a relative constant trend with small drops in May and April. Monthly infiltration rates over the southern portion of the BRAA are roughly 18% higher than infiltration rates over the northern portion of this area.

(a) Monthly runoff rates

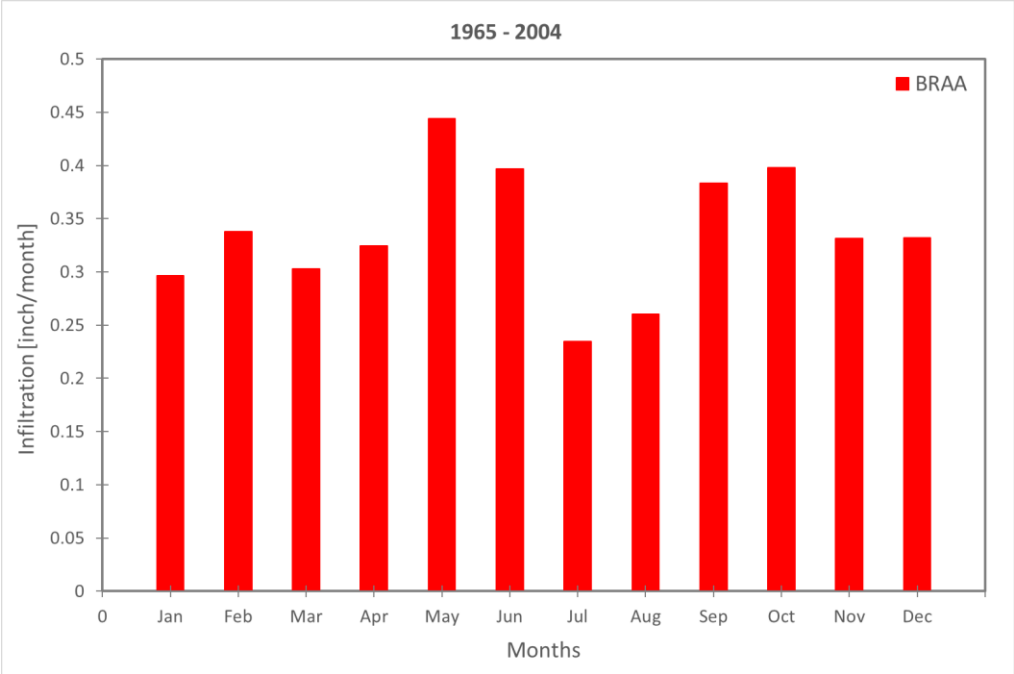

(b) Monthly infiltration rates

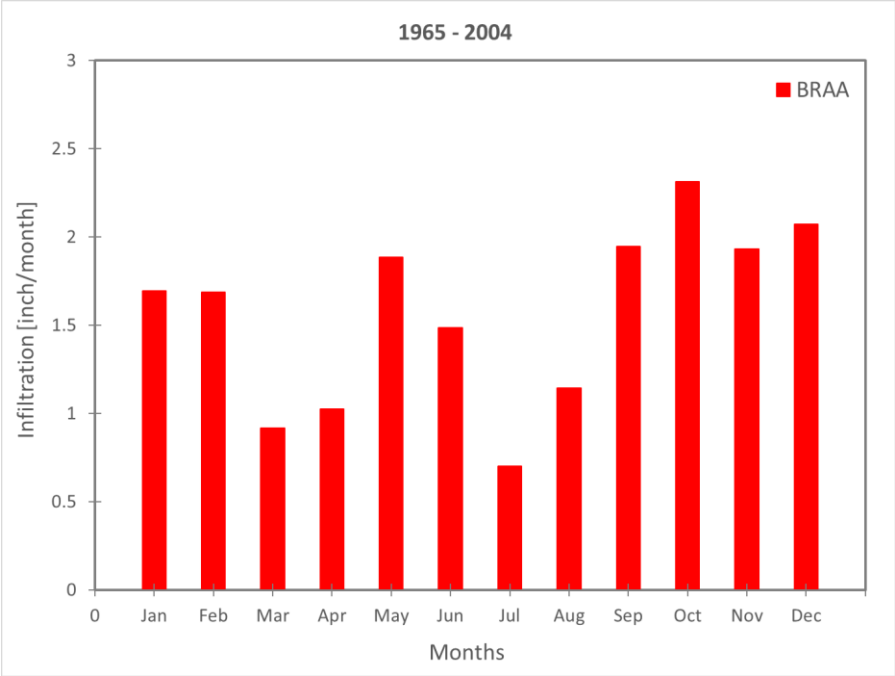

Figure 13: Monthly change of runoff and infiltration rates

3.4 Recharge

3.4.1 Statistical Analysis

There does appear to be a relationship between the time of the day and recharge rates (recharge data does not appear to be completely random) in the distribution of recharge rates for 40-years along a day (Figure 14). There is also an upward trend in the morning and then it falls down at 3 pm. This is a cyclical trend which on average is the same for this whole period. The simplest model to explain this relationship is to use a linear model. However, as we can see in figure 14a and 14b, the best model which fits recharge data is the polynomial degree 3 ($r^2 = 0.96$) and 6 ($r^2 = 0.48$). It is clear that recharge cannot be explained just by precipitation rates. It implies that recharge rates are not only affected by a specific time of the day when precipitation takes place but are also affected by other factors such as irrigation return flow, surface soils, topography, and surface water features. An alternative trend for recharge rates along the 40-years period implies that either linear and polynomial models are not enough tools to explain relationship between recharge and precipitation (Figure 14b). Moreover, it appears to be a more complex relationship between them (periodicities, and the other factors we stated above). The first QQ plot indicate that averaged daily recharge rates are normally distributed (Figure 14c); however, the second QQ plot indicate that this dataset is right skewed since some observations do not lie closely to the trendline.

(a) Linear and polynomial fit of daily recharge data.

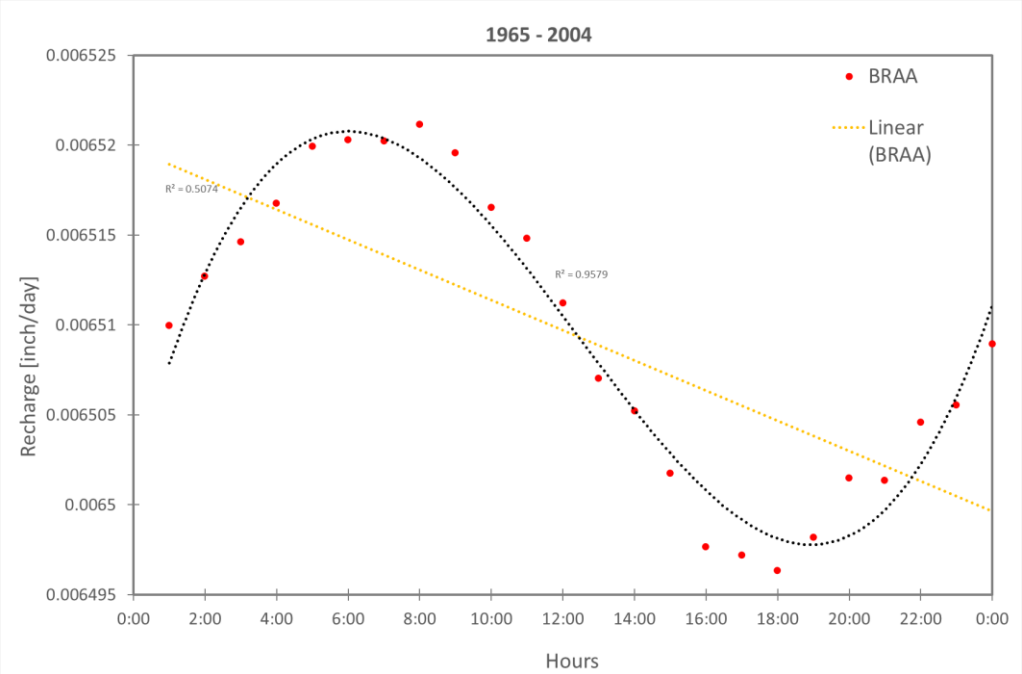

(b) Linear and polynomial fit of annual recharge and rainfall data.

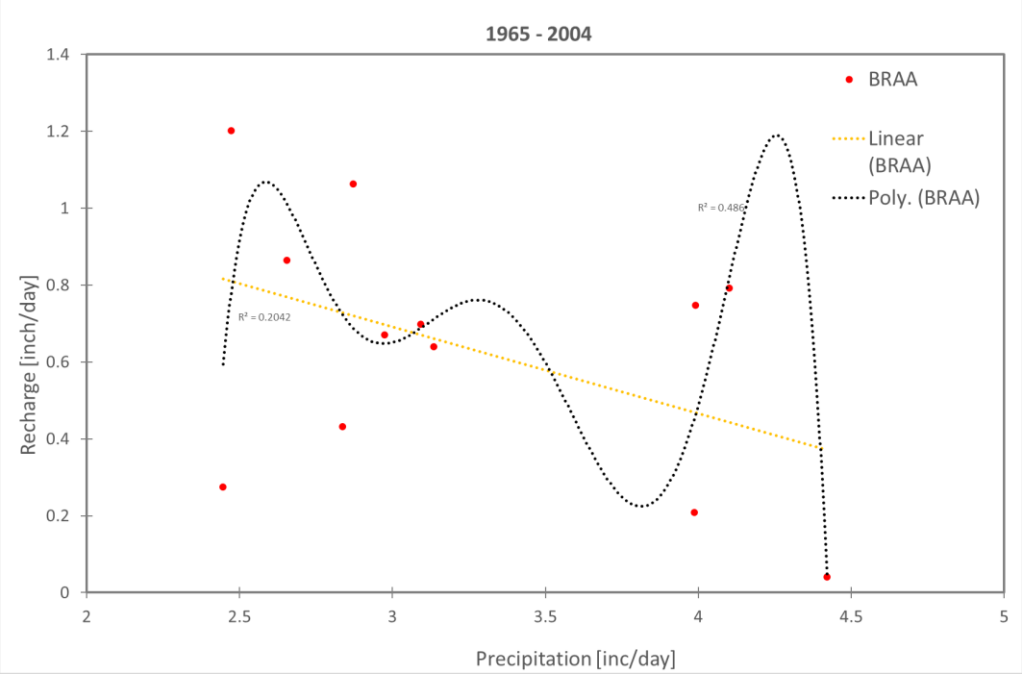

Figure 14: Statistical analysis

(c) QQ plot for daily averaged recharge data.

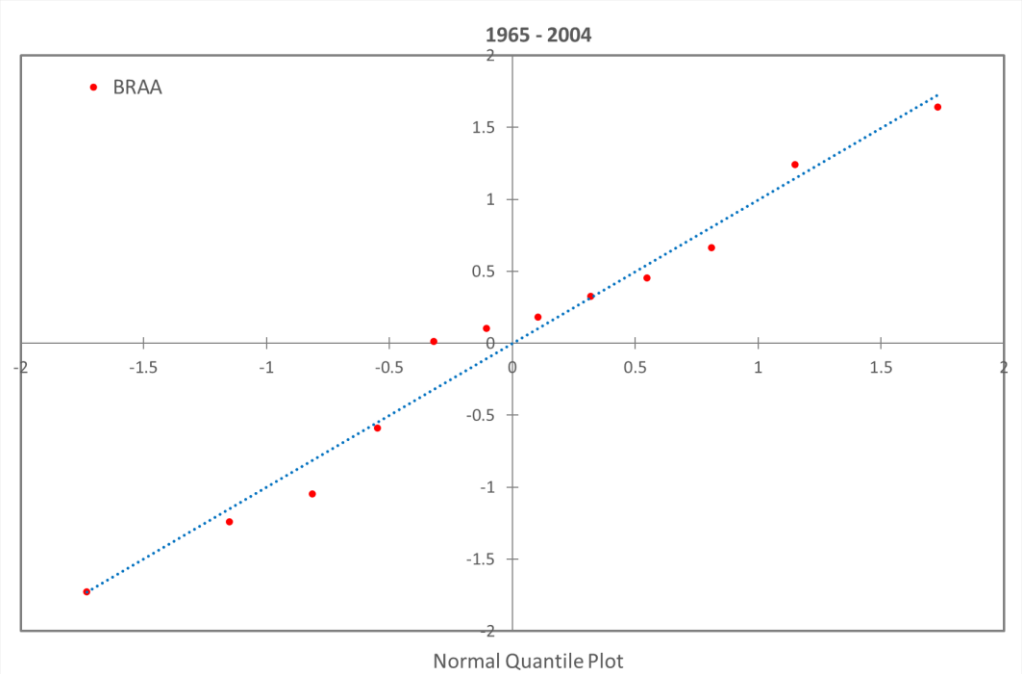

(d) QQ plot for daily recharge data observations.

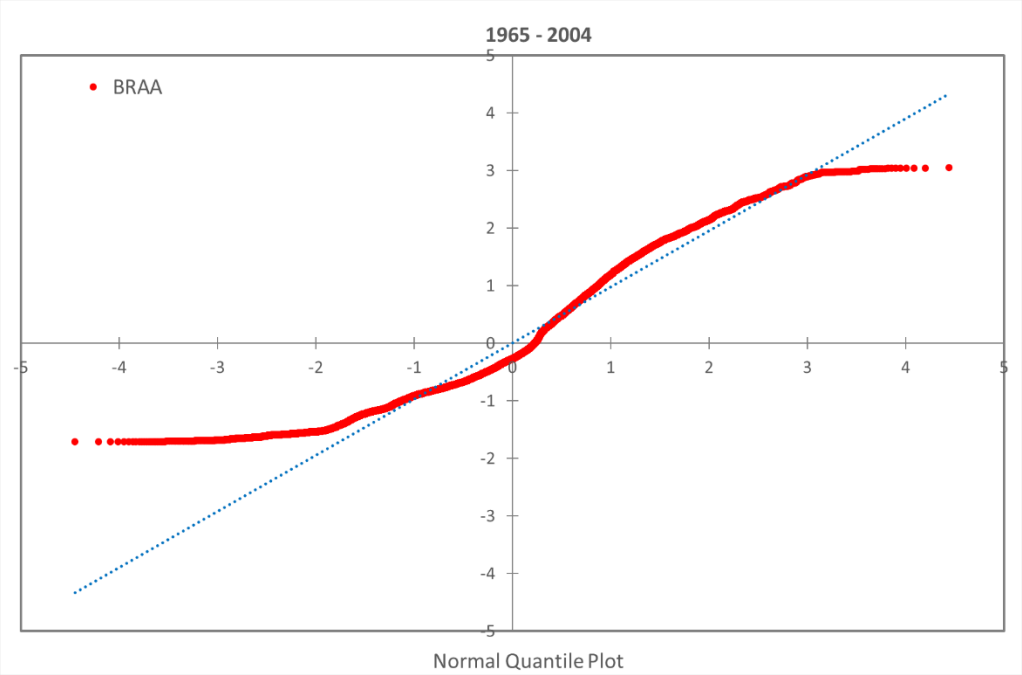

Figure 14: Continued

In conclusion, after conducting a t-test and checked for normality (p-value and standard deviation error), slope of the dataset is statistically significant and a 95% confidence interval for the slope (for the 40-years simulation period) is [1.33; 3.42] inch/year (Appendix A), which is an acceptable range as we will discuss below according the BRAA GAM, the USGS guideline, and previous studies.

3.4.2 Sensitivity Analysis

Averaged daily recharge rates over the BRAA for a 40 years period from 1965 to 2004 varied from 0.006496 in/day to 0.006521 in/day (Figure 15). Average recharge rates are higher during mornings with peaks of 0.006521 inches per day. It has a drop from 4:00 pm to 7:00 pm when recharge rate has a lowest value of 0.006496 inches per day. There is a cycle along the day for this parameter since it starts with a rate of 0.0065 inches per day roughly, afterwards it goes up and have a peak at 8:00 am, therefore it decreases and has its lowest value at 6:00 pm. Standard deviation which ranges from 0.00329 to 0.00332 is higher than other standard deviations for other parameters. Precipitation from the atmospheric forcing input data has a similar cycle. It has peaks during the morning at 10 or 11 am and a drop after 5 pm.

Similar to most of the parameters discussed above, southern portion of BRAA has higher recharge rates than northern portion of the BRAA. One reason this is happening is because the southern portion of BRAA has higher precipitation rates than the northern portion (about 13% higher). Annual precipitation in the study area increases from northwest to southeast, with the highest precipitation rates nearest the coast (TWDB, 2016). Additionally, topography affects the distribution of recharge, concentrating recharge especially in highlands and discharge in lowlands (Meyboom, 1966). Since northern portion of the BRAA is an area with slopes higher than 5%, it is less likely to have higher recharge rates.

Brazos River Alluvium Aquifer

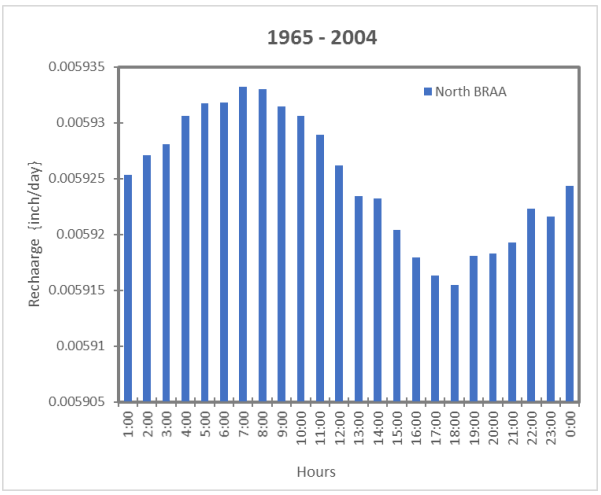

Daily Recharge

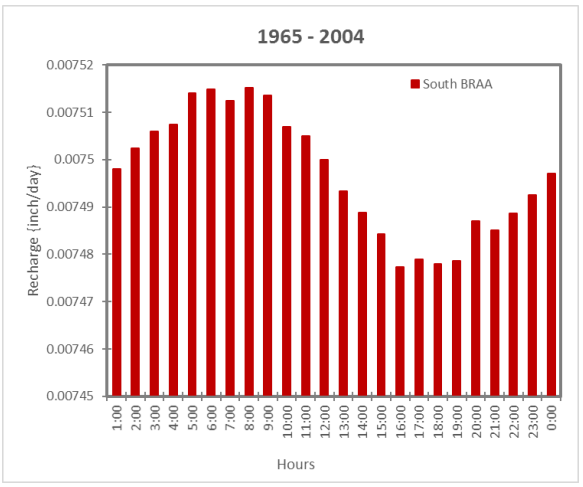

Daily Recharge

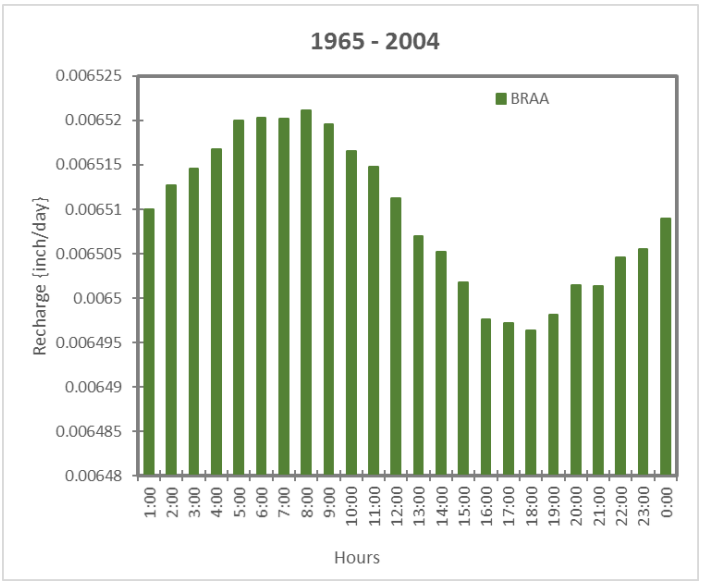

Daily Recharge

Figure 15: Daily recharge rates

Monthly recharge rates over the BRAA from 1965 to 2004 ranges from 0.2 to 1.2 inches/month (Figure 16). Highest recharge rates occur from January to May (with a peak value in January). Lowest recharge rates took place in June and July which are historically the driest months in Texas (National Weather Service). There is small variability for this parameter which

had a standard deviation ranges from 0.1 to 0.4 inches per year. Since precipitation is a strong factor affecting recharge rate and the lowest precipitation rates from the Quian atmospheric forcing data occurred in summer season especially in June and July, it was expected that during these months recharge rates were the lowest. In addition, as we stated before, parametrization has been done at 0.125 degrees for computational and time-consuming purposes, therefore, an error associated for these results was expected because we used more refined grid cells. Moreover, monthly recharge rates follow the same behavior as the previous parameters (i.e. infiltration, ET, runoff). Recharge rates in the southern portion of the BRAA are about 20% higher than recharge rates in the northern portion in average. As it was expounded previously, precipitation rates and topography along the BRAA mainly are the main reasons why these rates are higher in the southern portion of the BRAA.

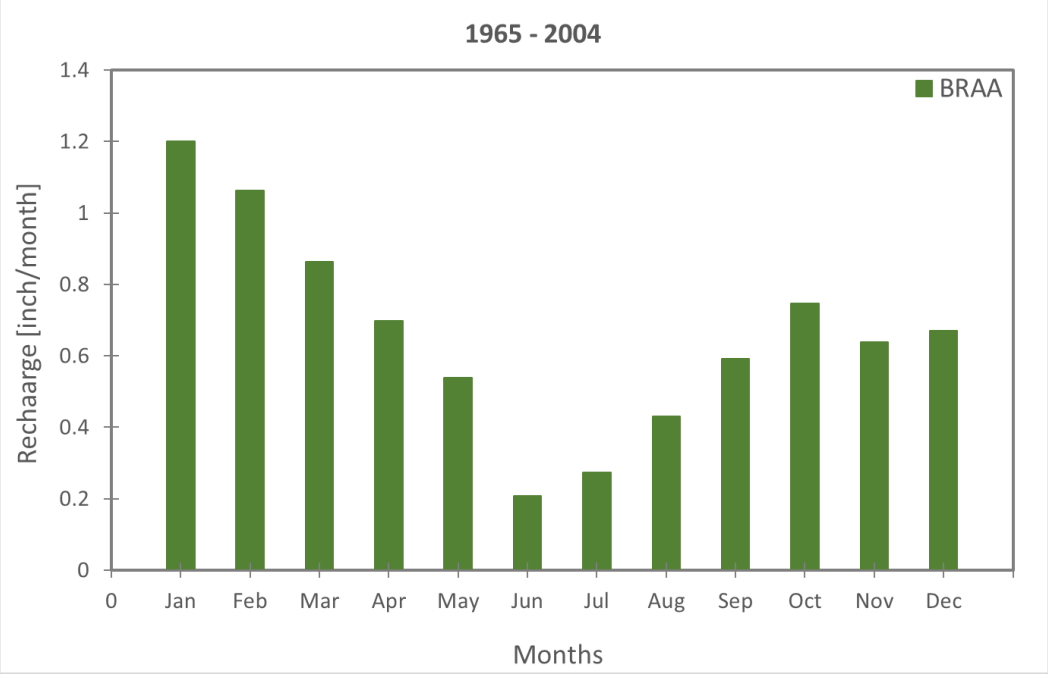

Figure 16: Monthly recharge rates

Annual recharge rates in the BRAA range from 0.076 to 9.730 inches per year with an annual average value of 3.01 inches per year. Variability is relatively low and standard deviation ranges from 0.64 to 3.39 inches per year. The highest value occurred in 1992 and the lowest value took place in 1982 (Figure 17). One manner to explain why recharge rates fluctuates in that range and is not constant, is analyzing weather during these years. Drought seasons produce lower recharge rates and storms seasons cause higher recharge rates. Therefore, it depends on how significant a storm occurred during that year. Table 13 explains in further details some important weather conditions for the 40 years period (from 1965 to 2004) that could affect these rates (National Weather Service, 2005; NOAA, 2002; Texas State Climatologist, 2019). For instance, in 1992 there were several hurricanes and tornadoes which produced severe thunderstorms and recharge rates for that year was the highest one during this 40-years period especially in the last semester of that year. On the contrary, in 1982 there were not any major weather condition in the area and recharge rate at that year was one of the lowest rates (Figure 18). Recharge rates are about 21% higher in the southern portion than in the northern portion of the BRAA per year.

Precipitation in Texas is quite variable, both in space and time. Much of the state has two rainy seasons, with the rainiest months on average being May, June, September, and October. Rainfall amounts increase from west to east, with the southeast corner of the state near Beaumont averaging over eight times the annual rainfall of some areas near El Paso. The long-term trend of precipitation in Texas has been positive. Over the past century, parts of central and eastern Texas have experienced precipitation increases of 15% or more, while in much of the western part of the state the long-term trend is flat or even downward.

On top of extreme weather conditions, El Nino and its counterpart La Nina, are weather patterns that can affect weather around the world. They usually appear every two to seven years.

El Nino is characterized by above-average temperatures in the Pacific Ocean. La Nina bring below-average temperatures. In Texas, El Nino patterns generally mean wetter weather (stronger storms). Comparison of the South Texas annual rainfall with the Southern Oscillation Index (SOI) time series over the last century typically shows higher amounts of rainfall during the warm phase of ENSO (El Niño events) and lower rainfall amounts during the cold phase of ENSO (generally La Niña events). In addition, ENSO seems to impact the rainfall variability more during the cold season (October-March) than in the warm season from April to September (Murgulet et al., 2012). Moderate and strong El Nino events in 1968, 1991, 1992, and 1997 produced higher rainfall over this area and consequently generated greater recharge rates. Moreover, moderate and strong La Nina events in 1965, 1975, 1989, 1995, and 2000 produced lower rainfall in the area, and therefore, less recharge rates over the BRAA.

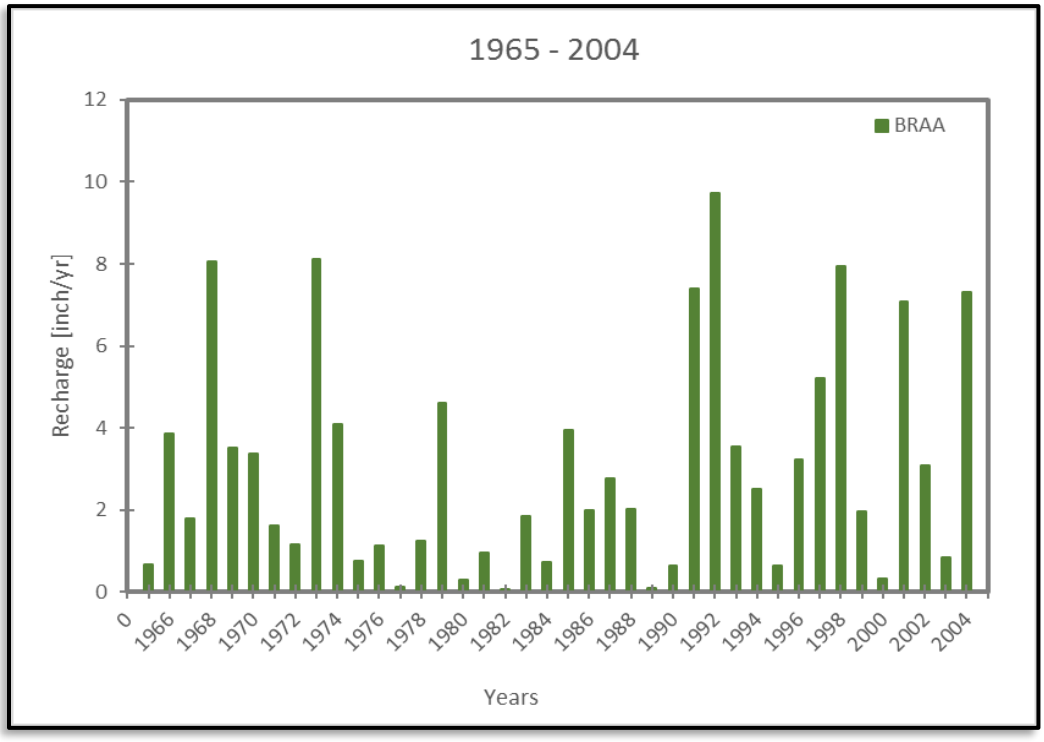

Figure 17: Annual recharge rates

Table 13: Severe weather conditions from 1965 to 2004.

Year	Severe Weather Conditions
1965	Dust storms in January and February La Nina event caused less rainfall in the area.
1966	Flash flooding in Dallas County.
1967	No important or severe events reported in the area.
1968	Tropical Storm Candy caused heavy flooding, crop damage, and tornadoes over the Southeast area in July. Moderate El Nino event over south Texas.
1969	No important or severe events reported.
1970	Tropical Storm Felice affected South east area of Texas in September. It caused rainfall of 6 inches and heavy flooding.
1971	No important or severe events reported in the area.
1972	No important or severe events reported in the area.
1973	Rainstorm over Southeastern Texas in June. From 10 to 15 inches of rain recorded.
1974	Flash flooding in South Central Texas in November.
1975	Low rainstorms in Austin and Waller County caused by La Nina event.
1976	Rainstorm in Harris County. Rains in excess of 13 inches.
1977	Hurricane Anita made medium rainfall throughout the South East portion of Texas in September.
1978	No important or severe events reported in the area.
1979	Tropical Storm Claudette produced a 24-hour rainfall record of 43 inches in July.
1980	Harris County reported 32 days with high temperatures at or exceeding 100° F. High record of 107 degrees on August 23 in Harris County. Brazos County reported 43 days with high temperatures exceeding 100° F.
1981	Severe flooding in Austin County in May
1982	No important or severe events reported in the area.
1983	Hurricane Alicia produced 23 tornadoes and several storms.
1984	Remnants of Tropical Storm Edward causes several flooding in South Texas, where some counties receive totals in excess of 20 inches in September.
1985	A record-breaking snowstorm struck in South Central Texas with up to 15 inches of snow that fell at several locations.
1986	Hurricane Bonnie makes landfall in Southeast Texas as a Category 1 hurricane affecting Galveston, Harris, and Waller counties. Rainfall peaks at 13 inches in June.
1987	No important or severe events reported in the area.
1988	Tropical Storm Beryl produced heavy rainfall over Southeast Texas (rainfall peaks of 4.25 inches) in August. Tropical Depression Ten produced heavy rain over Southeast Texas peaking at 8.16 inches in September.

Table 13: Continued.

Year	Severe Weather Conditions
1989	December was the second coldest month in history for Harris and Brazos County. It was the coldest month in history for Galveston County. Harris, Waller, Grimes and Brazos County recorded coldest temperatures in December (La Nina event)
1990	No important or severe events reported in the area.
1991	Tropical Depression Two caused isolated rainfall over South Texas, with a maximum total of 3 inches in July. Precipitation from November to January was considered wet (20 to 30 inches per month) due to ENSO event this year.
1992	A line of thunderstorms produced 18 tornados across all the counties in Southeast Texas in November. Precipitation in January was considered wet (20 to 30 inches per month) due to ENSO event this year.
1993	Hurricane Lidia moves into South Texas. Lidia's remnant caused moderate rainfall across this area in September.
1994	Heavy Rain produced widespread flooding over much the Southeast Region for almost a week in October. Many rivers reached record flood levels. ENSO effects caused precipitations of 25 inches in average in this area.
1995	Tropical Storm Gabrielle made landfall in South East Texas as a tropical Storm in August. It produced rainfall with peaks of 6.26 inches along the area.
1996	No important or severe events reported in the area.
1997	Moderate El Nino event caused moderate rainfall of 10 – 15 in.
1998	Tropical Storm Charley brought torrential rains and flash floods to the Hill County in August. Rainstorm in October in Hill County. A massive and devasting flood set all-records for rainfall and river levels.
1999	Golf-ball and softball-sized hail fell in Brazos County.
2000	Excessive heat resulted from high-pressure ridge over the summer, especially in July. College Station had 12 consecutive days of 100° F or greater (caused by La Nina event in the area).
2001	Tropical storm Allison hit Harris County area, which dumped large amounts of rain on the city in June. Rainstorms in South Central Texas caused flash flooding and some weak tornadoes in November.
2002	Rainstorm in South Central Texas. It was reported more than 30 inches of rain in June and July. Rainstorms in South Texas. Several thunderstorms produced heavy rain, causing flooding and small tornadoes.
2003	Flooding in South Texas during September in Galveston, Harris, and Fort Bend County.
2004	Hurricanes Javier and Ivan generated a tropical storm along South East Texas and Louisiana in September and October with over 7 inches of rain.

Year	Severe Weather Conditions
1968	Tropical Storm Candy caused heavy flooding, crop damage, and tornadoes over the Southeast area in July.
1973	Rainstorm over Southeastern Texas in June. From 10 to 15 inches of rain recorded.
1979	Tropical Storm Claudette produced a 24-hour rainfall record of 43 inches in July.
1991	Tropical Depression Two caused isolated rainfall over South Texas, with a maximum total of 3 inches in July.
1992	A line of thunderstorms produced 18 tornados across all the counties in Southeast Texas in November.
1997	No important or severe events reported in the area.
1998	Tropical Storm Charley brought torrential rains and flash floods to the Hill County in August. Rainstorm in October in Hill County. A massive and devasting flood set all-records for rainfall and river levels.
2001	Tropical storm Allison hit Harris County area, which dumped large amounts of rain on the city in June. Rainstorms in South Central Texas caused flash flooding and some weak tornadoes in November.
2004	Hurricanes Javier and Ivan generated a tropical storm along South East Texas and Louisiana in September and October with over 7 inches of rain.

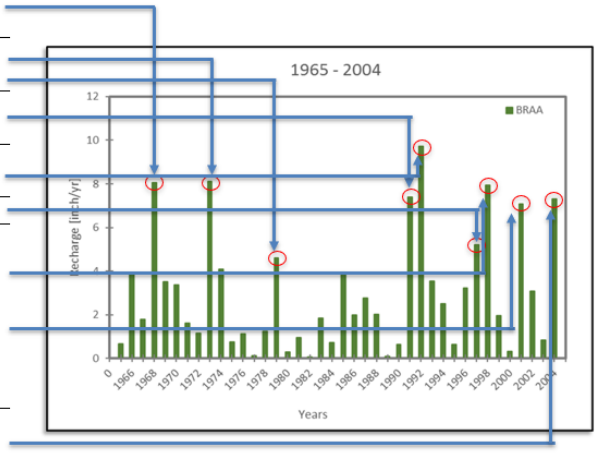

Figure 18: Extreme weather conditions

Annually recharge rates distribution over the BRAA from 1965 to 2004 are illustrated in Figure 14. We can see the grid cells used in this model simulation (0.01 x 0.01 degrees) and the corresponding recharge rates values for each one. Standard deviation is about 1.74 inches per year which implies there is low variability along this time period for each grid cell.

The average value for recharge rates is 3.01 inches/year (about 0.07 m/year) and represents roughly 169,690-acre feet per year over the entire aquifer. USGS suggests that recharge rates for this area are between 2 and 5 inches per year depending on the method used to obtained these results (Table 3). Overall, recharge rates obtained using CLM4.5 is in the suggested range. However, there are differences between the recharge rates obtained using CLM4.5 and the methods used in the GAM and in the previous studies (Table 14). CLM4.5 has the lowest difference with the Flow between flow lines method (about 14%) and the highest difference with the mass chloride and baseflow methods (from 69 to 89%). Since both digital baseflow separation and chloride mass balance were estimated over just one station gauge near either Bryan or Hempstead and CLM4.5 estimated recharge rates over the whole BRAA, difference between recharge rates from these

methods are the highest. Base flow separation estimated recharge rates using 20 station gauges over the BRAA and that is why difference between recharge rates using both methods were lower.

Table 14: Comparison between CLM4.5 and previous studies in the area.

	CLM4.5 (in/year)	**Alternative method (in/year)**	**% Difference**	**Comments**
CLM4.5 vs Flow between flow lines	3.01	3.5	14.0	Alternative method was used over the whole BRAA for a 15 years' time period.
CLM4.5 vs digital baseflow separation	3.01	0.74	75.40	Alternative model was used just in two-gauge stations near Bryan for a 10-years' time period.
CLM4.5 vs digital baseflow separation	3.01	0.95	68.9	Alternative model was used just in two-gauge stations near Hempstead for a 10-years' time period.
CLM4.5 vs Chloride mass balance	3.01	0.33	89.0	Alternative model was used over just one-gauge station near Hempstead for a 55-years' time period.
CLM4.5 vs MODFLOW (GAM)	3.01	4.83	37.6	Alternative method was used over the whole BRAA for a 65 years' time period.

In addition, there are differences between the GAM reported values and the rates obtained using CLM4.5 (0.019 m/year versus 0.07 m/year, about 60% of difference). An analysis for mainly characteristics of both methods can reveal more about discrepancy between these annual rates. CLM4.5 estimated recharge rates using a non-standard resolution of 0.01 x 0.01 degrees (1.1 km x 1.1 km in average); however. MODFLOW estimated recharge rates based on a smaller grid cell which range from 0.2 to 1.6 km in average which produced more accurate results. Furthermore, another source of discrepancy is the time period both models simulated. CLM4.5 simulated a time period of 40 years from 1965 to 2004 and MODFLOW simulated a time period of 63 years from

1950 to 2012. Diverse severe weather conditions contributed to get a different average recharge rate such some hurricanes (i.e. Audrey in 1957), torrential rains, and drought seasons (especially in 1956 and 2011). Another major source of discrepancy is that aquifer was recharged not only by precipitation, irrigation, or river interaction but also by cross-formational flow in the MODFLOW simulation; however, this last factor was not taken account in the CLM4.5 simulation.

A more detailed comparison using the time period suggested in the previous studies and just over the region they tested recharge rates (Bryan/CS, and Hempstead, and the whole BRAA) was developed (Table 15). Recharge rates obtained using these models were spatially and historically averaged. Since datasets for the time period of the first alternative model was not available in CLM4.5, a comparison with the others models was developed. The difference between values of recharge rates obtained by those alternative values and CLM4.5 decreased about 5 or 6%. Using this detailed approach of comparison, the main source of discrepancy is the model used to test the area and the way data was collected. As it was stated before, previous studies except for the GAM report collected information from the area based on one- or two-gauge stations near the areas of Bryan and Hempstead. However, when CLM4.5 was applied, information collected from the area was for the whole area tested and not just for one or two sites in order to be more accurate.

Table 15: More detailed comparison between CLM4.5 and previous studies in the area.

	Time period	CLM4.5 (in/year)	Alternative method (in/year)	% Difference	Comments
CLM4.5 vs Flow between flow lines	1957 – 1961	N/A	3.5	N/A	Cannot make a fairly comparison because we do not have data for this period time.
CLM4.5 vs digital baseflow separation	1994 – 2004	2.64	0.74	72.00	Alternative model was used just in two-gauge stations near Bryan for a 10-years' time period. CLM4.5 estimated recharge rates for the same time period in the Bryan/CS area.
CLM4.5 vs digital baseflow separation	1965 – 1998	2.33	0.95	59.22	Alternative model was used just in two-gauge stations near Hempstead for a 10-years' time period. CLM4.5 estimated recharge rates for the same time period in the Hempstead area.
CLM4.5 vs Chloride mass balance	1965 – 1998	2.33	0.33	85.84	Alternative model was used over just one-gauge station near Hempstead for a 55-years' time period. For this comparison, CLM4.5 estimated recharge rates for a time period of 34 years in the Hempstead area.
CLM4.5 vs MODFLOW (GAM)	1965 – 2004	3.01	4.83	37.6	Alternative method was used over the whole BRAA for a 65 years' time period.

Additionally, since recharge rates mainly depends on precipitation rates, location, and topography, a comparison between recharge a precipitation rates were developed. Annual averaged recharge rates over the BRAA represents a low percentage of the total precipitation rates in this area roughly. This percentage ranges from 0.20 to 21.00 % (Figure 19a) and the average for this

time period is 7.20%. These values lie over the range suggested by the USGS (10 to 20 %). Moreover, precipitation is strong correlated to recharge rates. R2 is almost 0.80 in the scatter plot generated with result obtained (Figure 19b).

(a) Annual precipitation and recharge rates

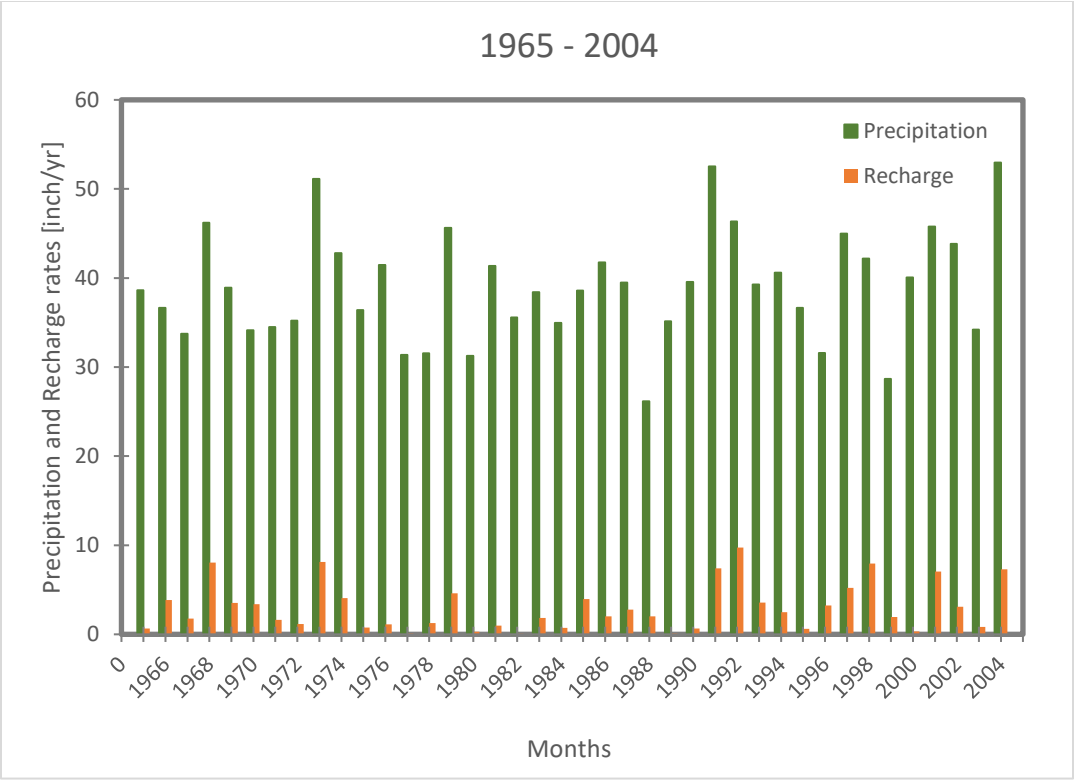

Figure 19: Precipitation and recharge rates

(b) Precipitation vs Recharge rates

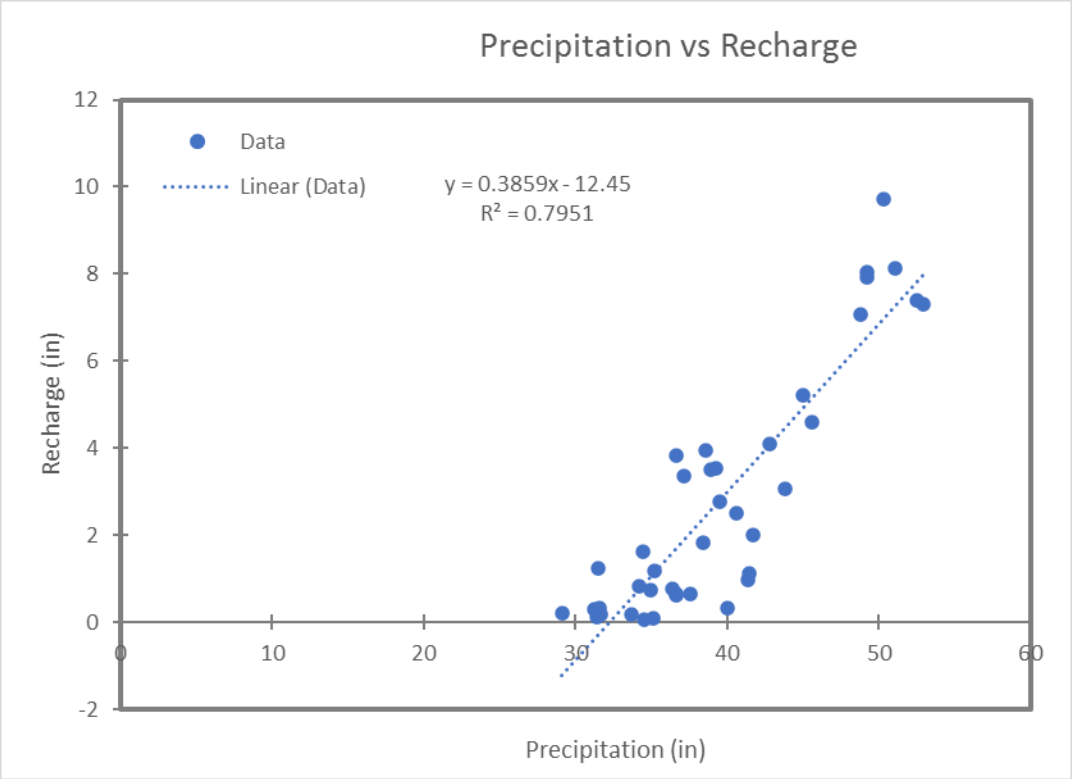

Figure 19: Continued

Recharge rates are higher in the south BRAA than in the northern east portion of this aquifer (about 21% in average). The effects of location and topography clearly influenced range of recharge rates in the northern and southern portion of the BRAA (Figure 20). Northern portion of the BRAA has stepper slopes and, as a consequence, tend to have enhanced runoff and are less likely to be an area where recharge rates are higher comparing it to the southern portion of the BRAA. Slopes over the northern portion of the BRAA are clearly higher (> 5%) than the southern portion (TWDB, 2012). This trend is not only noticeable in an annual recharge rates analysis but also it is noticeable historically. In 1982 was reported the lowest recharge rate over the time period simulation.

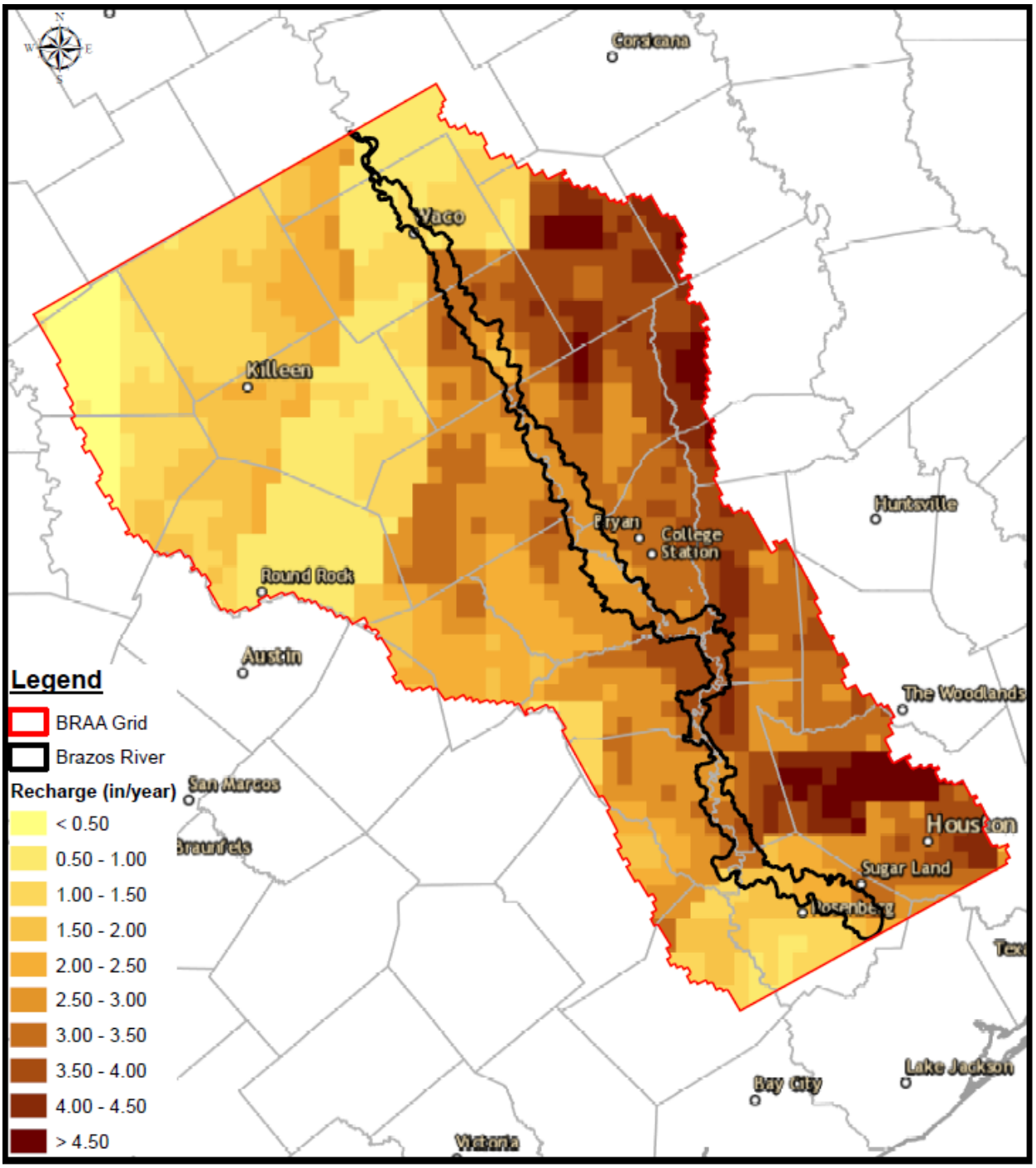

Figure 20: Average recharge rates in the BRAA

Northern portion of the BRAA registered rates of less than 1 inches per year with included a vast area of rates of less than 0.5 inches per year especially in the north west of the BRAA (Figure

21). The average annual recharge rate for the northern portion of the BRAA is 0.10 inches per year and for the southern portion of the BRAA is 0.40 inches per year.

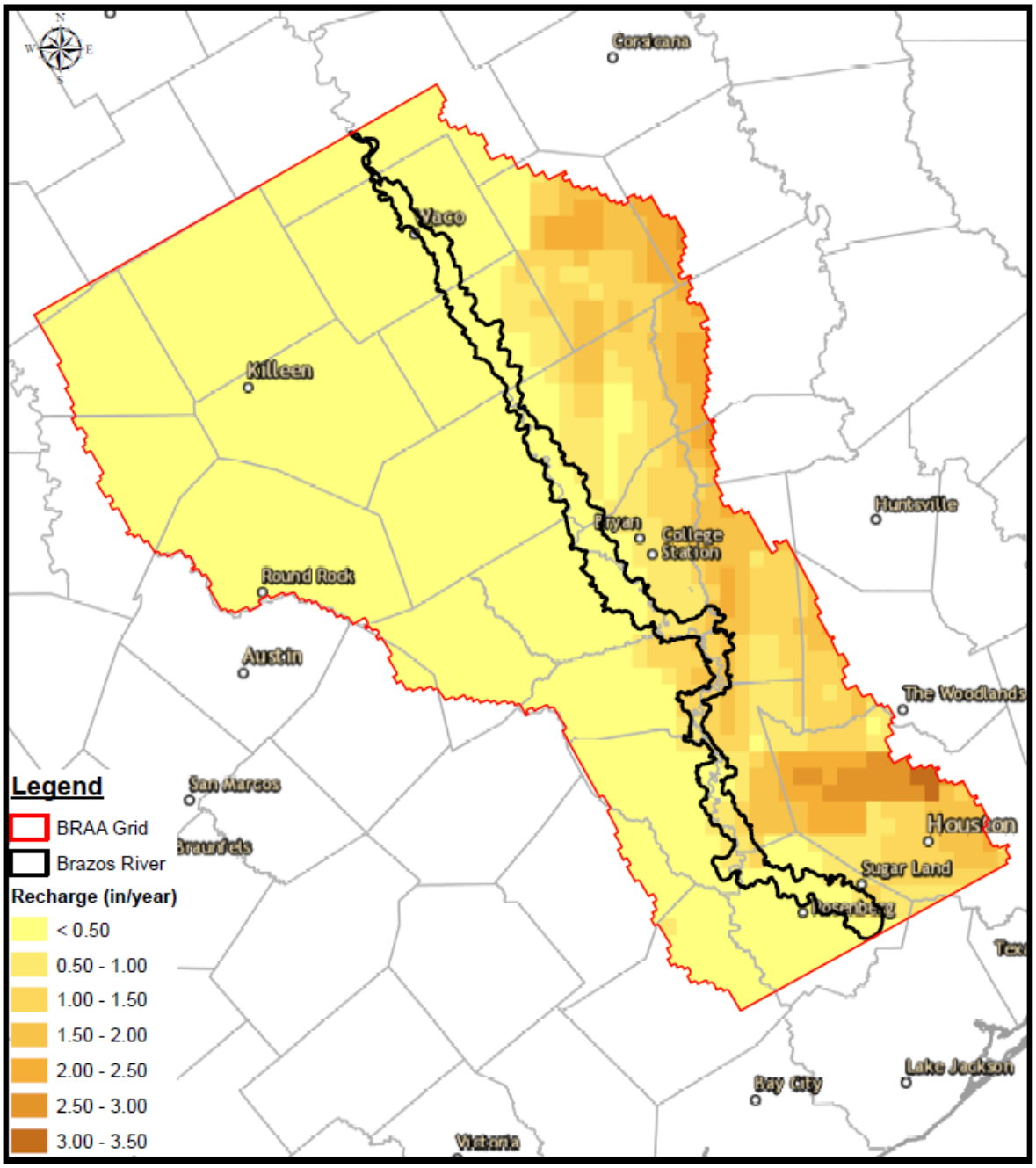

Figure 21: Average recharge rates in the BRAA in 1982

On the contrary, in 1992 was reported the highest recharge rates over the time period simulation with a mean rate of 9.60 inches per year (Figure 22). Northern portion of the BRAA registered rates of less than 7.00 inches per year while the southern portion of the BRAA registered rates of 9.85 inches per year in average.

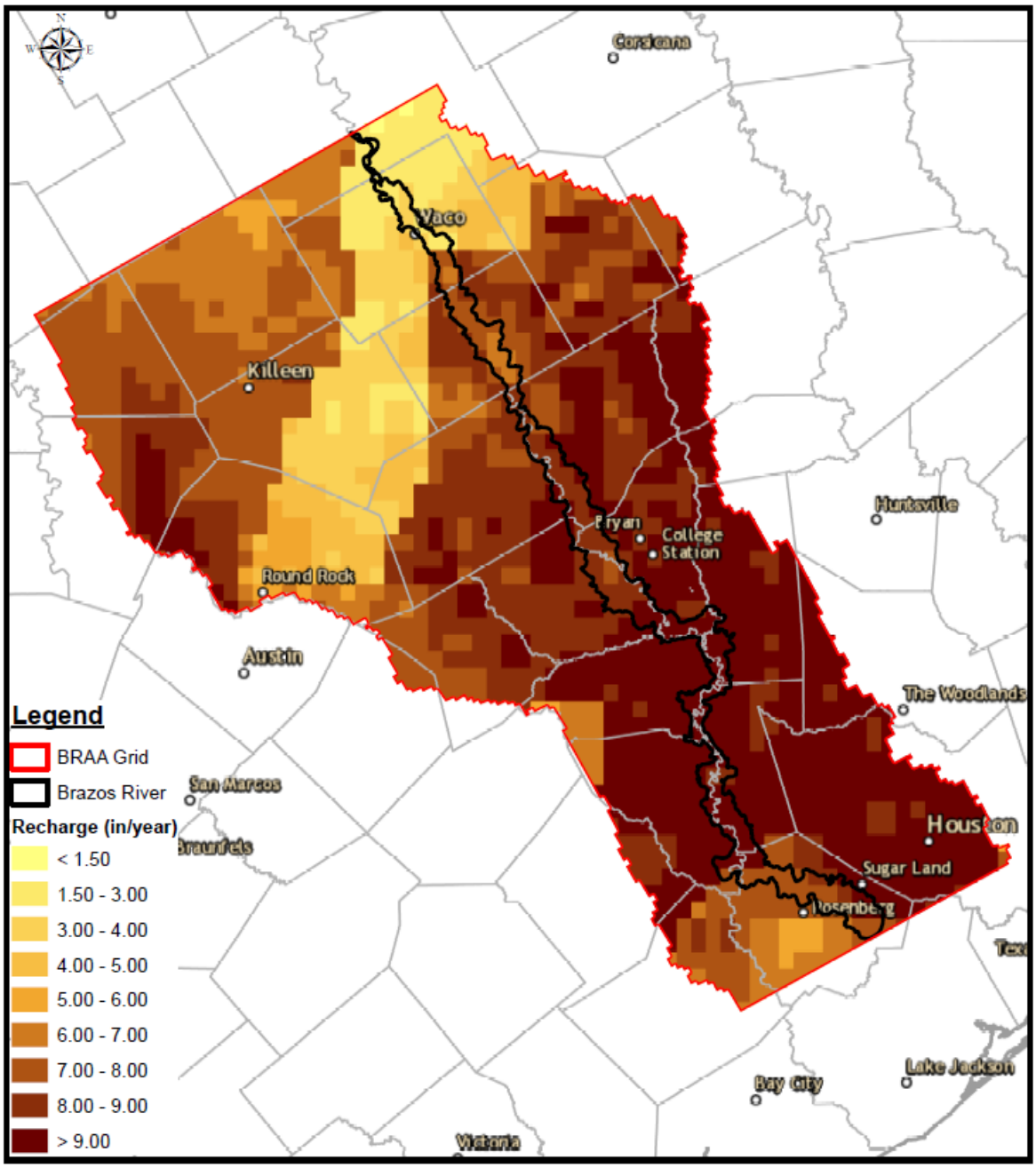

Figure 22: Average recharge rates in the BRAA in 1992

In 1979 the annual recharge rate was 4.61 inches per year (higher than the average annual recharge rate fort the time period simulation). Northern portion was clearly the region with lower recharge rates (Figure 23). Several portions of this regions reported less than 1.0 or even 0.5 inches per year while in the southern portion of the BRAA the average rate was 5.9 inches per year.

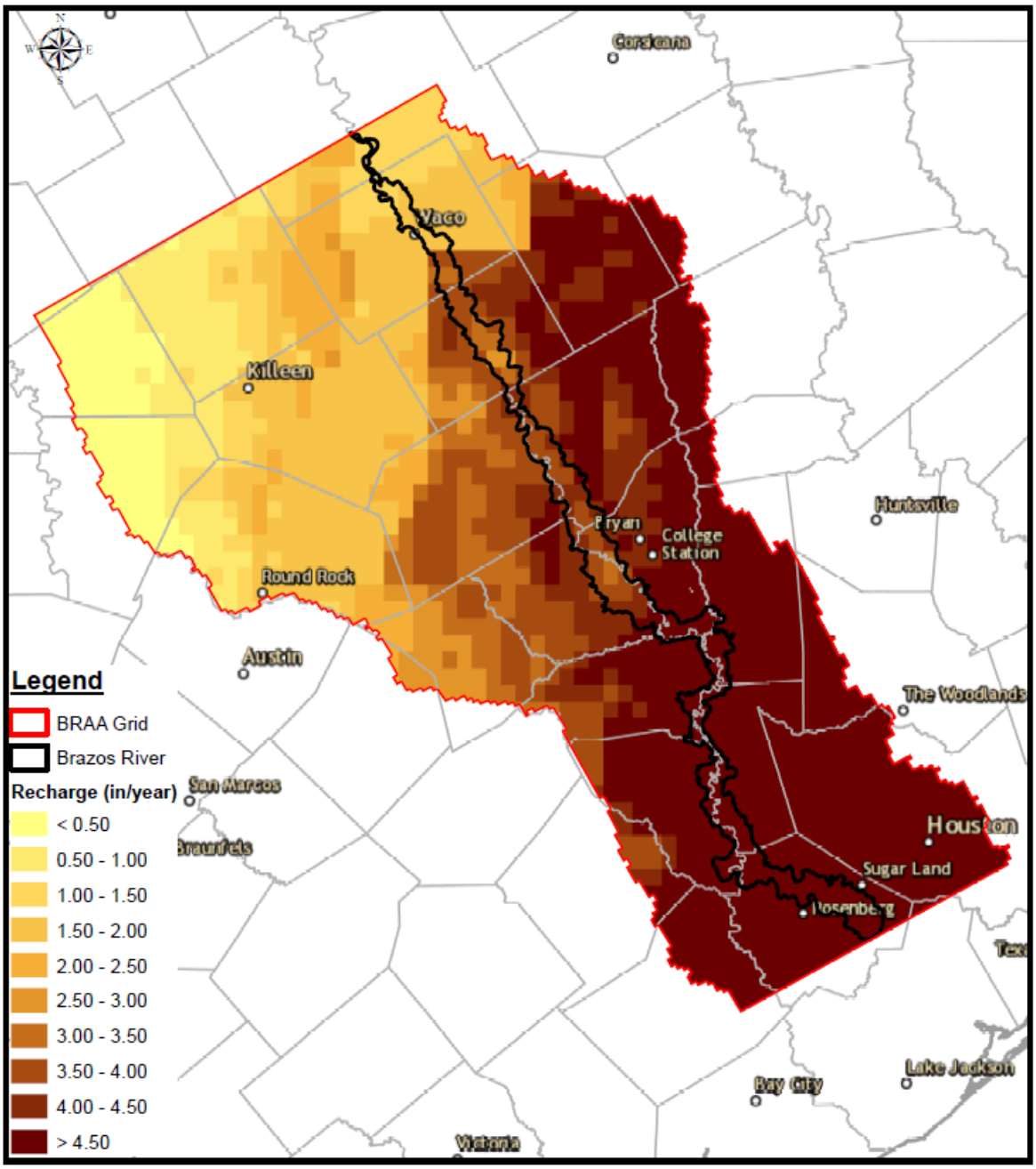

Figure 23: Average recharge rates in the BRAA in 1979

These results indicated that location and topography are factors that affect recharge rates in this area. However, it is also clear that a finer resolution with detailed and updated information of topography could better represents the BRAA since it is a small region. Some alternatives would be to create a finer resolution with more computational resources or make a study in several sites (as the previous studies from Cronin and Wilson and Chowdhury) using a point scale resolution available in CLM4.5 or CLM5.0.

Recharge rates were spatially and historically higher in the southern portion of the BRAA than in the northern portion. According our previous classification of soil type within the BRAA, there are a mixture of soils (Figure 2); however. the upper portion of the Brazos River Alluvium Aquifer has relatively higher clay content than the lower portion, which has relatively higher sand and gravel content (Appendix C). Since sandy soils typically accept more infiltration for a given precipitation event than clayey soils and clay soils tend to retain water, allowing more time for evapotranspiration by vegetation ($K_{clay} < K_{sand}$), it is clear that clay soils which are present in more areas in the northern portion of the BRAA allowed more evapotranspiration and less infiltration, which generated less recharge over this region. On the contrary, higher recharge rates were founded in the southern portion because there is another type of soil in this region with a higher hydraulic conductivity which allows higher infiltration rates and, as a consequence, higher recharge rates as well.

Since the grid cells used in this simulation were small squares of approximately 0.01 x 0.01 degrees without any rotation or translation as GAM report developed in their model using MODFLOW, maps generated from the outputs obtained present some linear shapes, An optimal solution would be to create a finer resolution and rotate it to follow the direction of the river and the aquifer as the GAM report did.

Overall results show that simulating groundwater in CLM4.5 is limited in a regional scale without more work on 1) a high computational resources needed to run the code even for a regional case with a fine resolution especially for the time requested to spin up the simulation; 2) a better understanding of groundwater dynamics such as the impact of soil depth and aquifer depth and lateral connectivity between the grid cells; and 3) quantifying the effects of soil water, surface runoff, and baseflow recharge separately on groundwater. These limitations and some bugs that CLM4.5 presents could be solved using the newest version of this LSM: CLM5.0.

Finally, climate change could potentially be an important factor affecting recharge rates in this region. Since CLM4.5 is a Land Surface Model, it would be useful for future works to develop a simulation over the BRAA using the carbon-nitrogen cycle component in order to obtain accurate results. Since rainfall and surface runoff play important roles in the cycling of some elements such as carbon and nitrogen, it would be interesting to see in a future work how this interconnection influence in the estimation of recharge rates and other parameters.

The reliability of an assessment depends on the validity of the approach for the particular application and the quality and currency of the data used. Thus, even if the modeling technique selected is valid, the use of poor-quality input data could introduce uncertainty into the results of the assessment. Uncertainties resulting from input data quality problems can be reduced by ensuring that the variability in the attributes over the area is accurately reflected in the interpolated values of the spatial and nonspatial attributes.

SSURGO database was gathered by walking over the land and observing and testing the soil. Soil samples were analyzed in laboratories. Maps generated from this in situ information describes properties of soil and other components. The information was collected at scales ranging from 1:12,000 (1,000 ft per in) to 1:63,360 (0.189 ft per in). STATSGO database was created by

generalizing more detailed soil survey maps. Data on geology, topography, vegetation, and climate were assembled and related to Land Remote Sensing Satellite (LANDSAT) images. This dataset basically consists of georeferenced, vector, and tabular data. The map data were collected in 1- by 2- degree topographic quadrangle units and merged into a seamless national dataset. Since resolution used in CLM4.5 was 0.01 x 0.01 degrees, datasets provided by SSURGO and STASTGO introduced uncertainty into results. A finer resolution in both datasets would generate more accurate results (i.e. recharge, precipitation, and infiltration rates).

Because of a lack of observations, historical simulations of land surface conditions using land surface models are needed for studying variability and changes in the continental water cycle and for providing initial conditions for seasonal climate predictions. Atmospheric forcing datasets are also needed for land surface model development. The quality of atmospheric forcing data greatly affects the ability of land surface models to realistically simulate land surface conditions. For this model simulation, Quian et al. was the dataset selected. It includes global forcing dataset for 1948 to 2004 with 3-hourly and 1.875-degree resolution for precipitation, radiative fluxes, and temperature. An error associated to the parametrization and interpolation of input datasets to the resolution selected in CLM4.5.

Theoretically, hydrology calculations should be calculated explicitly from a discrete cumulative distribution function (CDF) at each grid cell at the resolution the model was running such as 0.01 x 0.01 degrees for this particular case (Oleson, 2013). Unfortunately, because this is a computationally intensive and time-consuming task even for regional applications in CLM4.5, results are calculated at 0.125° resolution using HYDRO1K dataset from USGS following the algorithm in Niu et al which is more than 12 times higher than the desired resolution. Some grid cells with topographic indices exceeding the 95-percentile threshold at this resolution are excluded

from the calculation to eliminate biased estimation of statistics because of large CTI values at pixels on stream networks (Oleson, 2013). As a consequence, an error associated with this parametrization was expected and, therefore, results obtained were not 100% accurate.

Finally, since the grid cells used in this simulation were small squares of approximately 0.01 x 0.01 degrees without any rotation or translation as GAM report developed in their model using MODFLOW, maps generated from the outputs obtained present some linear shapes, An optimal solution would be to create a finer resolution and rotate it to follow the direction of the river and the aquifer as the GAM report did.

4. CONCLUSIONS

This thesis documents the application of a coupled land surface model in the Brazos River Alluvium Aquifer (BRAA) for a time period of 40 years (from 1965 to 2004).

CLM4.5 is a coupled and integrated land surface model that also incorporates hydrological, urban, carbon, and vegetation processes. For this simulation period, we used a 0.01 x 0.01-degree resolution (grid cell); however, for future research projects it would be better to refine this resolution to obtained more accurate results and, consequently, have a more precise comparison between these recharge rates using MODFLOW (GAM) and CLM4.5. Moreover, it would take more computation time to do this new simulation and most likely higher performance computing resources (such as disk storage and permissions).

Comparison to the GAM may provide insight to water resources planners. The purpose of using an alternative code (for this particular case, a land surface model) was to try to replicate each part of the water cycle at several levels (i.e. land, groundwater, atmospheric, vegetation) instead of relying on long-terms estimates for baseflow or recharge and, ultimately, compare final results to determine if a land surface model such as CLM4.5 could be used in the future for developing state and regional water plans. It is clear that more studies in a regional scale should be done to scientifically accept this code; however, this research work shows that results are reliable since recharge rates lies in the range suggested by the USGS.

The obtained datasets from the Community Land Model 4.5 (CLM4.5) yielded the expected average recharge rates suggested by the USGS which ranges between 2 and 5 inches per year supporting the hypothesis that a Land Surface Model (LSM) could be applied in a regional scale in order to acquire hydraulic parameters such as recharge, infiltration, or even runoff rates if

needed. Even though some grid cells reported more recharge rates more than 5 inches per year depending on any weather conditions happened in that time, the historically average value lies on the suggested range. The main differences between results reported in the Brazos River Alluvium Aquifer's GAM and the results obtained using CLM4.5 were mainly grid cell size, time period simulation, and code approach (groundwater vs land).

Recharge rates mainly depends on precipitation rates, location, and topography. The effect of precipitation clearly affects recharge rates and the location where we can find the highest rates. Annual precipitation in the southern portion of the BRAA is in average 49 inches per year and in the northern portion is 40 inches per year. The simulated recharge rates tended to be higher in the southern portion of the BRAA than in the northern portion. Additionally, topography and location have a strong relationship to recharge rates. Slopes over the northern portion of the BRAA are clearly higher (> 5%) than the southern portion, therefore, this area is less likely to has higher recharge rates. It was clear that southern portion of the BRAA had higher recharge rates than the northern portion in average and this trend was registered not only spatially but also historically over the whole simulated time period.

Furthermore, for future research projects, it would be ideal if time period simulation was the same for both codes. In GAM report, they simulated the time period from 1950 to 2012 (62 years) and for the present research carried on in CLM4.5 it was simulated a time period of 40 years from 1965 to 2004 (using QUIAN et al datasets for precipitation, atmospheric forcing, and solar fluxes data). There are a couple of ways to solve this model limitation. The first one, is using a different component set (COMPSET) in CLM4.5. Any of the compset including CRUNCEP Atmospheric Forcing Data could solve this limitation since it includes historical data from 1901 to 2010. However, choosing some of these component sets would have a cost: any of those ones

does not include the Satellite Phenology component. The second solution would be using the new version of the code: CLM5.0, which includes atmospheric forcing data from 1948 to 2016. Additionally, in order to observe how climate change affects recharge rates, CLM4.5 or CLM5.0 would be run using a carbon-cycle component to obtain accurate results as well over this aquifer. Since climate change influences weather conditions, recharge rates would be different from the results we obtained using CLM4.5 without the carbon-nitrogen cycle component.

Several parameters in addition of recharge rates for the BRAA have been simulated in this research project. Solar fluxes such as Latent Heat, Ground Flux, Infrared Radiation, Atmospheric Radiation, Sensible Heat, and Solar Radiation on either a monthly or daily basis were simulated. Net Radiation equation have been applied to make a plot for this aquifer. Since there is not available information of significant previous studies about these parameters over the Brazos River Alluvium Aquifer, result obtained using CLM4.5 were contrasted to NASA datasets. Solar fluxes lie on the range provided by NASA information on these parameters. In addition, we simulated hydrologic fluxes such as infiltration, interception, evaporation, and evapotranspiration (ET). After analyzing all these parameters over northern, southern, and the whole BRAA, we concluded that there is enough evidence that all of these fluxes are higher in the southern portion of the Brazos River Alluvium Aquifer than in the northern portion of it as we stated in the recharge objectives section. and secondly, due to more severe weather exposition which increase precipitation rates in this area. Variability for each grid cell over the 40 years of simulation is not high as expected.

In order to obtain a more accurate perspective of how CLM4.5 performs and if this code is useful to reach recharge rates over an entire aquifer in a regional scale, future researchers can use this code to the rest of aquifers in Texas, starting for the minor ones and later extend the study to the major aquifers in Texas. If recharge rates obtained using CLM4.5 match or have some

similitude with the ones reported in the GAMs, therefore, we can conclude that using a land surface model in a regional scale would be implemented and developed in a future GAM update as an alternative tool. Moreover, comparison between computational time and resources need to run the simulation should be performed to determine which code is better. This way atmospheric, land, vegetation, hydrologic properties, and crop data would be the same for all the models and up to date.

CITED LITERATURE

Abromopoulos, F. et al (1988). Improved ground hydrology calculation for global climate models (GCMs): Soil water movement and evaporation. *Journal of Climate*, 1, 921-941.

Ajami, H., McCabe, M. F., and Evans, J. P. (2015). Impacts of model initialization on an integrated surface water-groundwater model. *Hydrological Processes*, 29(17), 3790-3801

Alexeev, V. (2007): An evaluation of deep soil configurations in the CLM3 for improved representation of permafrost. *Geophysics Resources Letter*, *34* (9) https://doi.org/10.1029/2007GL029536

Allison, G., & Hughes, M. (1978). The use of environmental chloride and tritium to estimate total recharge to an unconfined aquifer. *Division of Soils, CSIRO*, 16(2), 181-195. https://doi.org/10.1071/SR9780181

Ashworth, J. & Hopkins, J. (1995). *Aquifers of Texas*. Texas Water Development Board.

Bartsch, S. et al (2014). River – aquifer exchange fluxes under monsoonal climate conditions. *Journal of Hydrology*, 509(1), 601-614. https://doi.org/10.1016/j.jhydrol.2013.12.005

Bonan, G. et al (2002): The land surface climatology of the community land model coupled to the NCAR community climate model. *National Center for Atmospheric Research Journal*, 15 (22), 3123-3149. https://doi.org/10.1175/1520-0442(2002)015%3C3123:TLSCOT%3E2.0.CO;2

Brook, R., and Corey, A. (1964). Hydraulic Properties of Porous Media. *Colorado State University.*

Bruun, B., Jackson, K., & Lake, P. (2017). *2017 State Water Plan*. Texas Water Development Board

Chakka, K. B., and Munster, C. L. (1996). Simulation of groundwater-surface water interaction on the lower reach of the Brazos River., *Universities Council on Water Resources 1996, Integrated Management of Surface and Ground Water*. Carbondale, 213-228.

Chowdhury, A. H., Osting, T., Furnans, J., and Mathews, R. (2010). "Groundwater surface water interaction in the Brazos River Basin: evidence from lake connection history and chemical and isotopic compositions." *Texas Water Development Report 375, Texas Water Development Board.*

Cronin, J. and Wilson, C. (1963). "Ground water in the floodplain alluvium of the Brazos River, Whitney Dam to vicinity of Richmond, Texas." *Texas Water Development Board Report 41*, 206.

Dassi, L. (2010). Use of chloride mass balance and tritium data for estimation of groundwater recharge and renewal rate in an unconfined aquifer from North Africa: a case study from Tunisia. *Environmental Earth Sciences, 60*(4), 861-871. doi:10.1007/s12665-009-0223-1

Ewing, J. E., Harding, J. J., & Jones, T. L. (2006). Final Conceptual Model Report for the Brazos River Alluvium Aquifer Groundwater Availability Model. *Texas Water Development Board*.

Ewing, J. E., & Jigmond, M. (2016). Final Numerical Model Report for the Brazos River Alluvium Aquifer Groundwater Availability Model. *Texas Water Development Board*.

Famiglietti, J. and Wood, F. (1991). Evapotranspiration and runoff from large land areas: Land surface hydrology for atmospheric general circulation models. *Surveys in Geophysics*, 12, 179-204. https://doi.org/10.1007/BF01903418

Fleckenstein, J. H., Niswonger, R. G., and Fogg, G. E. (2006). River-aquifer interactions, geologic heterogeneity, and low-flow management. *Groundwater*, 44(6), 837-852.

Furnans, J. et al (2017). Final Report: Identification of the vulnerability of the major and minor aquifers of Texas to subsidence with regard to groundwater pumping. *Texas Water Development Board.*

Harlan, S. (1990). Hydrogeologic assessment of the Brazos River alluvial aquifer from Waco to Marlin. Waco, TX: *Baylor University.*

Kumar, C. P. (2012). Climate Change and Its Impact on Groundwater Resources. *International Journal of Engineering and Science, 1*(5), 43-60.

Lawrence, D. & Slater, G. (2008). Incorporating organic soil into a global climate model. *Climate Dynamic Journal, 30*, 145-160. https://doi.org/10.1007/s00382-007-0278-1

Lawrence, D. et al (2011): Parametrization improvements and functional and structural advances in version 4 of the community land model. *Journal of Advances in Modeling Earth Systems, 3* (1). https://doi.org/10.1029/2011MS00045

Lee, T. & Pielke, R. (1992). Estimating the soil surface specific humidity. *Journal of Applicated Meteorology*, *31* (5): 480-484. https://doi.org/10.1175/1520-0450(1992)031%3C0480:ETSSSH%3E2.0.CO;2

Lombardozzi, D., et al (2016). CLM4.5 tutorial: Running CLM. *National Center of Atmospheric Research.*

Maples, S., Fogg, G., & Maxwell, R. (2019). Modeling managed aquifer recharge processes in a highly heterogenous, semi-unconfined aquifer system. *Hydrogeology Journal, 27*: 2869-2888. https://doi.org/10.1007/s10040-019-02033-9

MATLAB. (2016). MATLAB (Version R2016a). Natick, Massachusetts: The MathWorks Inc.

Maxwell, R. & Miller, N. (2005). Development of a coupled land surface and groundwater model. *Journal of Hydrometeorology, 6* (3), 233-247. https://doi.org/10.1175/JHM422.1

Meyboom, P. (1966). Unsteady groundwater flow near a willow ring in hummocky moraine. *Journal of Hydrology*, 4, 38-62. https://doi.org/10.1016/0022-1694(66)90066-7

Miall, A. (1996). The geology of fluvial deposits: sedimentary facies, basin analysis, and petroleum geology. *Springer, Berlin*; New York.

Mohan, C., Western, A. W., Wei, Y., & Saft, M. (2018). Predicting groundwater recharge for varying land cover and climate conditions – a global meta-study. *Hydrol. Earth Syst. Sci., 22*(5), 2689-2703. doi:10.5194/hess-22-2689-2018

National Aeronautics and Space Administration – NASA (2018). Land Surface Modeling: A mini workshop. *Goddard Institute for Space Studies.*

Natural Resources Conservation Service (2017). Web Soil Survey. *United States Department of Agriculture, USDA*

Nicolsky, D. et al (2007). Improved modeling of permafrost dynamics in a GCM land-surface scheme. *Geophysics Resources Letter, 34* (8). https://doi.org/10.1029/2007GL029525

Niraula, R. et al (2016). Comparing potential recharge estimates from three land Surface Models across the Western US. *Journal of Hydrology*, 1, 410-423. https://dx.doi.org/10.1016%2Fj.jhydrol.2016.12.028

Niu, G. & Yang, Z. (2005). A simple TOPMODEL-based runoff parametrization (SIMTOP) for use in global climate models. *Journal of Geophysics Resources*, 110 (D21). https://doi.org/10.1029/2005JD006111

Oleson, K. et al, 2013: Technical description of the community land model (CLM). *N*ational Center of Atmospheric Research.

Paniconi, C. and Putti, M. (2015). Physically based modeling in catchment hydrology at 50: Survey and outlook. *Water Resources Research*, 51, 7090-7129. https://doi.org/10.1002/2015WR017780

Peter, G. et al (2011). *Aquifers of Texas*. Texas Water Development Board.

Russell, G. and Miller, J. (1994). Continental-scale river flow in climate models. *Journal of Climate*, 7, 914-928. https://doi.org/10.1175/1520-0442(1994)007%3C0914:CSRFIC%3E2.0.CO;2

Sellers, P. et al (1996). A revised land surface parametrization (SiB2) for atmospheric GCMs. Part I: Model formulation. *Journal of Climate*, 9, 676-705. https://doi.org/10.1175/1520-0442(1996)009%3C0676:ARLSPF%3E2.0.CO;2

Shah, S., Houston, N., and Braun, C. (2007). Hydrogeologic Characterization of the Brazos River Alluvium Aquifer, Bosque County to Fort Bend County, Texas. *US Geological Service (USGS). https://doi.org/10.3133/sim2989*

Stockli, R. et al (2008) Use of Fluxnet in the community land model development. *Journal of Geophysics Resources, 113* (G1). *https://doi.org/10.1029/2007JG000562*

Tayyab, Mehmood (2018). Numerical Modeling of Water Flux Interactions Between the Brazos River Alluvium Aquifer and the Brazos River: Testing of Alternative Conceptual Models. College Station, TX: *Texas A&M University*.

Texas A&M University High Performance Research Computing (2019). ADA User's Guide. *Texas A&M University*.

Vaughan, E. G., Crutcher, J. M., W. Labatt II, T., McMahan, L. H., Bradford Jr, B. R., & Cluck, M. (2012). *2012 Water for Texas*. Texas Water Development Board

Vrzel, J. et al (2019). Hydrological system behavior of an alluvial aquifer under climate change. *Science of the Total Environment, 649* (1): 1179-1188. https://doi.org/10.1016/j.scitotenv.2018.08.396

Woessner, W. (2000). Stream and Fluvial Plain Ground Water Interactions: Rescaling Hydrogeologic Thought. *Groundwater*, 38, 423-429. https://doi.org/10.1111/j.1745-6584.2000.tb00228.x

Wong, S. (2012). Developing a Geospatial Model for Analysis of a Dynamic, Heterogeneous Aquifer: The Brazos River Alluvium Aquifer, Central Texas. Waco, TX: *Baylor University.*

Zeng, Z. & Decker, M. (2009). Improving the numerical solution of soil moisture-based Richard equation for land models with a deep or shallow water table. *Journal of Hydrometeorology*, *10* (1): 308-319. https://doi.org/10.1175/2008JHM1011.1

APPENDIX A

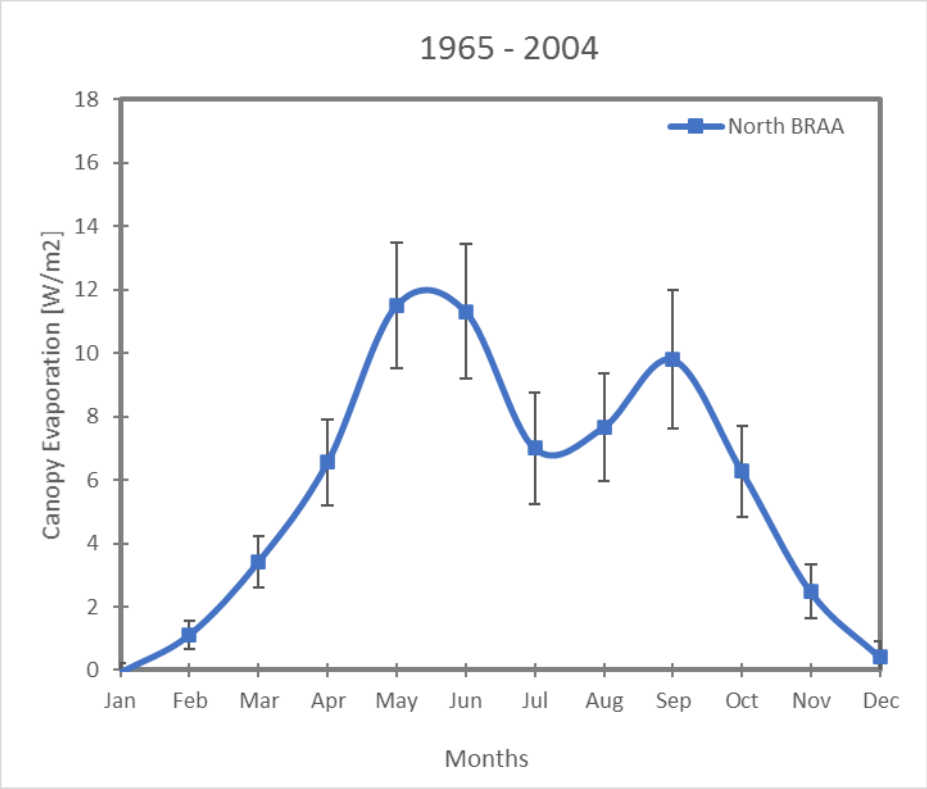

Figure A.1 Monthly canopy Evaporation in the northern portion of the BRAA

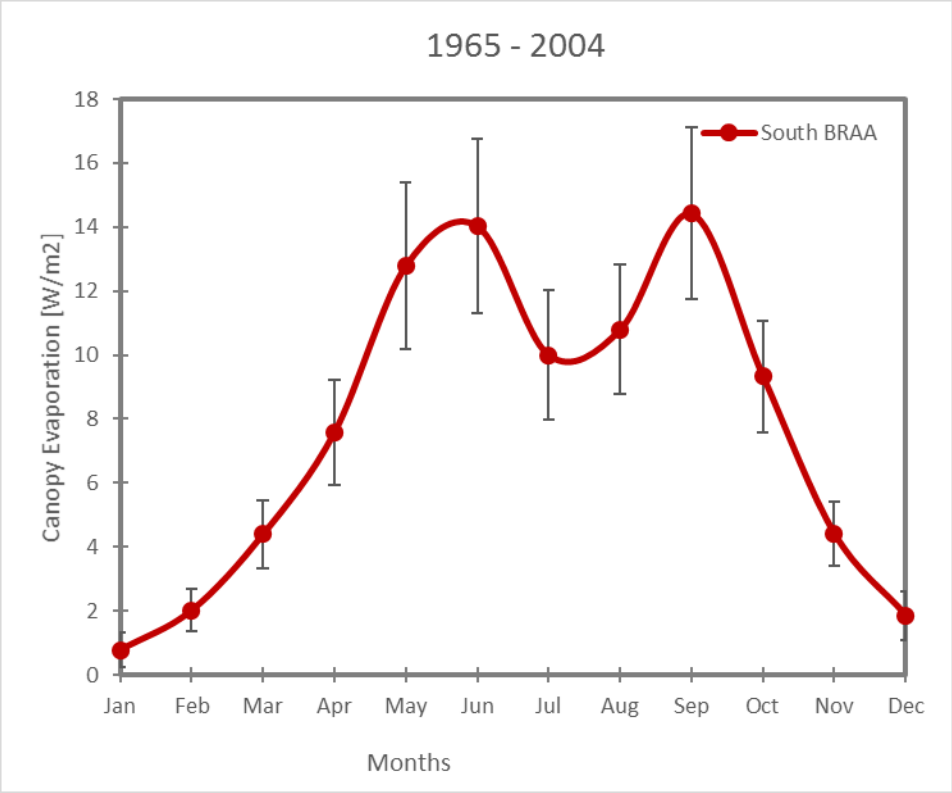

Figure A.2 Monthly canopy evaporation in the southern portion of the BRAA

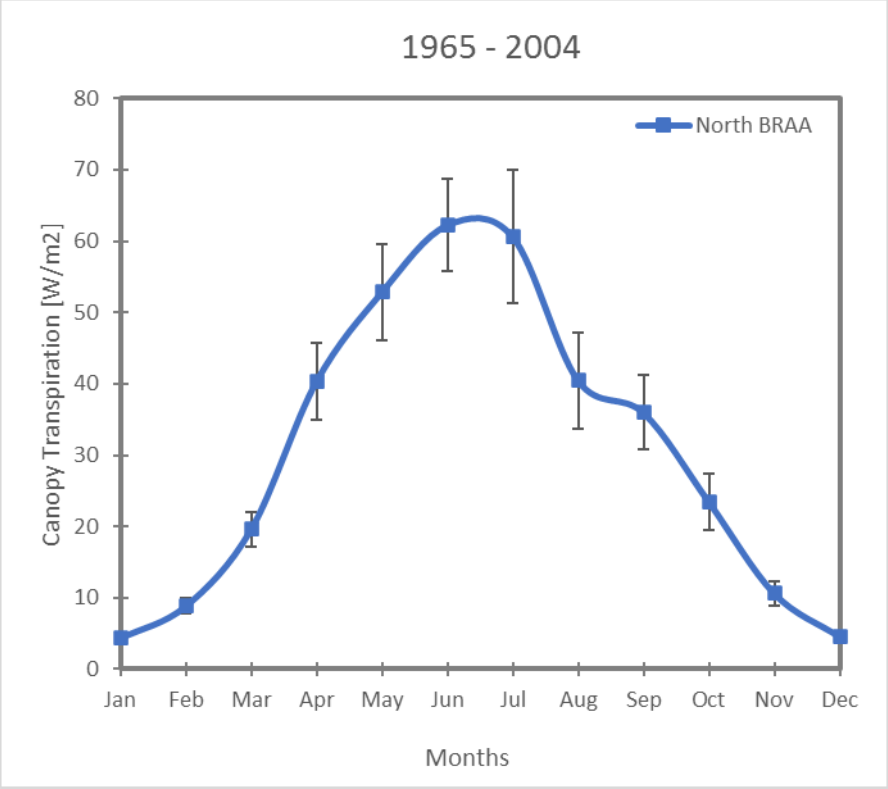

Figure A.3 Monthly canopy transpiration in the northern portion of the BRAA

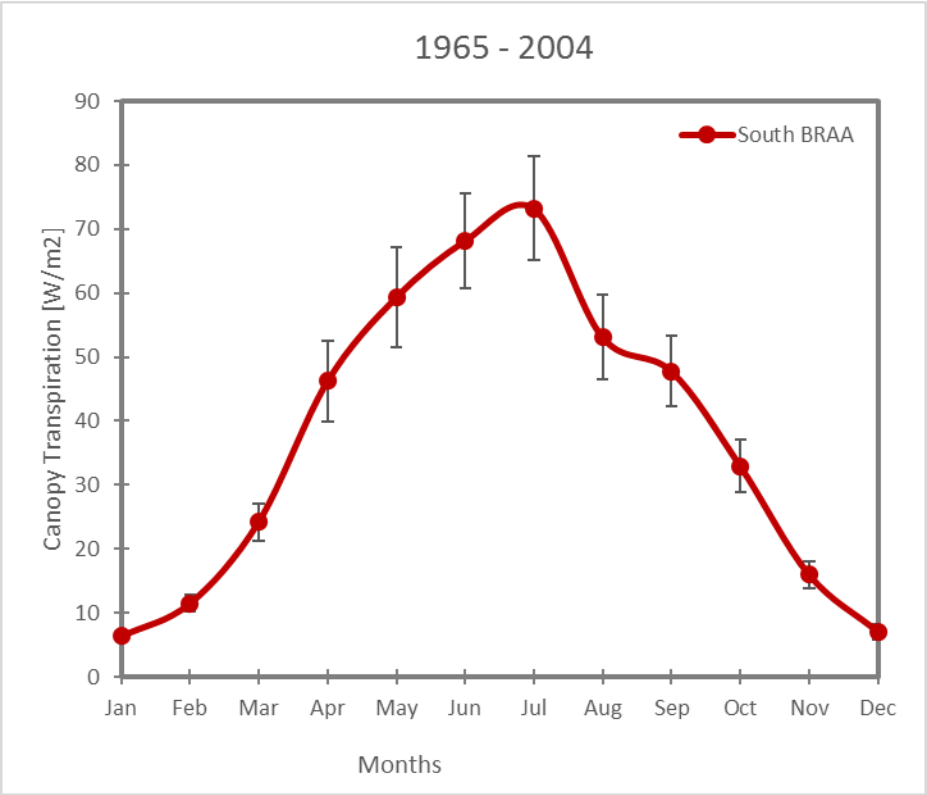

Figure A.4 Monthly canopy transpiration in the southern portion of the BRAA

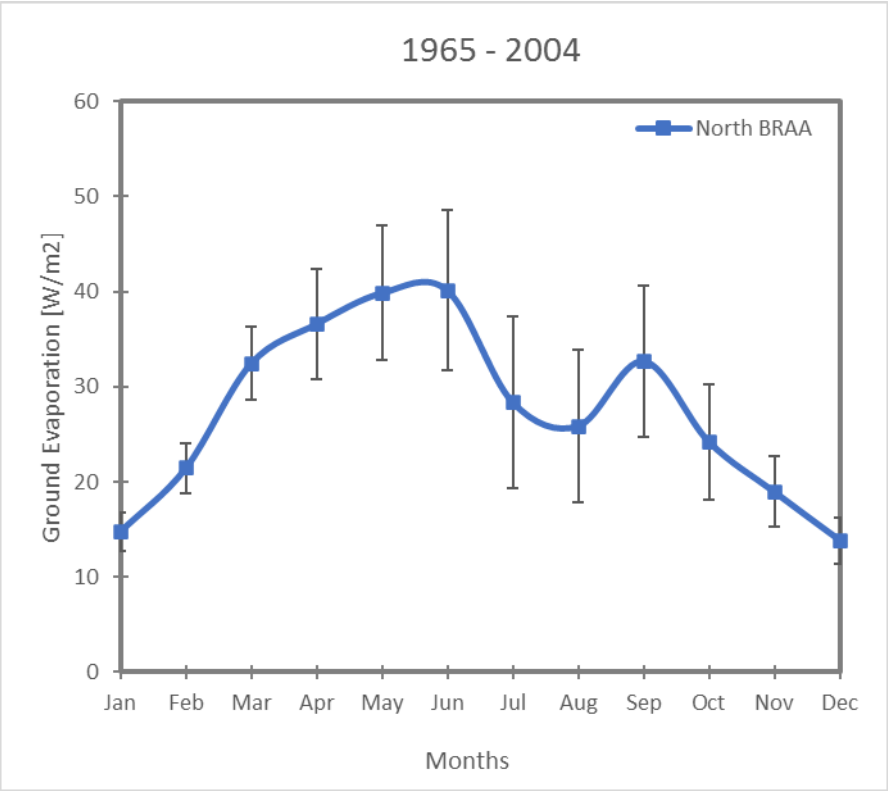

Figure A.5 Monthly ground evaporation in the northern portion of the BRAA

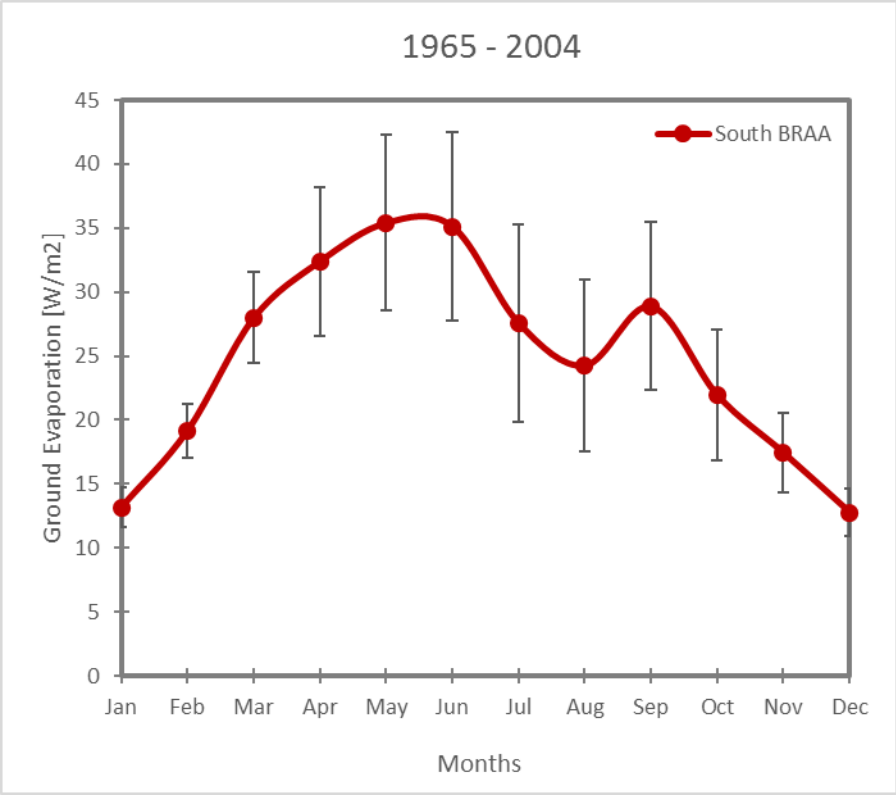

Figure A.6 Monthly ground evaporation in the southern portion of the BRAA

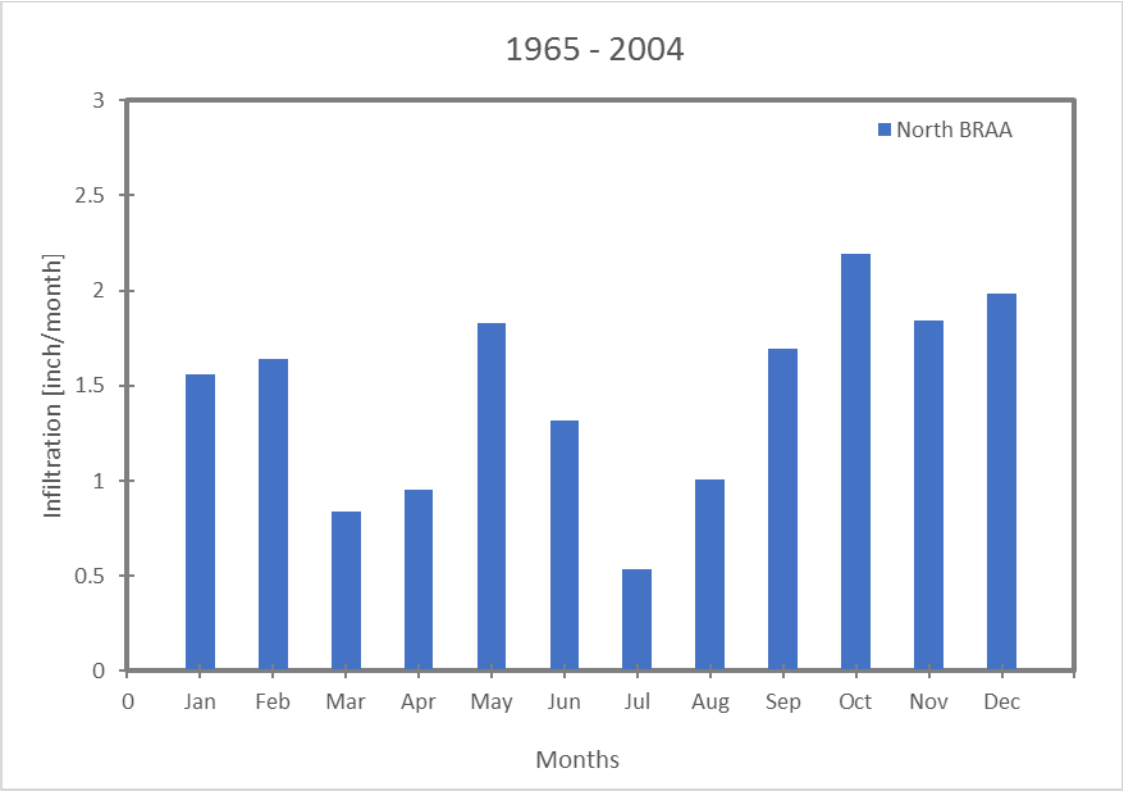

Figure A.7 Monthly infiltration in the northern portion of the BRAA

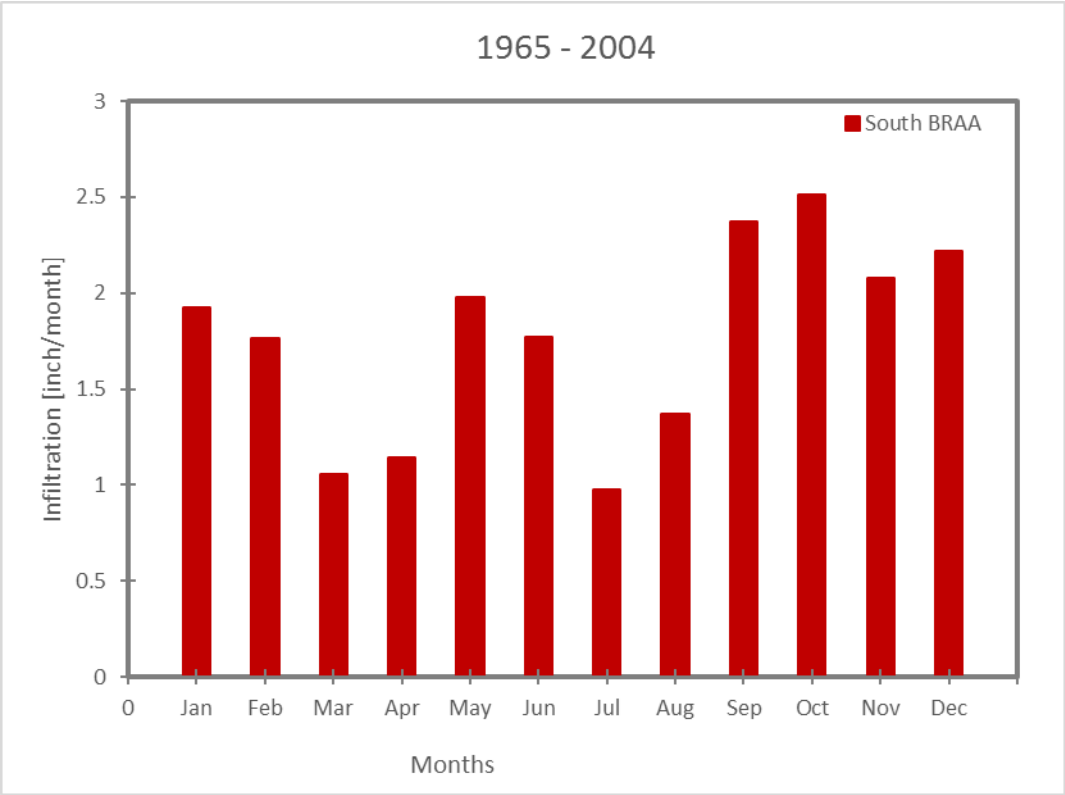

Figure A.8 Monthly infiltration in the southern portion of the BRAA

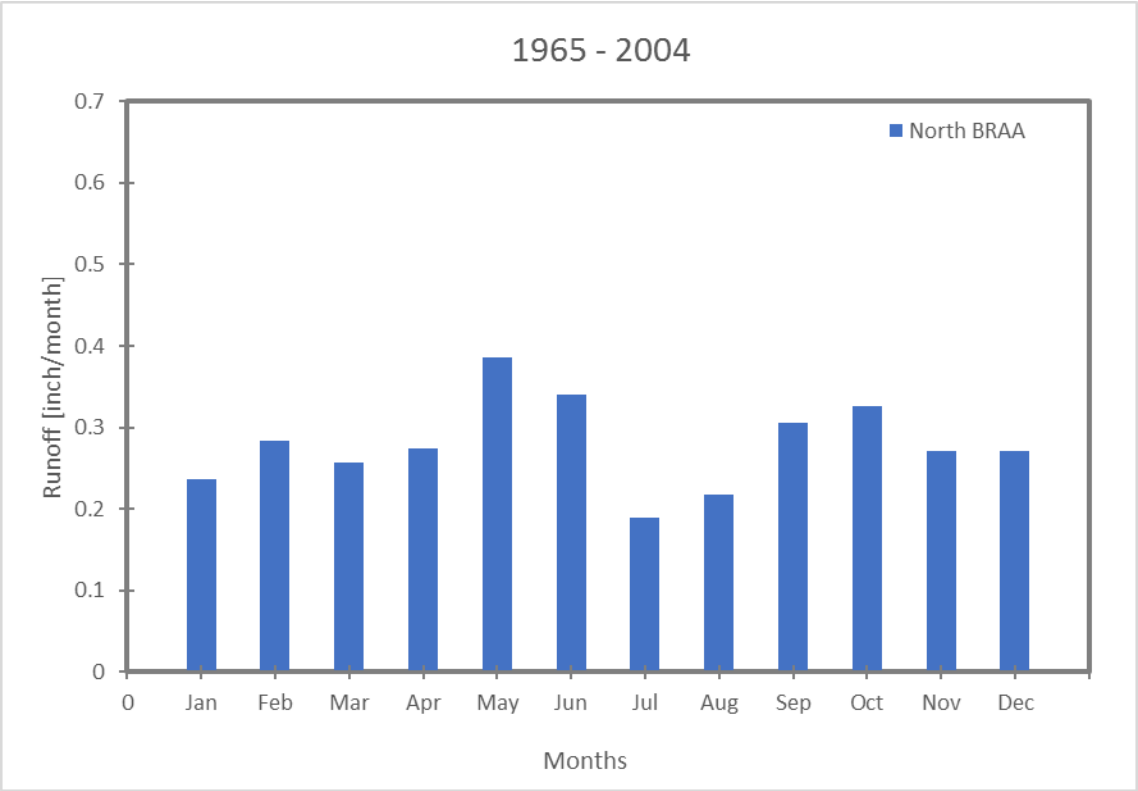

Figure A.9 Monthly runoff in the northern portion of the BRAA

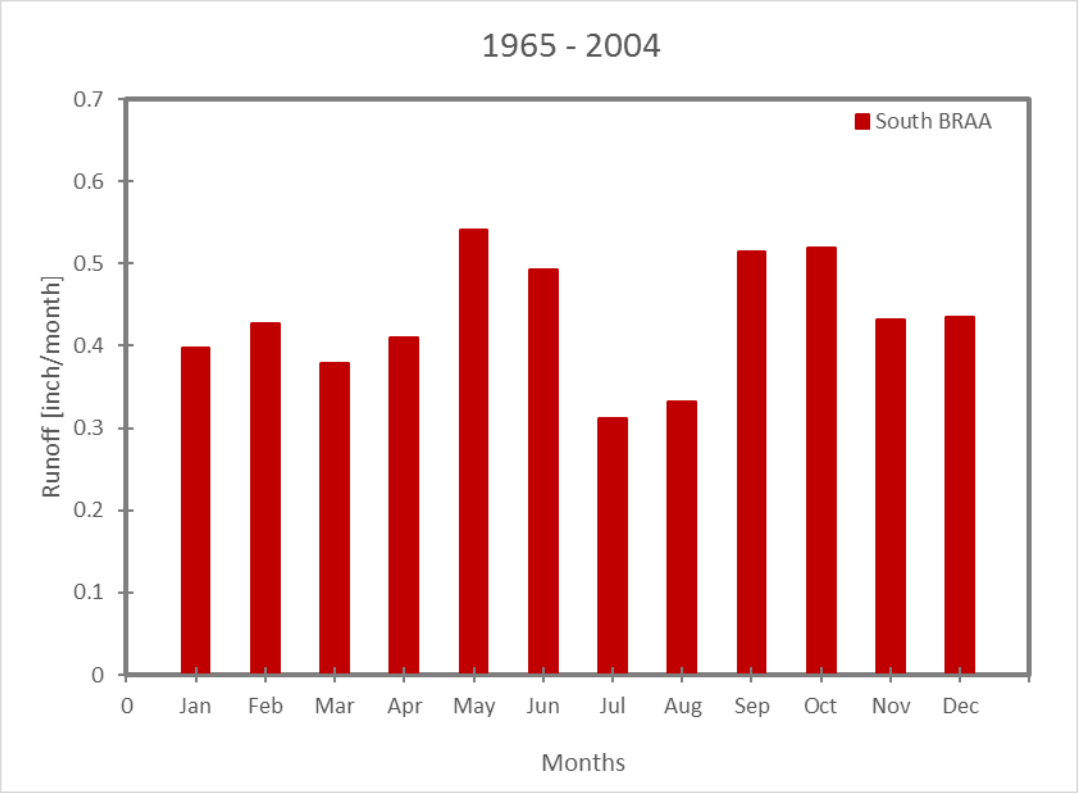

Figure A.10 Monthly runoff in the southern portion of the BRAA

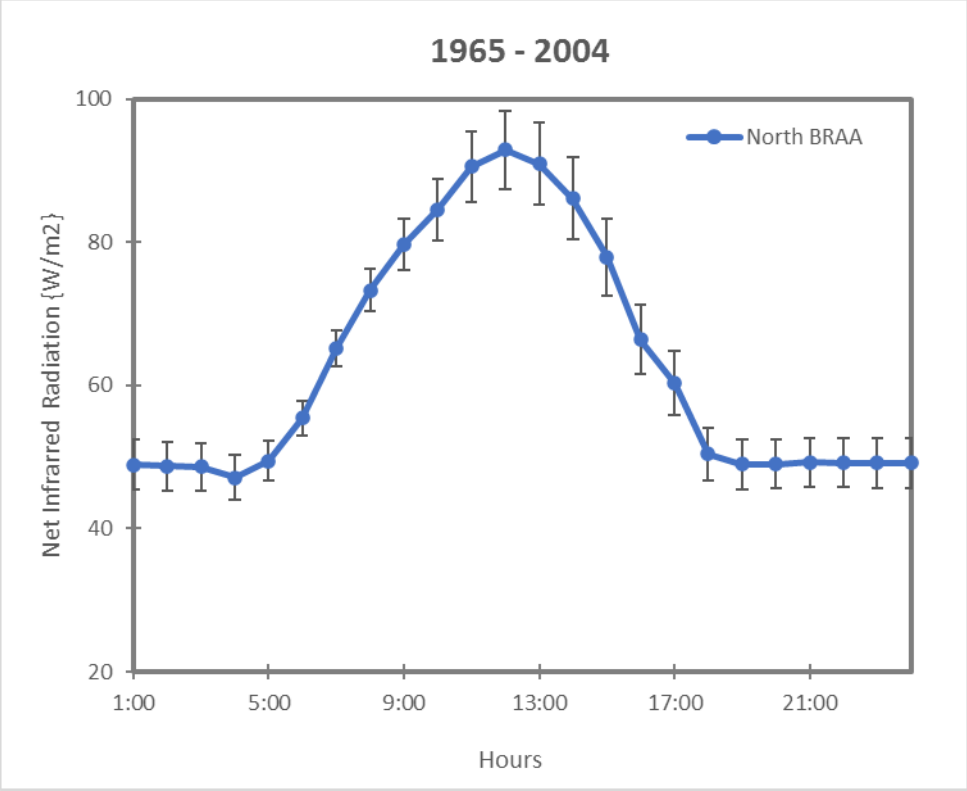

Figure A.11 Daily net infrared radiation in the northern portion of the BRAA

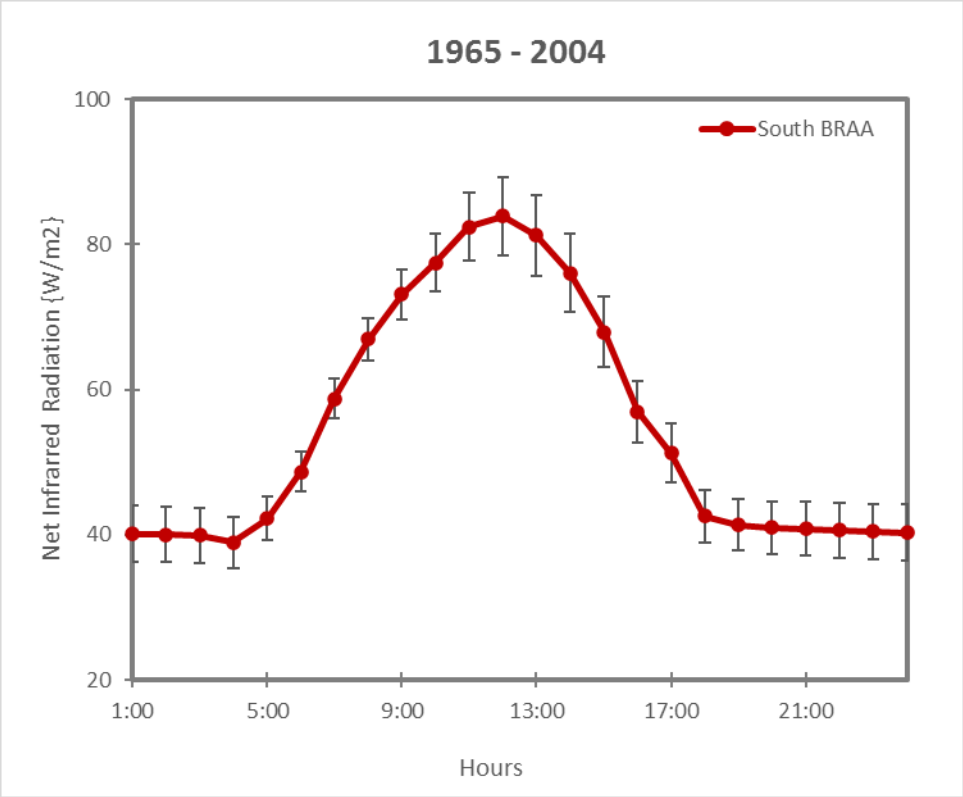

Figure A.12 Daily net infrared radiation in the southern portion of the BRAA

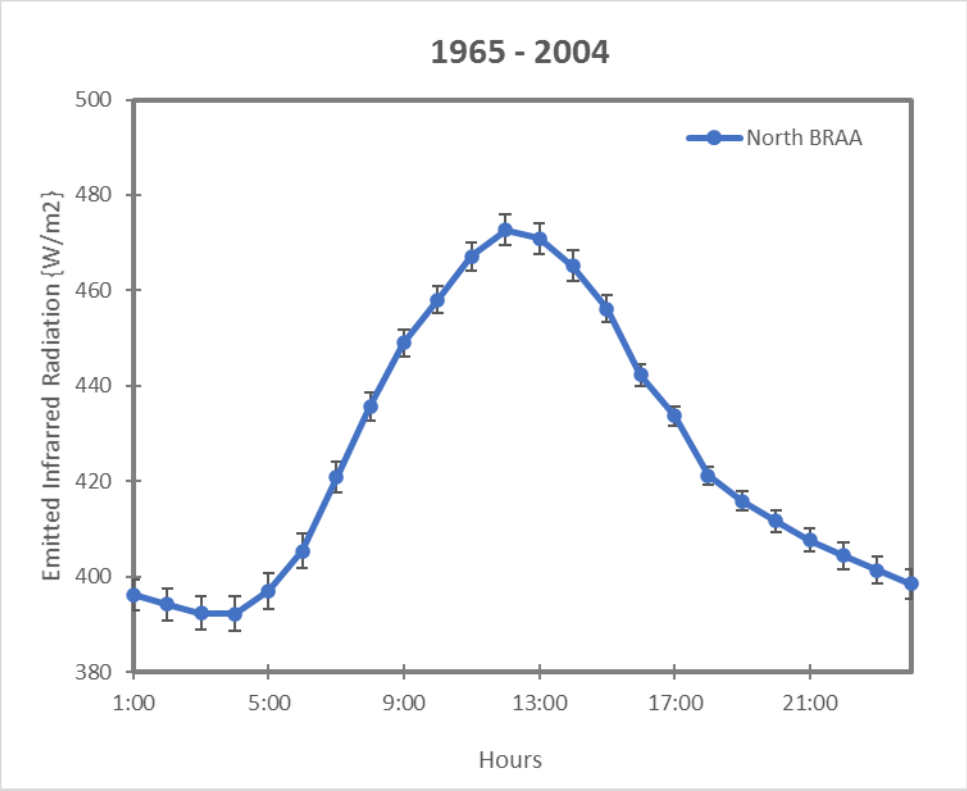

Figure A.13 Daily emitted infrared radiation in the northern portion of the BRAA

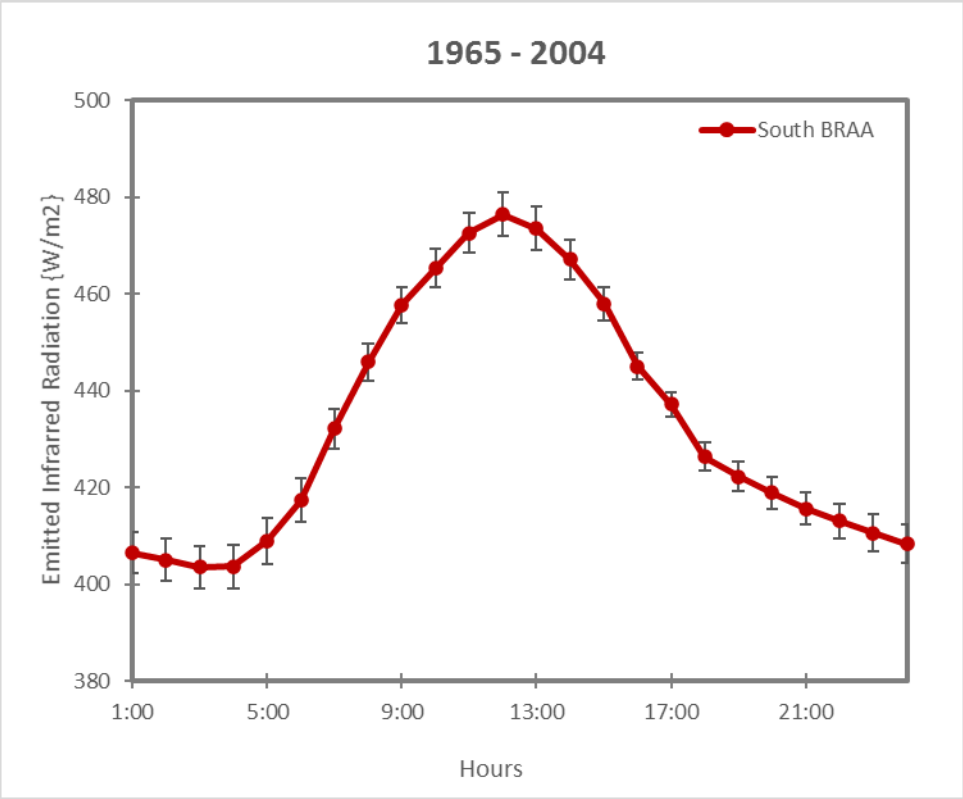

Figure A.14 Daily emitted infrared radiation in the southern portion of the BRAA

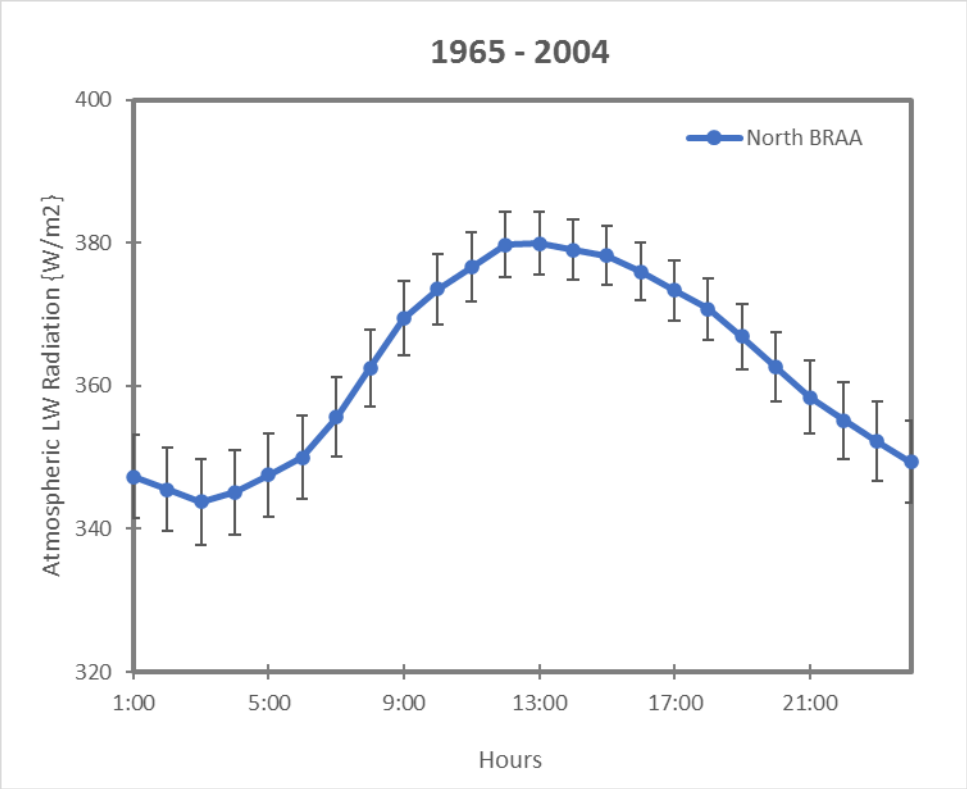

Figure A.15 Daily atmospheric longwave radiation in the northern portion of the BRAA

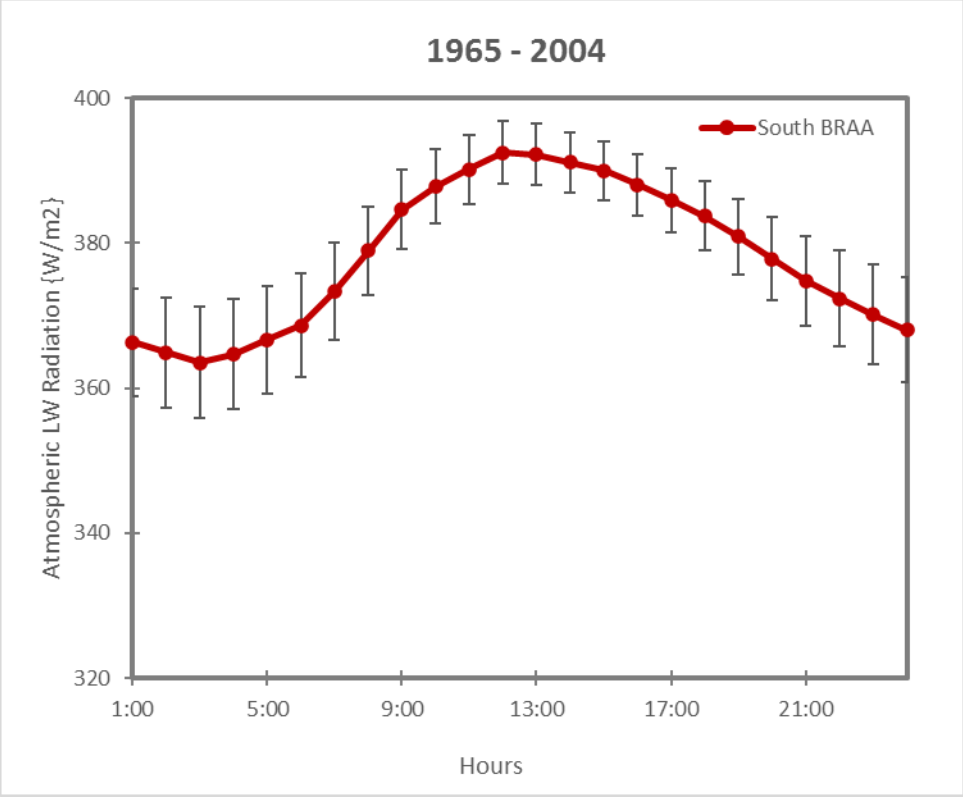

Figure A.16 Daily atmospheric longwave radiation in the southern portion of the BRAA

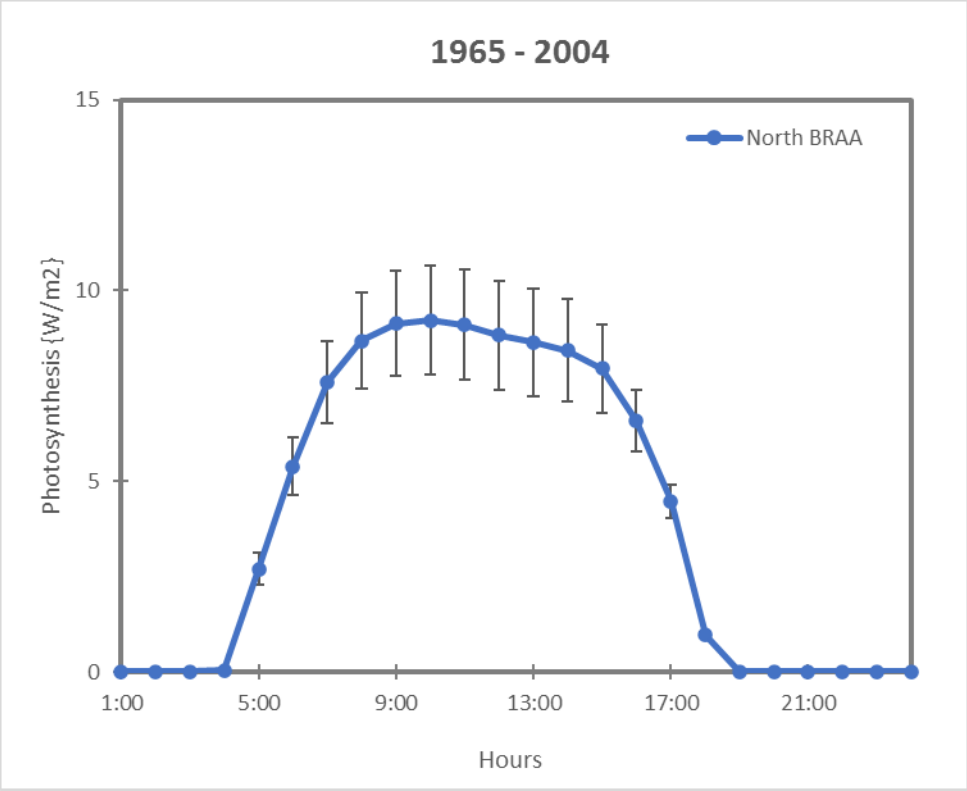

Figure A.17 Daily photosynthesis in the northern portion of the BRAA

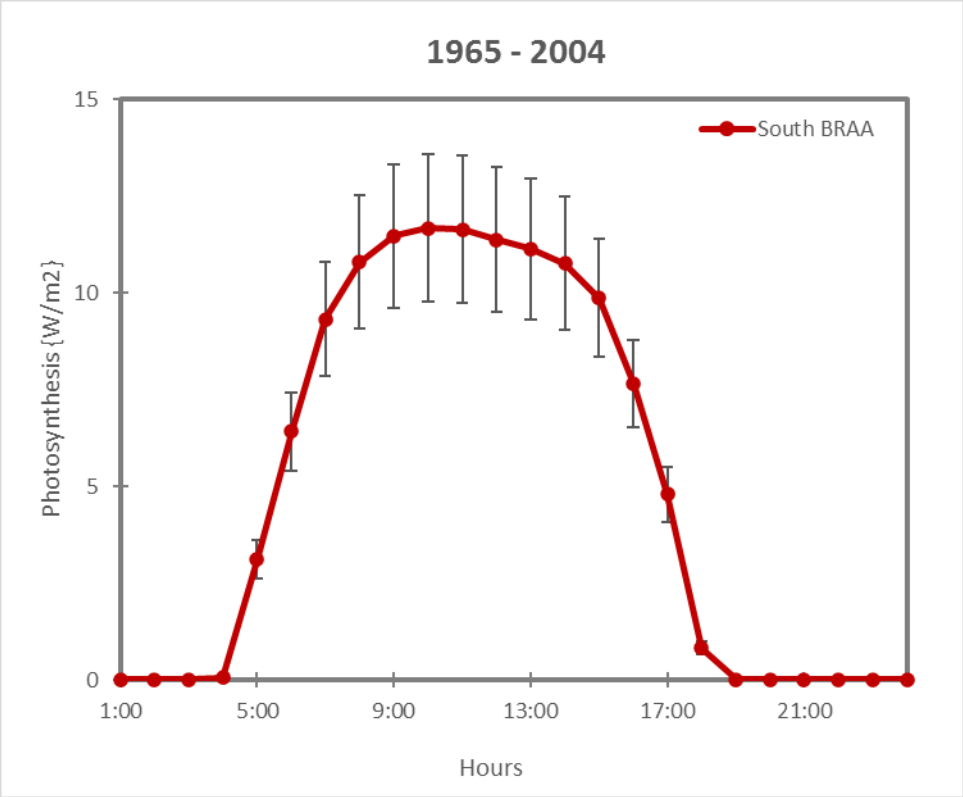

Figure A.18 Daily photosynthesis in the southern portion of the BRAA

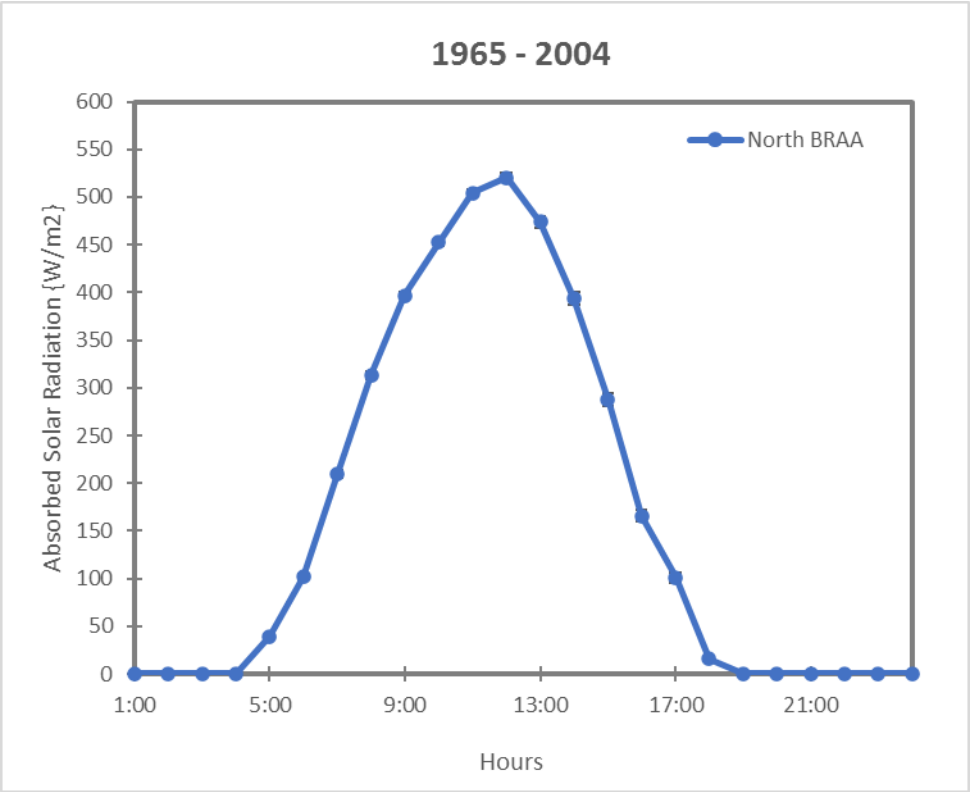

Figure A.19 Daily absorbed solar radiation in the northern portion of the BRAA

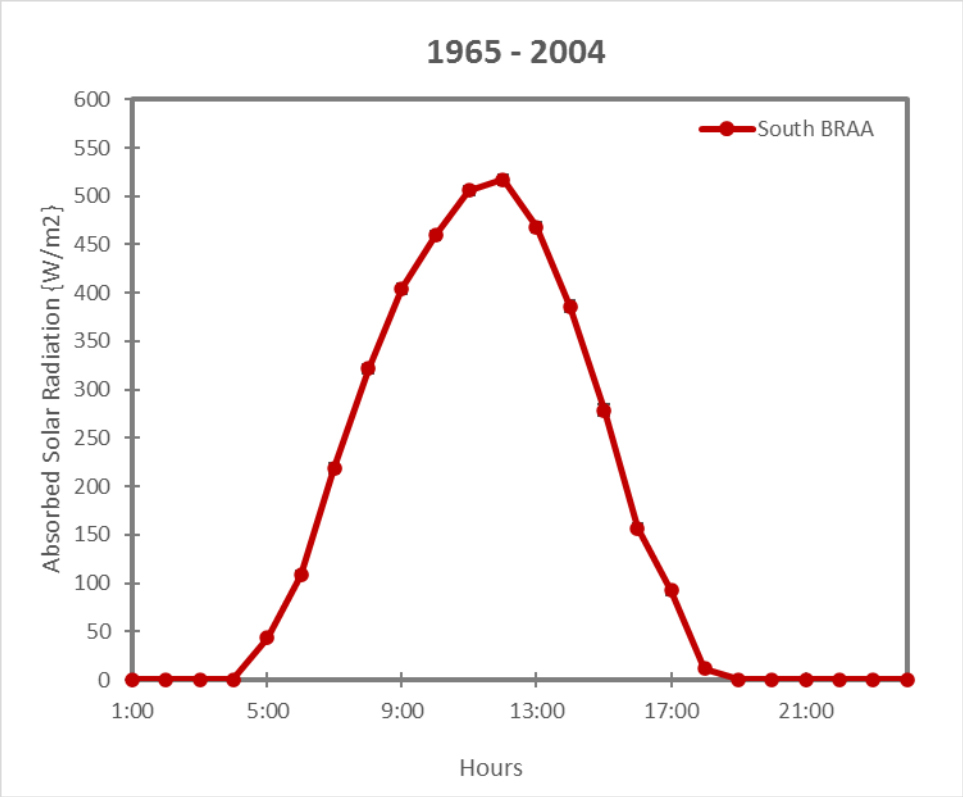

Figure A.20 Daily absorbed solar radiation in the southern portion of the BRAA

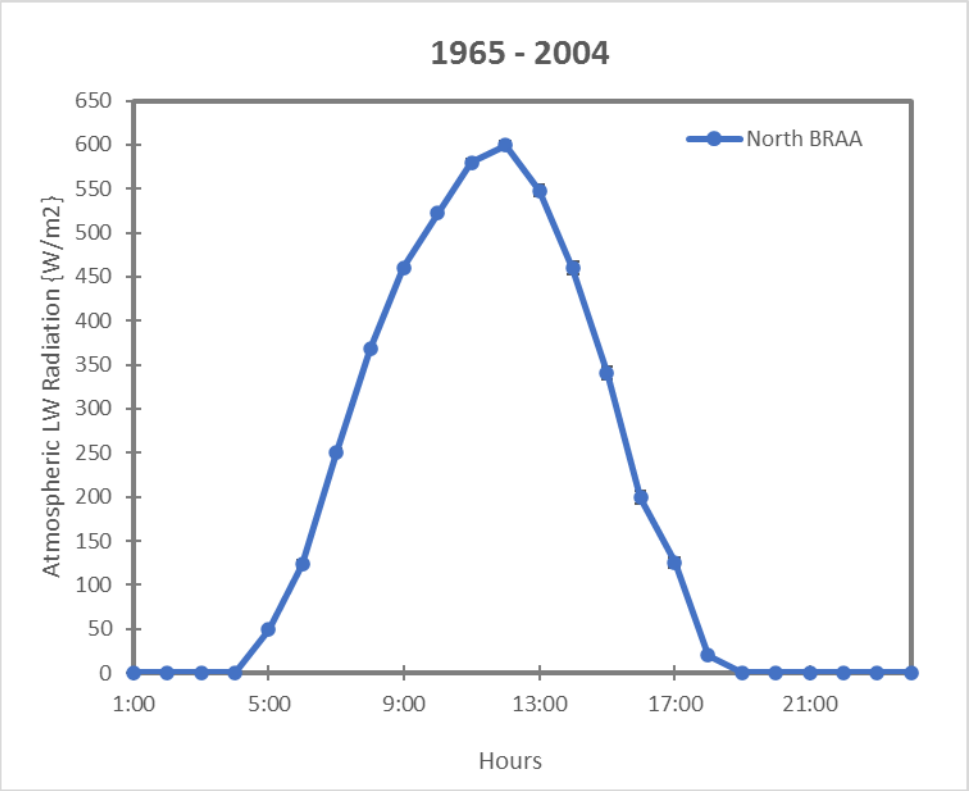

Figure A.21 Daily atmospheric incident solar radiation in the northern portion of the BRAA

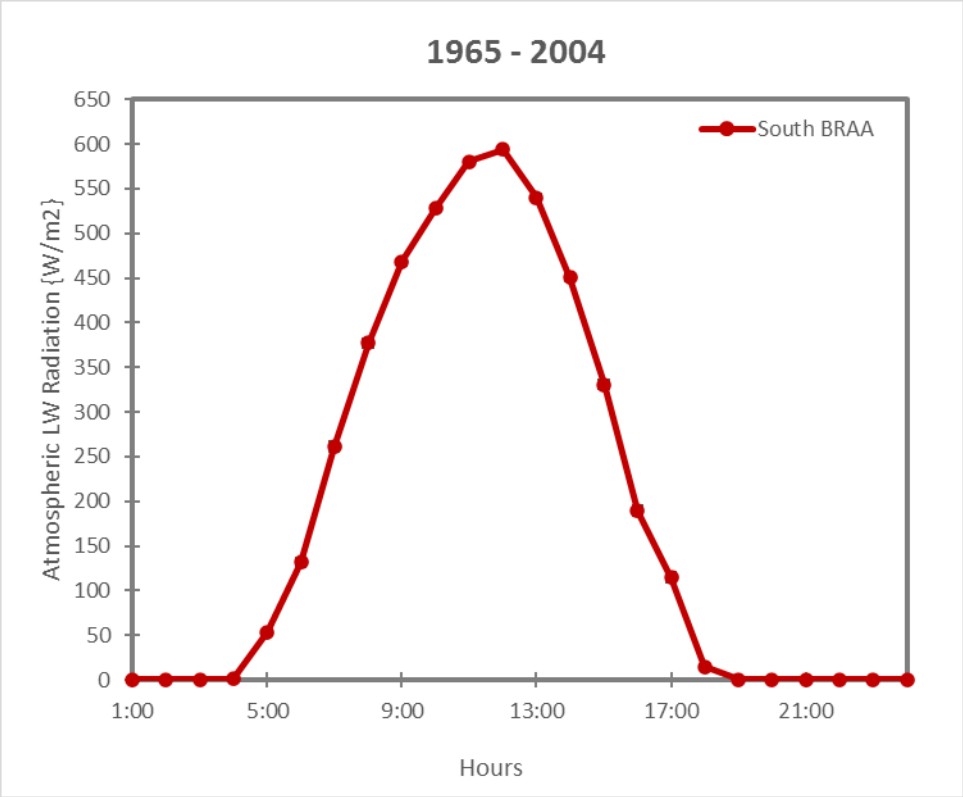

Figure A.22 Daily atmospheric incident solar radiation in the southern portion of the BRAA

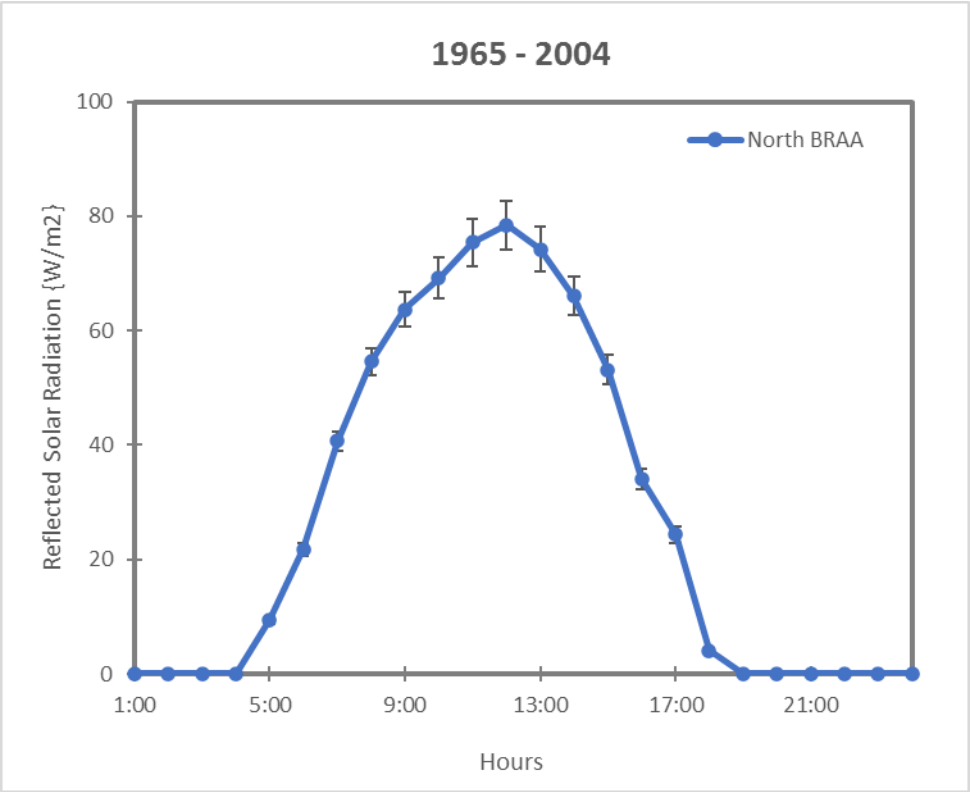

Figure A.23 Daily reflected solar radiation in the northern portion of the BRAA

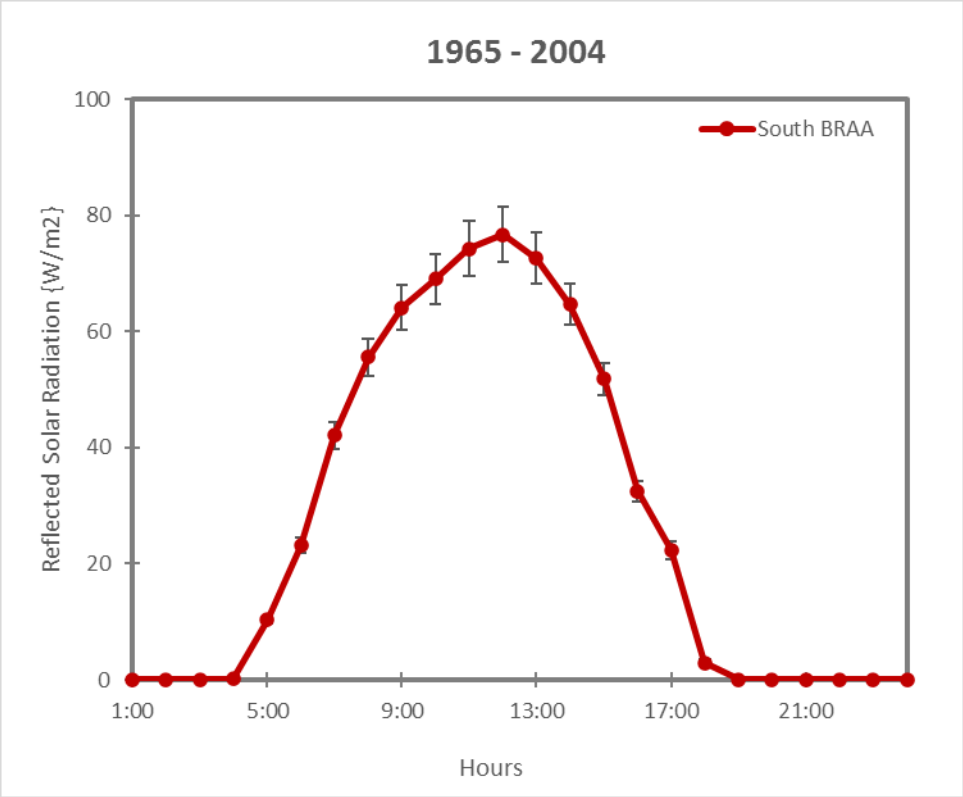

Figure A.24 Daily reflected solar radiation in the southern portion of the BRAA

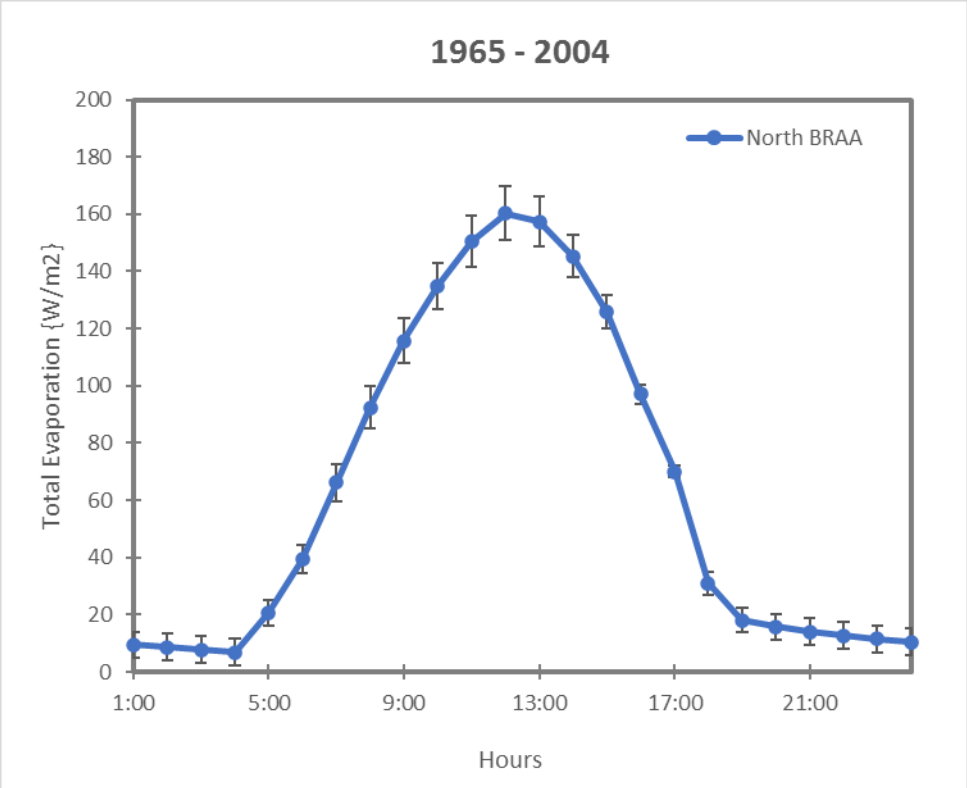

Figure A.25 Daily total evaporation in the northern portion of the BRAA

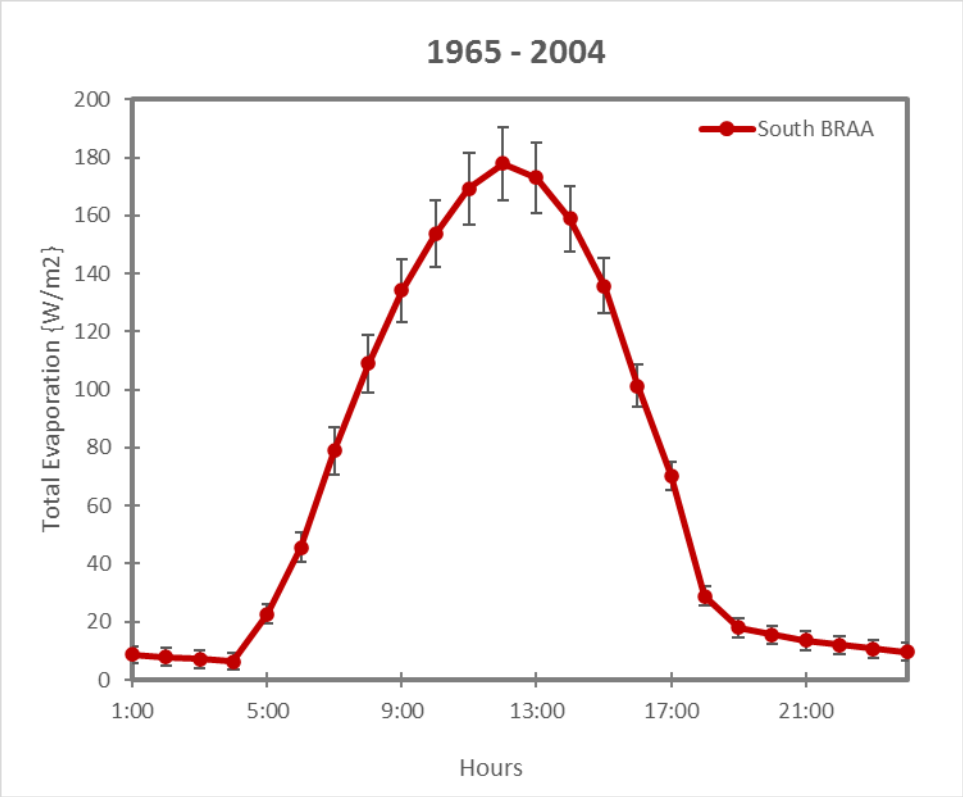

Figure A.26 Daily total evaporation in the southern portion of the BRAA

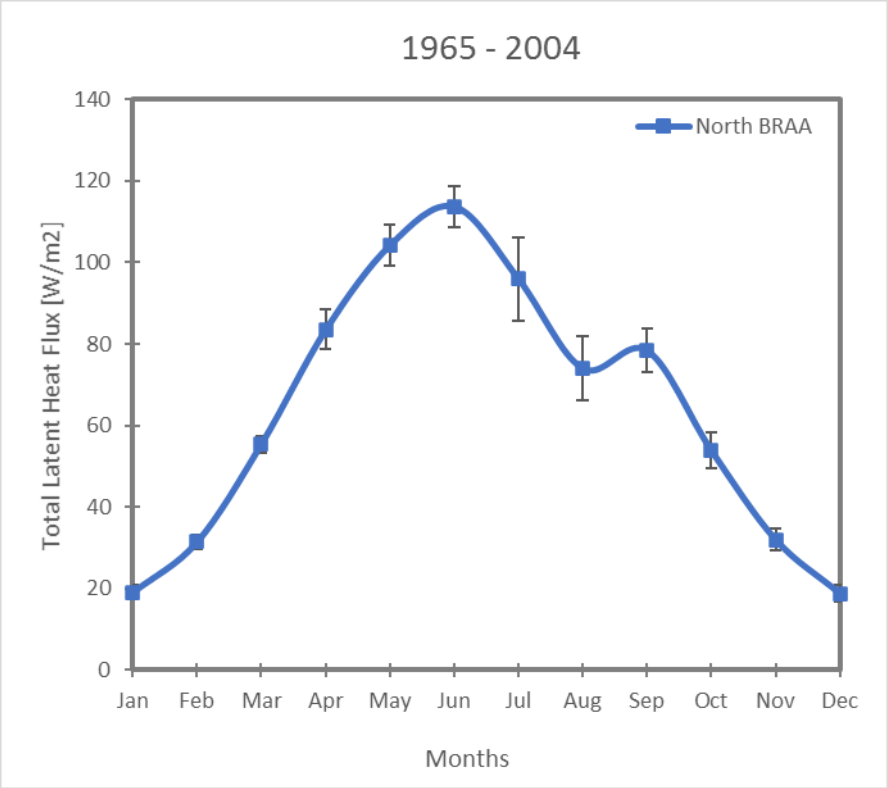

Figure A.27 Monthly latent heat in the northern portion of the BRAA

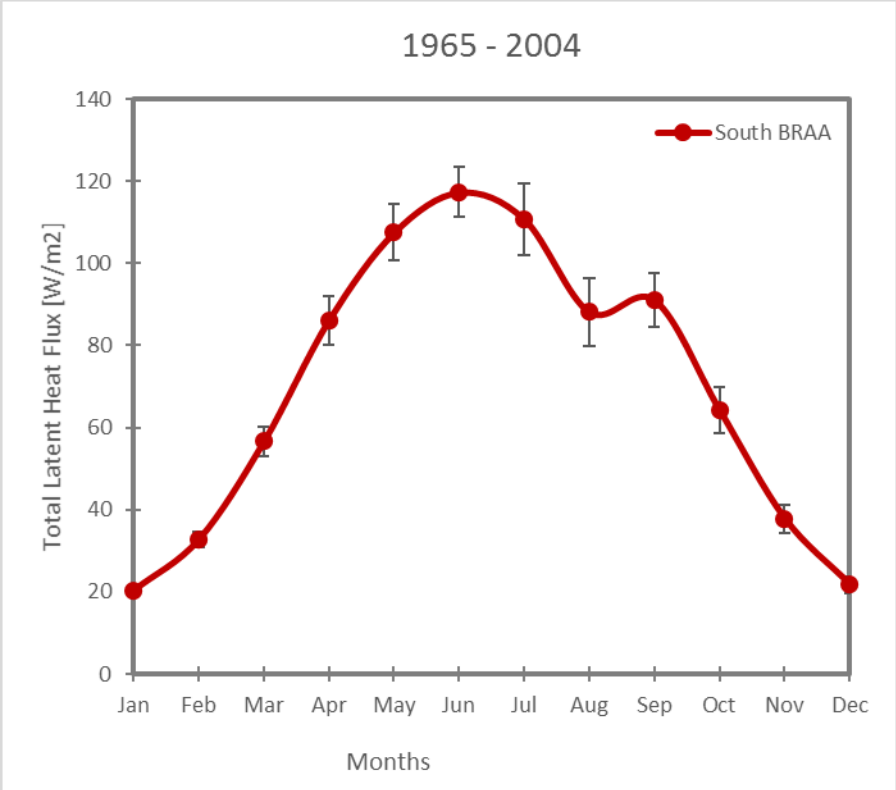

Figure A.28 Monthly latent heat in the southern portion of the BRAA

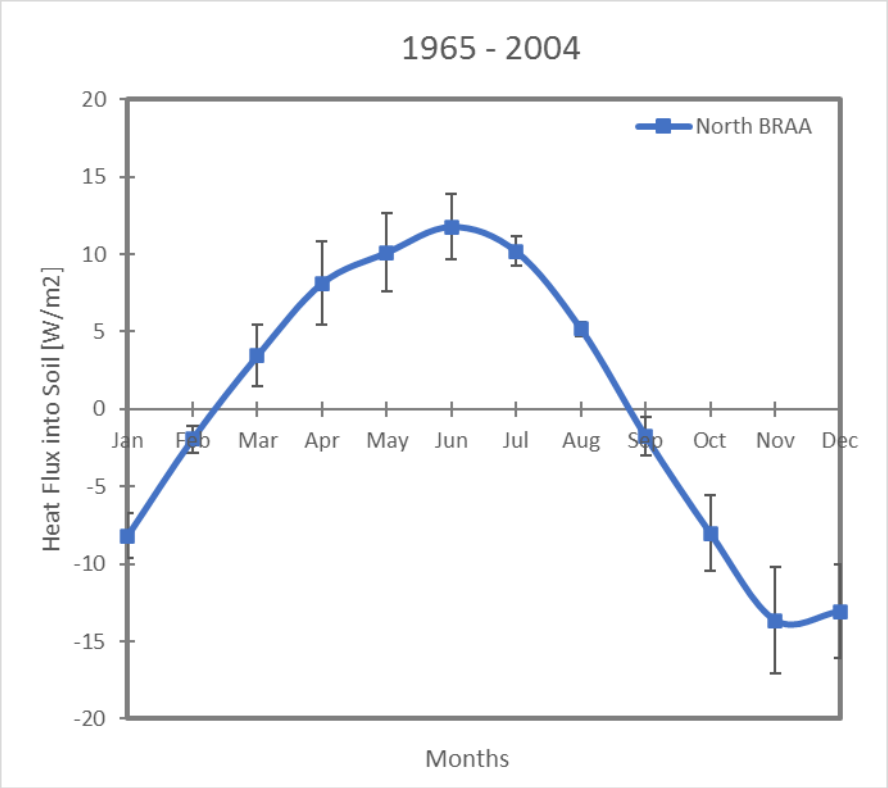

Figure A.29 Monthly heat flux into soil in the northern portion of the BRAA

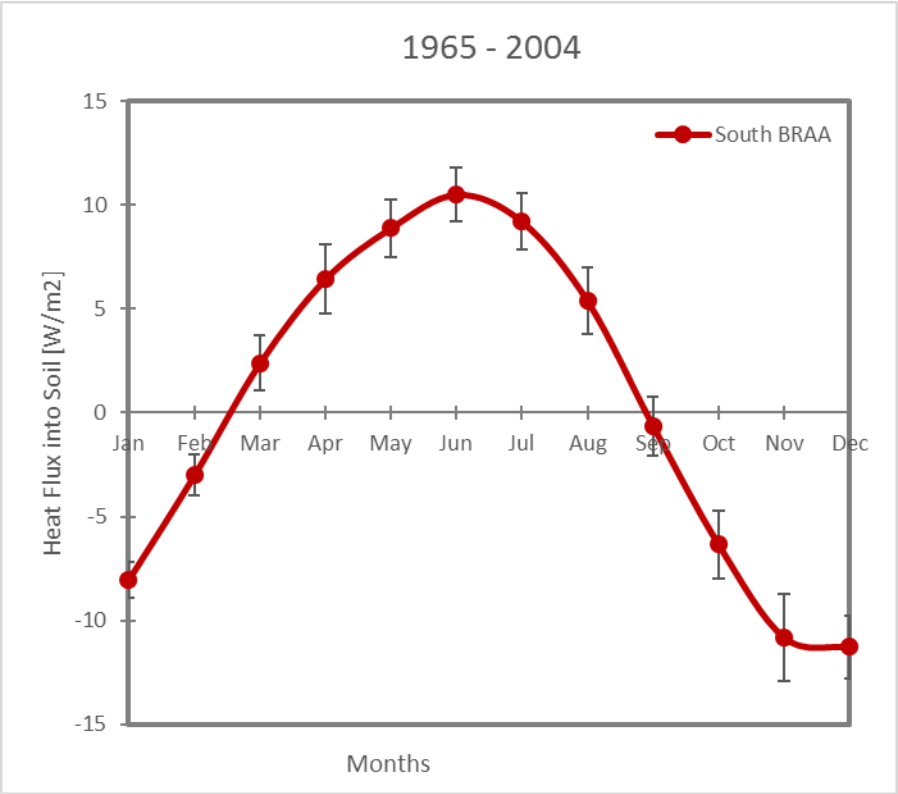

Figure A.30 Monthly heat flux into soil in the southern portion of the BRAA

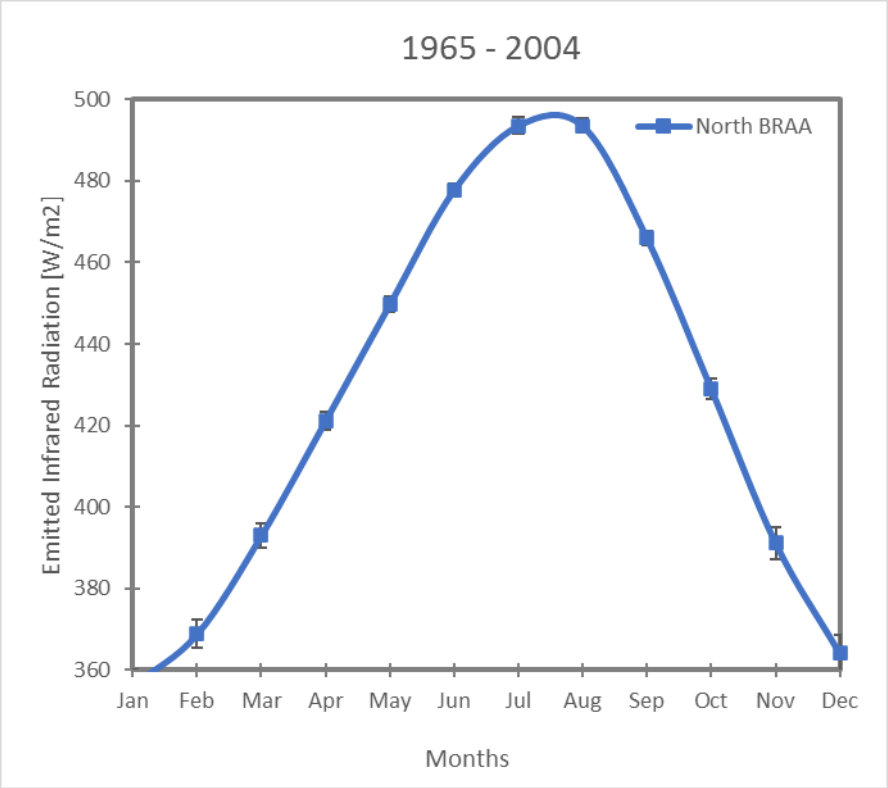

Figure A.31 Monthly emitted infrared radiation in the northern portion of the BRAA

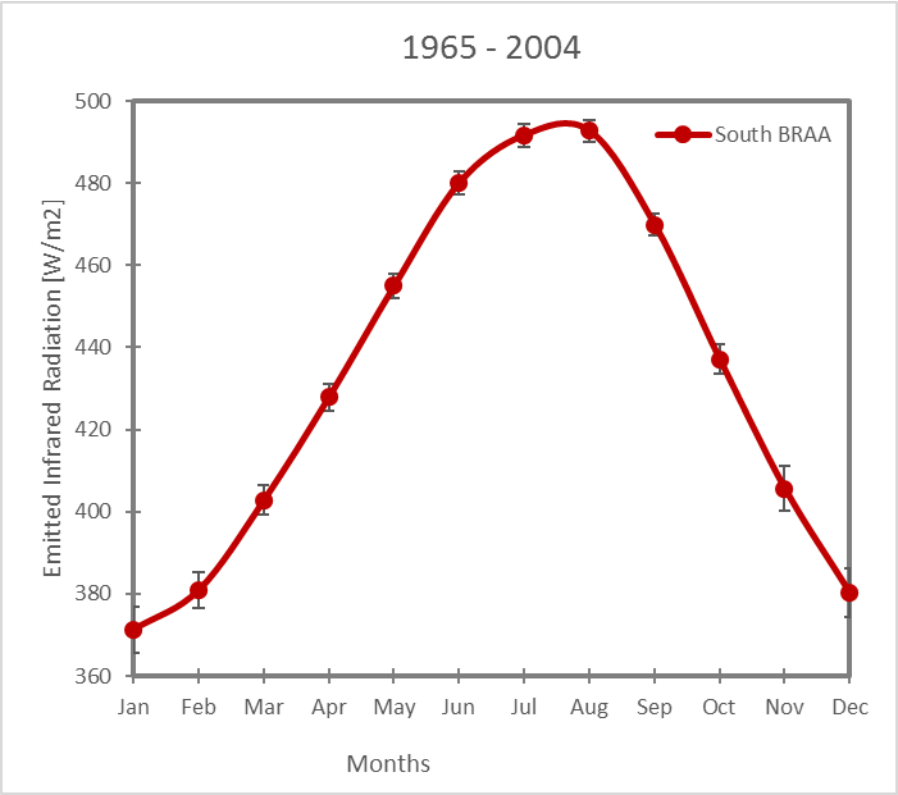

Figure A.32 Monthly emitted infrared radiation in the southern portion of the BRAA

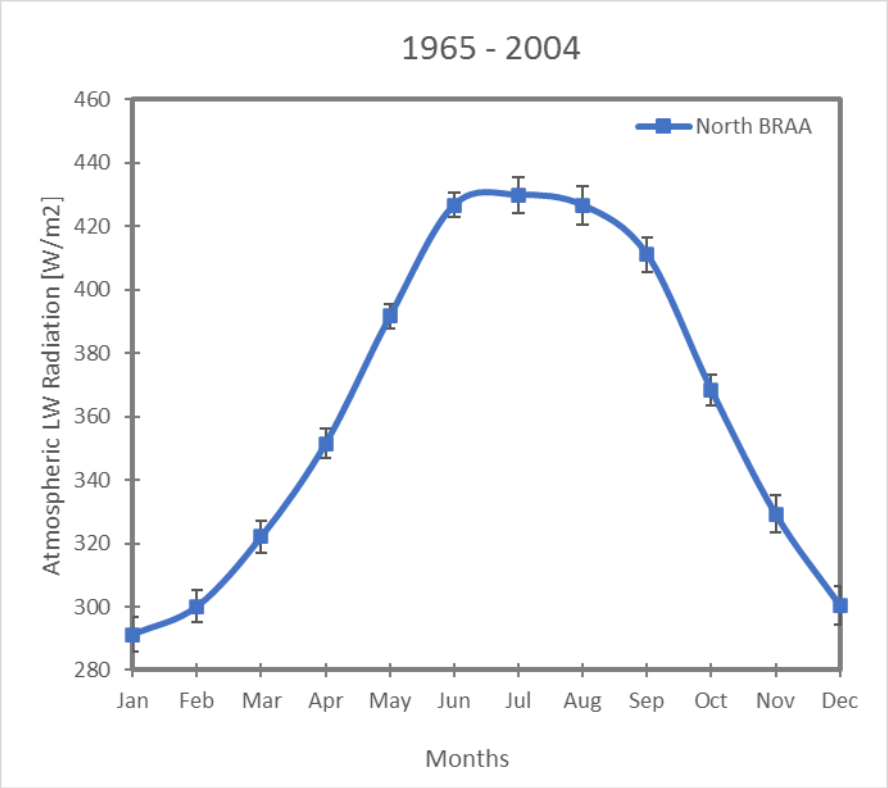

Figure A.33 Monthly atmospheric longwave radiation in the northern portion of the BRAA

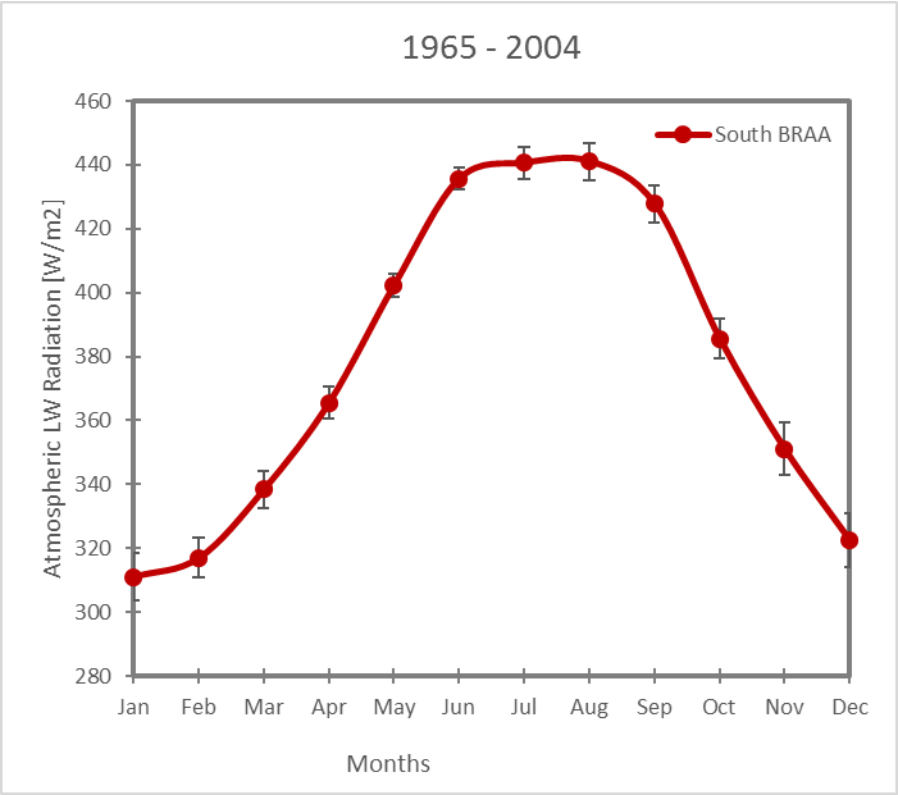

Figure A.34 Monthly atmospheric longwave radiation in the southern portion of the BRAA

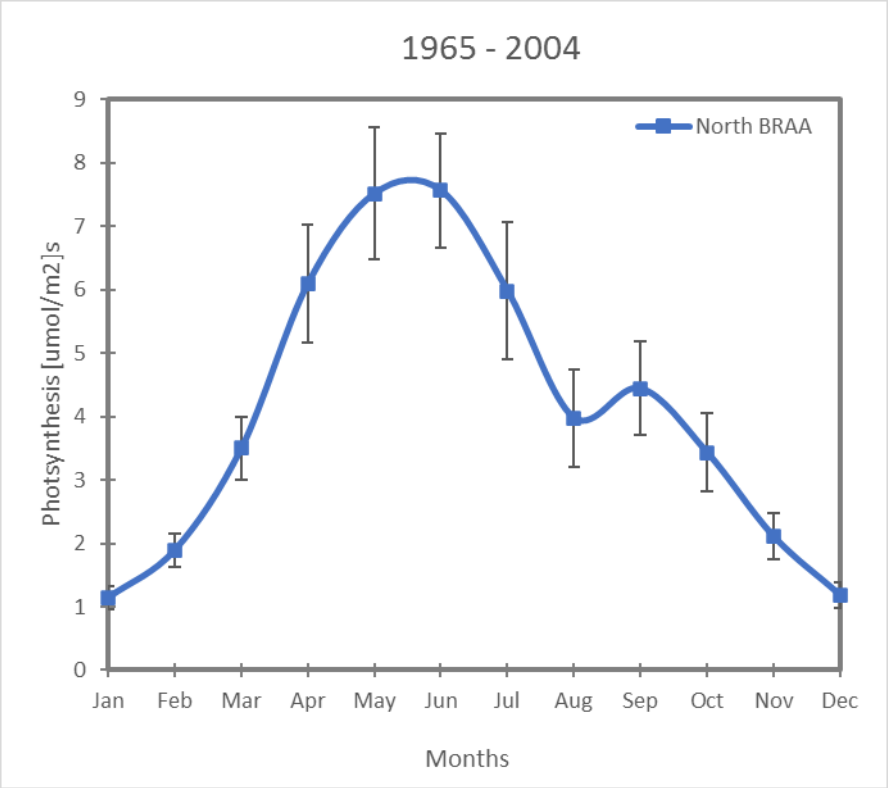

Figure A.35 Monthly photosynthesis in the northern portion of the BRAA

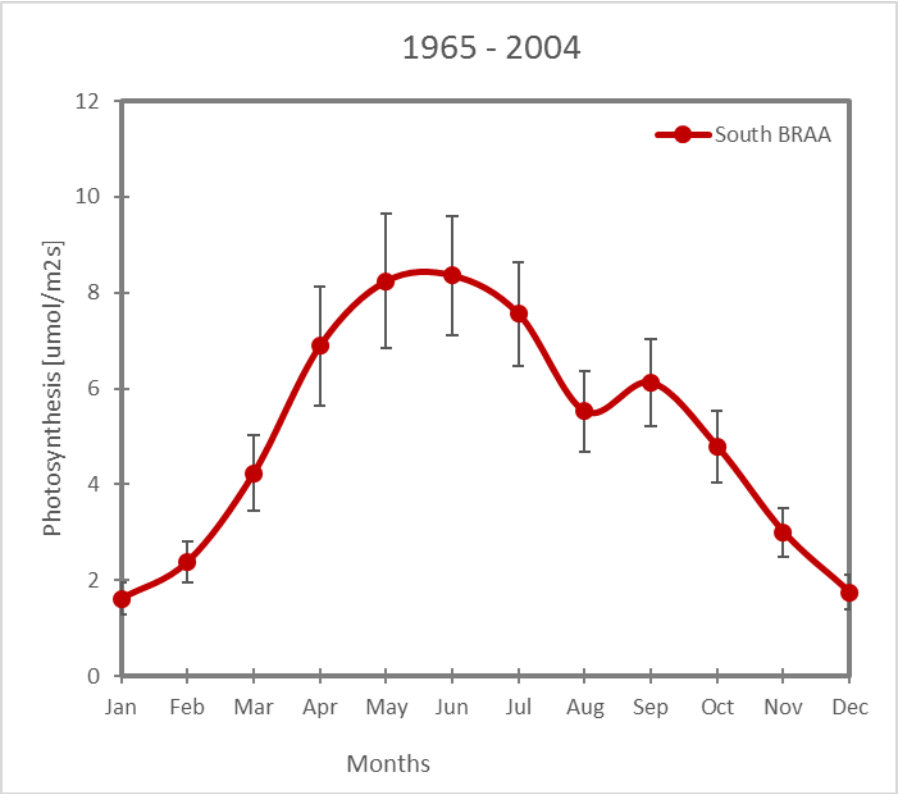

Figure A.36 Monthly photosynthesis in the southern portion of the BRAA

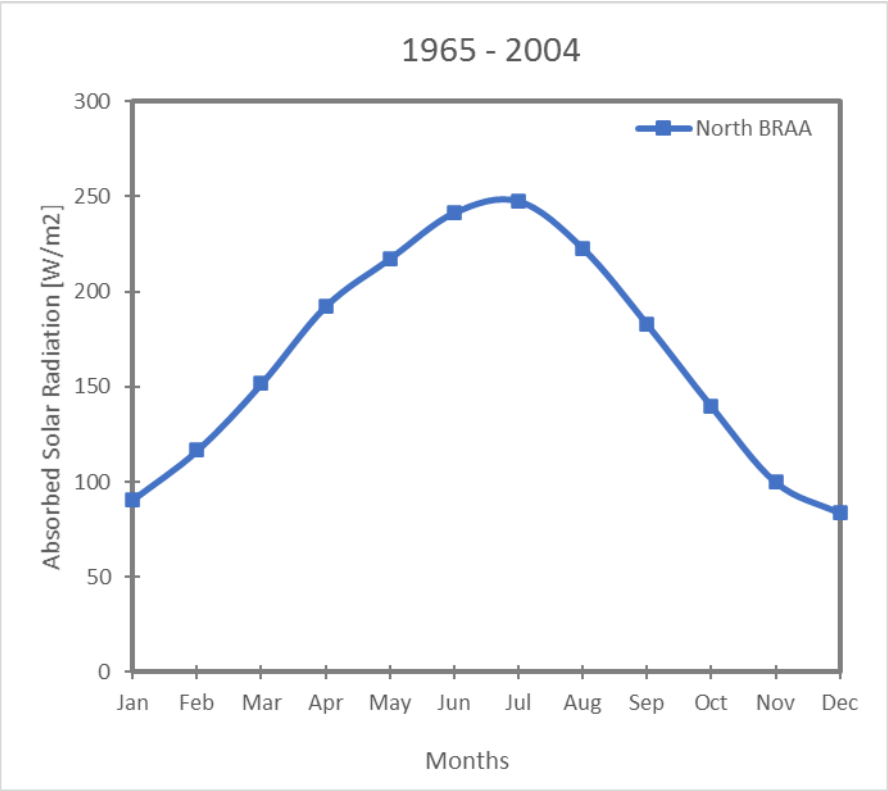

Figure A.37 Monthly absorbed solar radiation in the northern portion of the BRAA

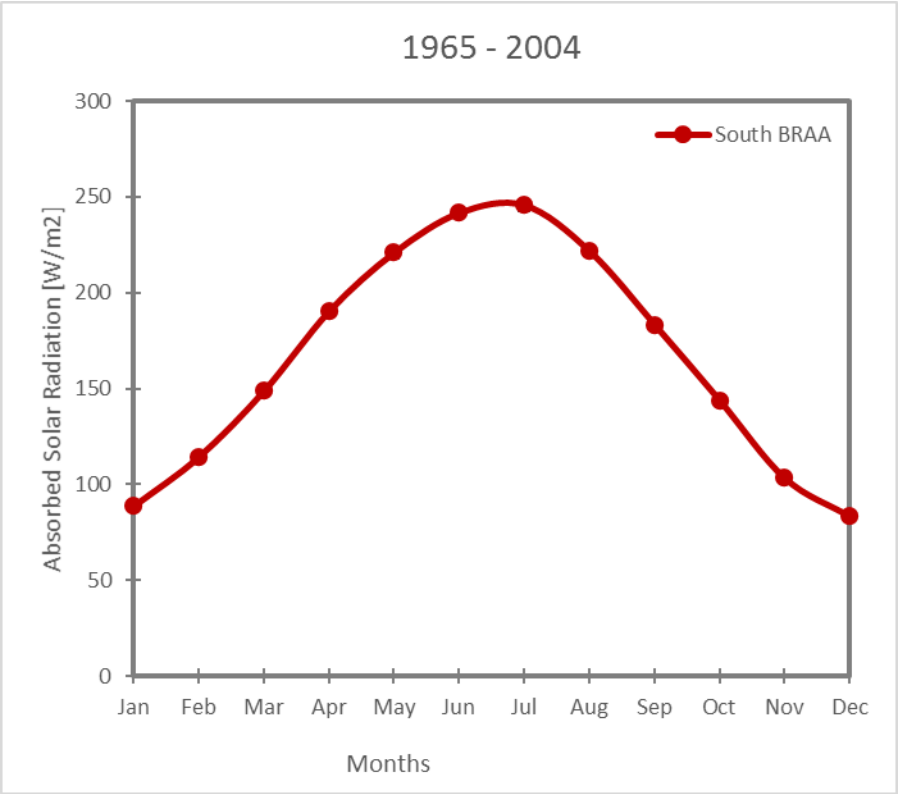

Figure A.38 Monthly absorbed solar radiation in the southern portion of the BRAA

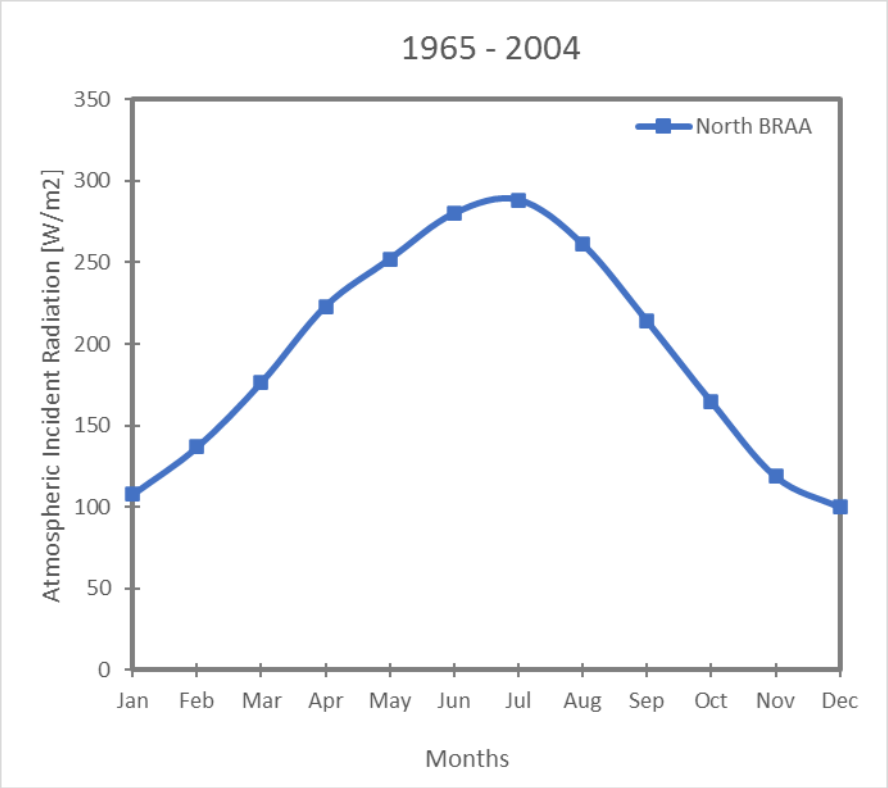

Figure A.39 Monthly atmospheric incident radiation in the northern portion of the BRAA

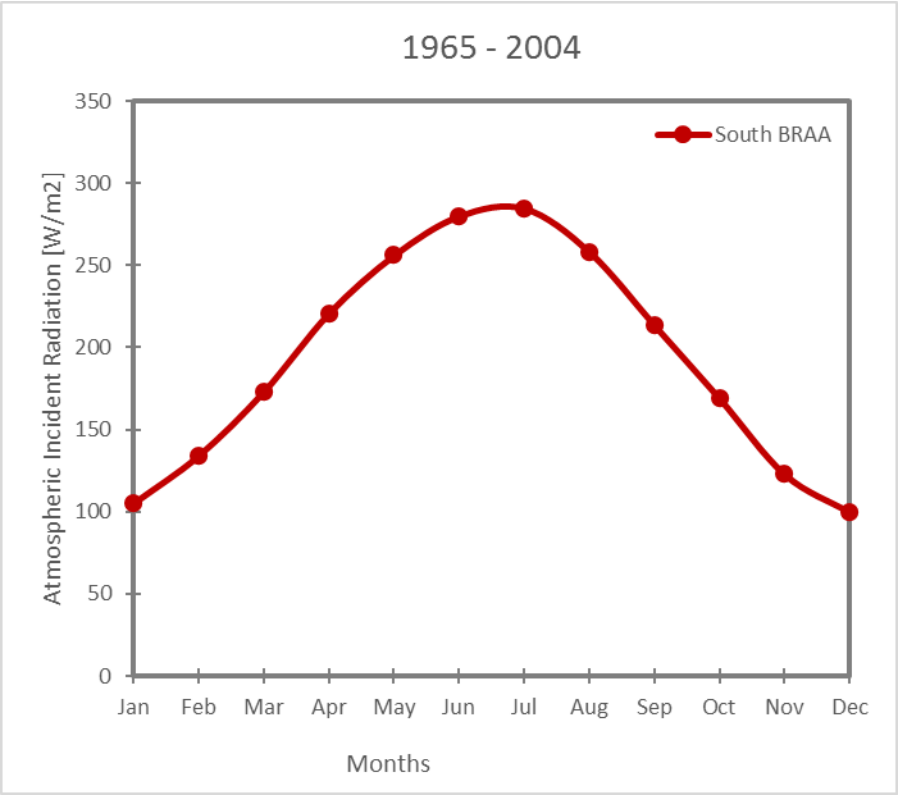

Figure A.40 Monthly atmospheric incident radiation in the southern portion of the BRAA

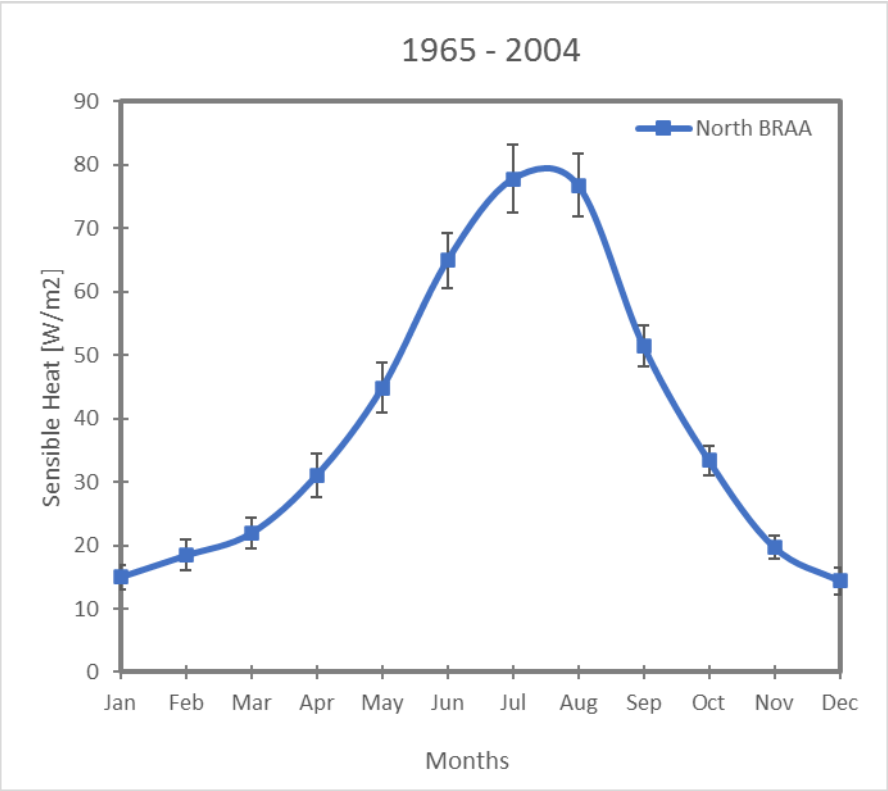

Figure A.41 Monthly sensible heat in the northern portion of the BRAA

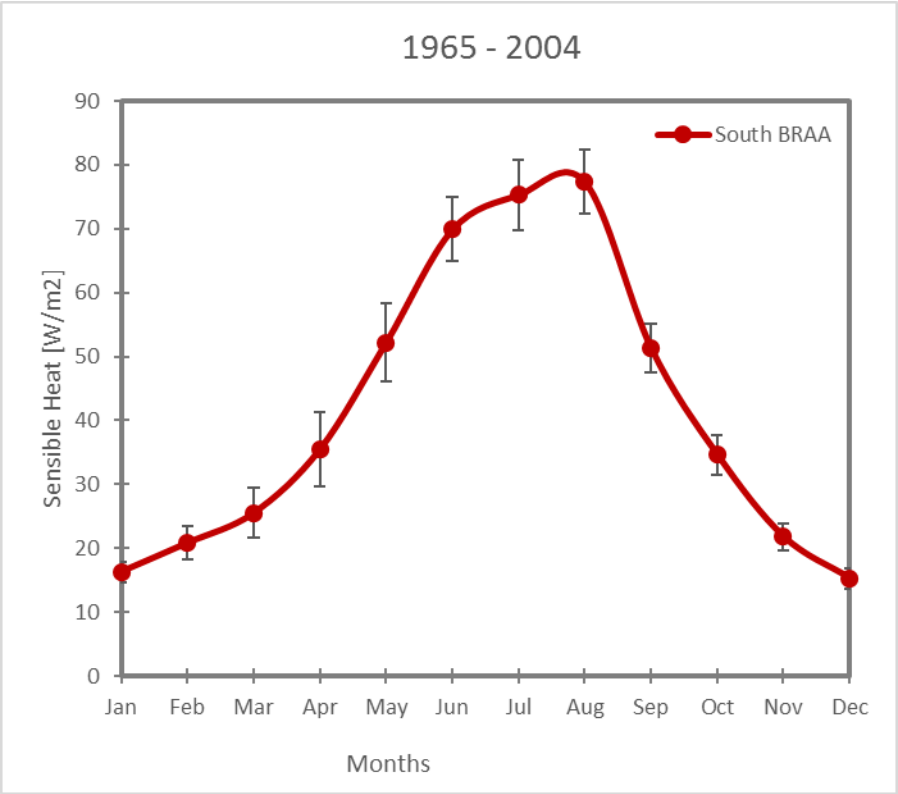

Figure A.42 Monthly sensible heat in the southern portion of the BRAA

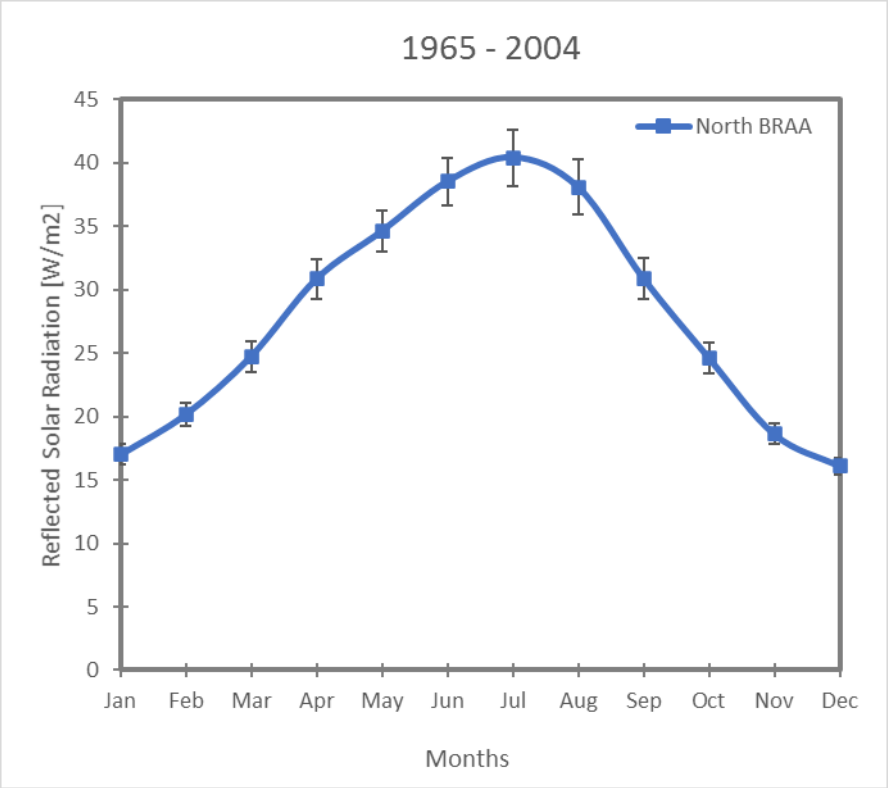

Figure A.43 Monthly reflected solar radiation in the northern portion of the BRAA

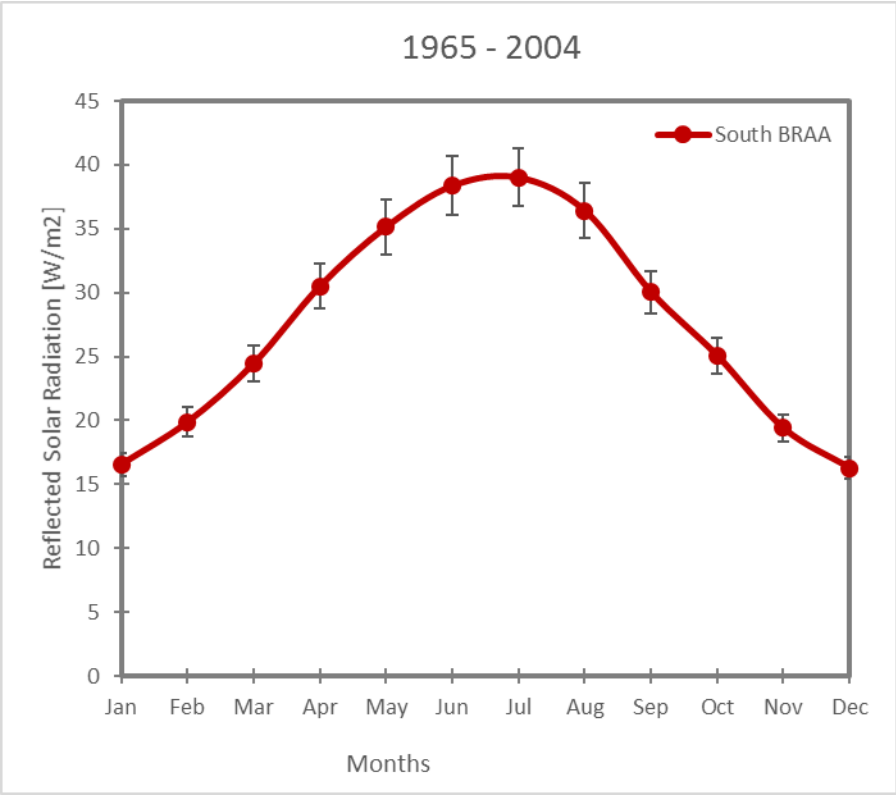

Figure A.44 Monthly reflected solar radiation in the southern portion of the BRAA

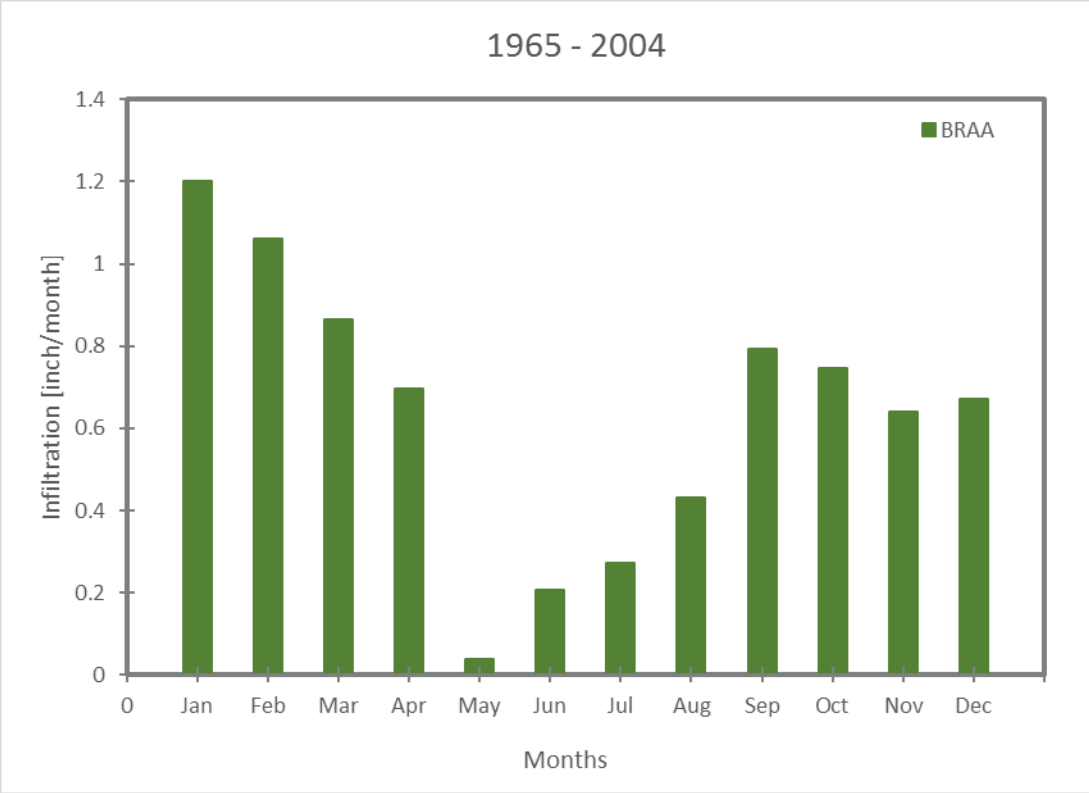

Figure A.45 Monthly infiltration in the BRAA

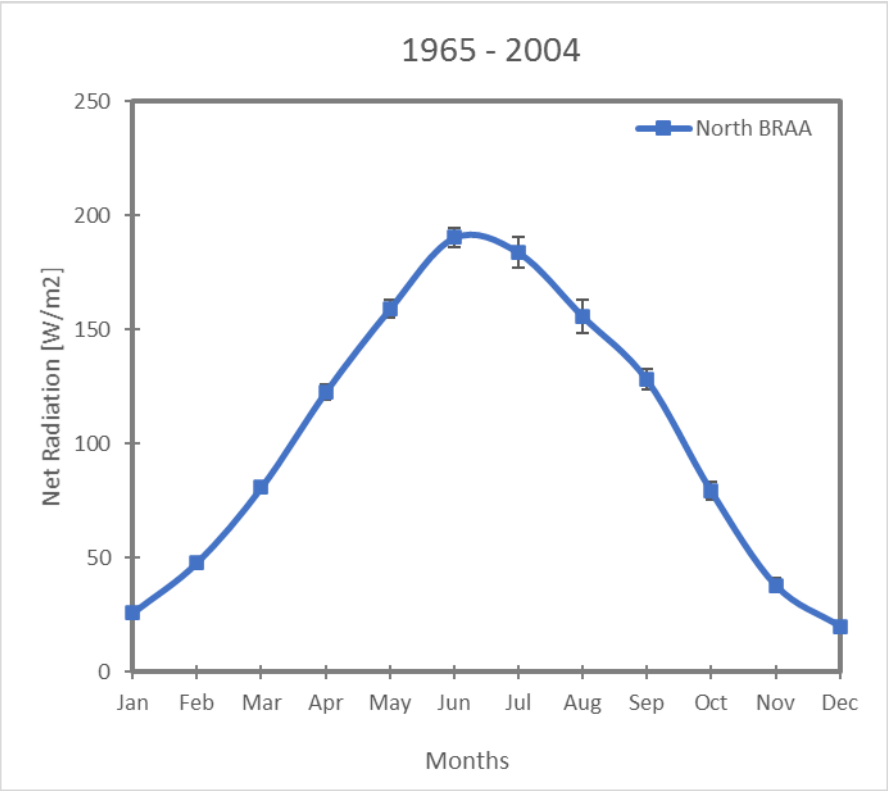

Figure A.46 Monthly net radiation in the northern portion of the BRAA

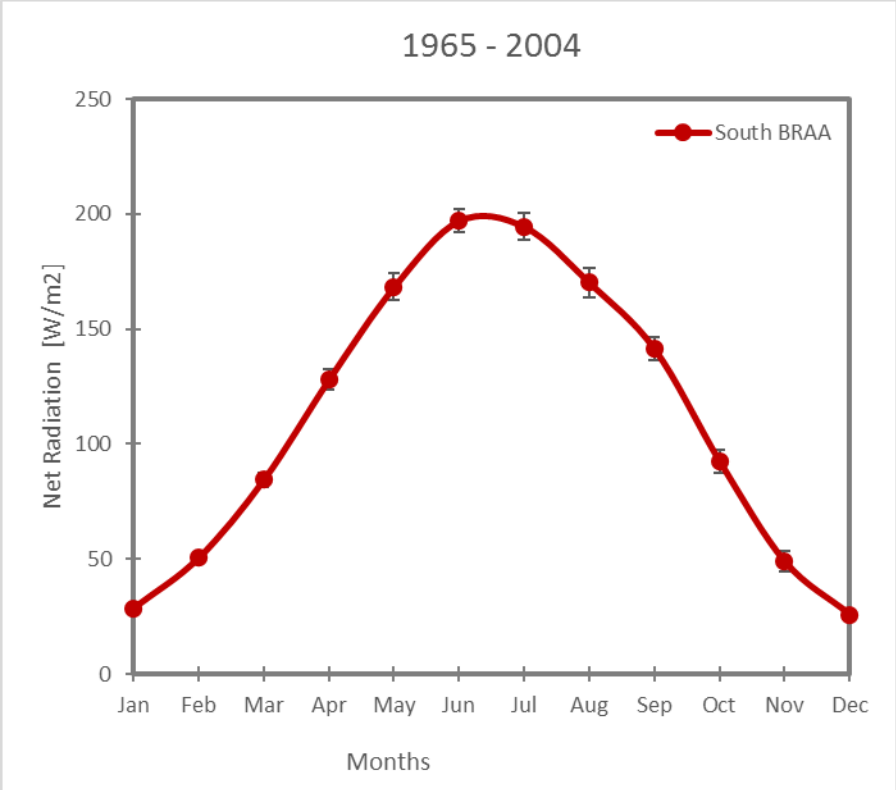

Figure A.47 Monthly net radiation in the southern portion of the BRAA

APPENDIX B

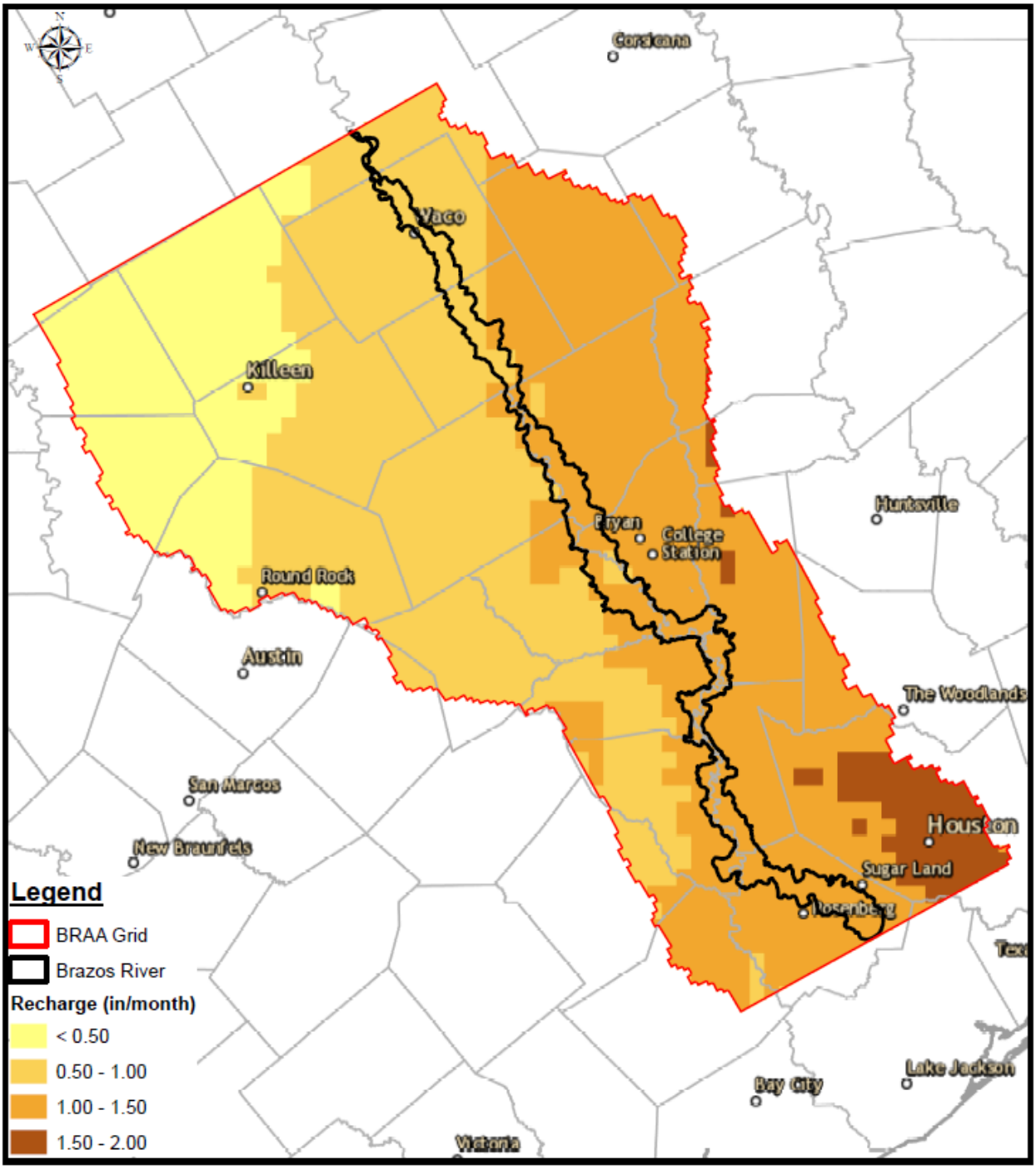

Figure B.1: Monthly average recharge rates in the BRAA (January)

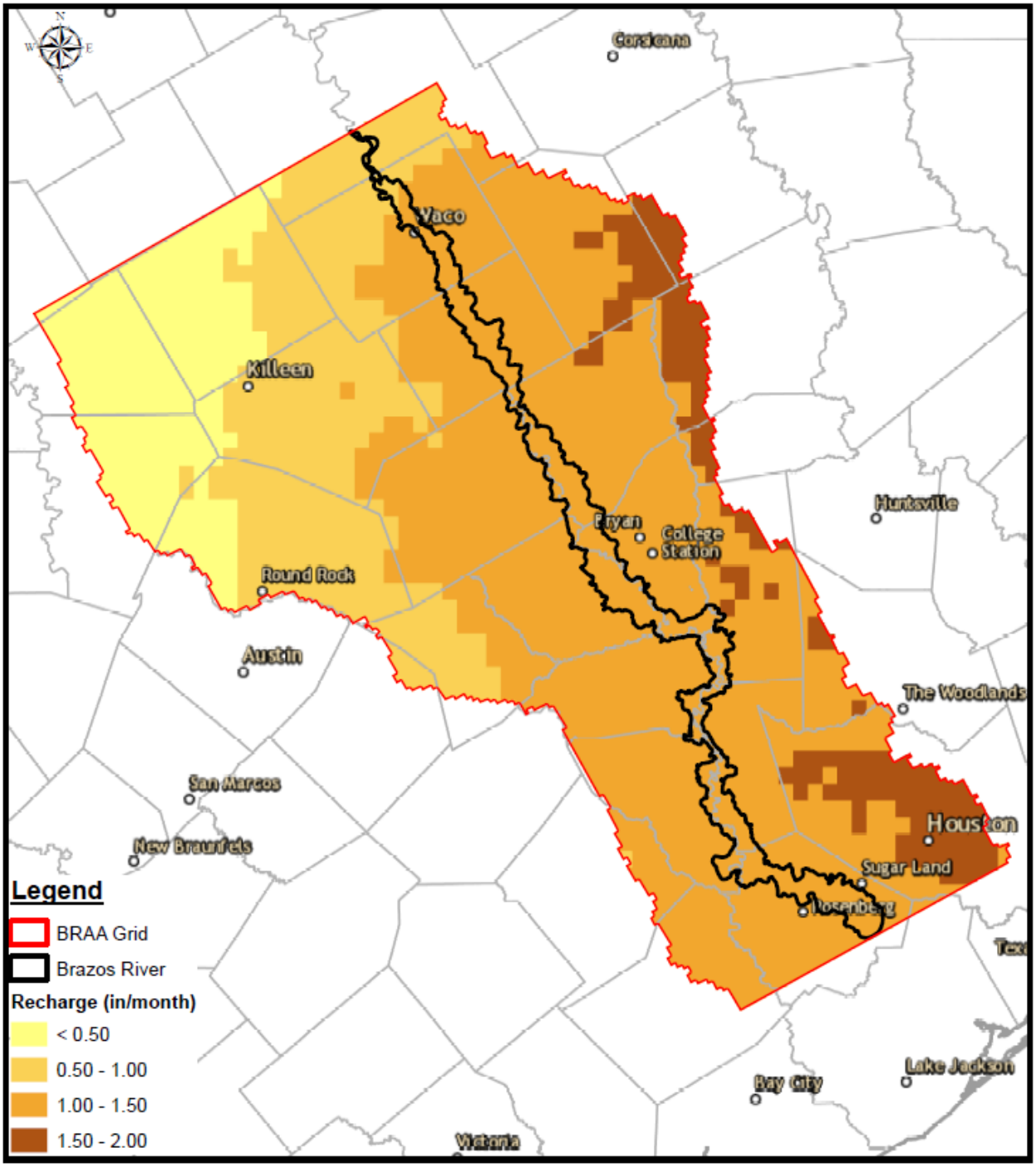

Figure B.2: Monthly average recharge rates in the BRAA (February)

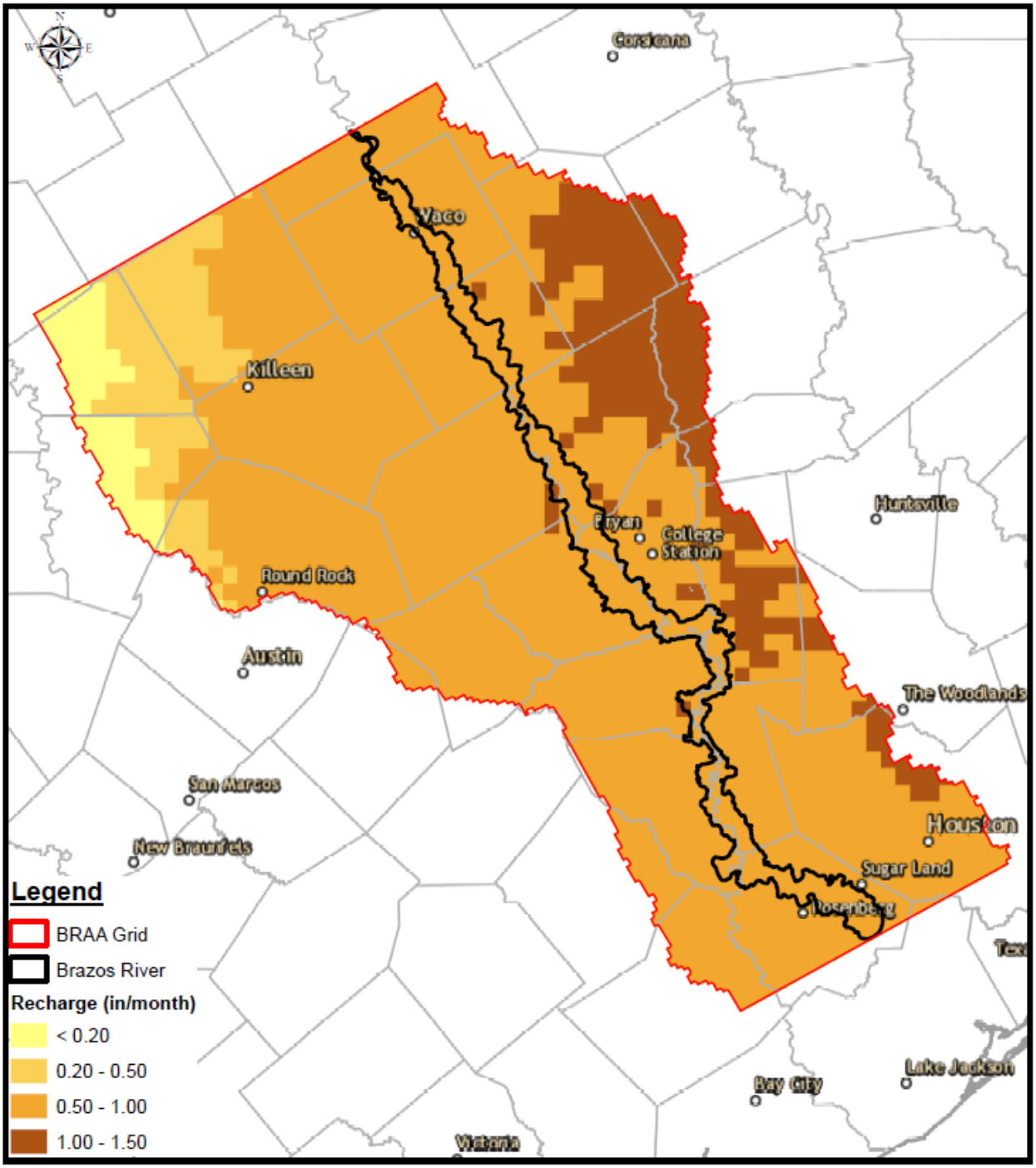

Figure B.3: Monthly average recharge rates in the BRAA (March)

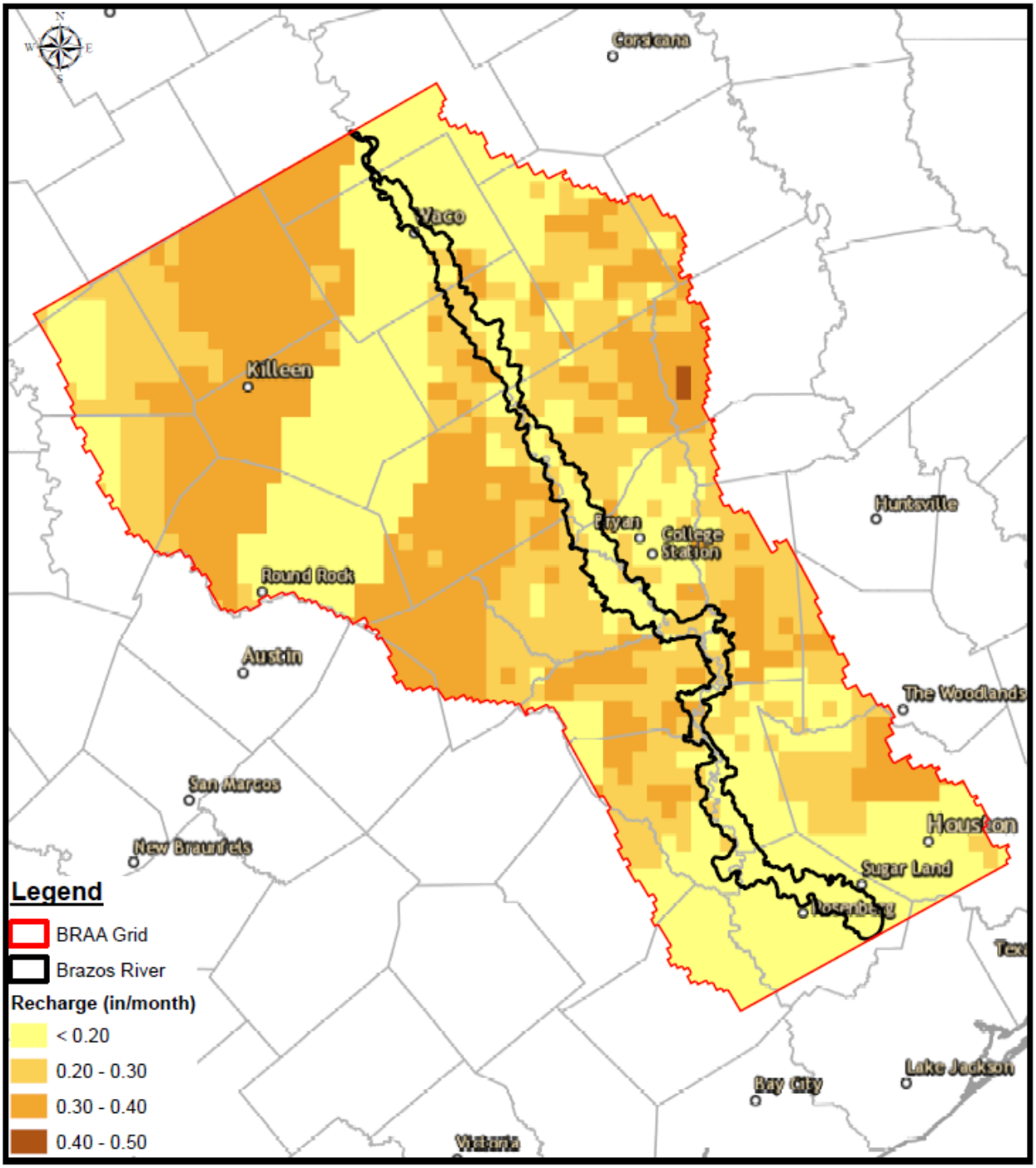

Figure B.4: Monthly average recharge rates in the BRAA (April)

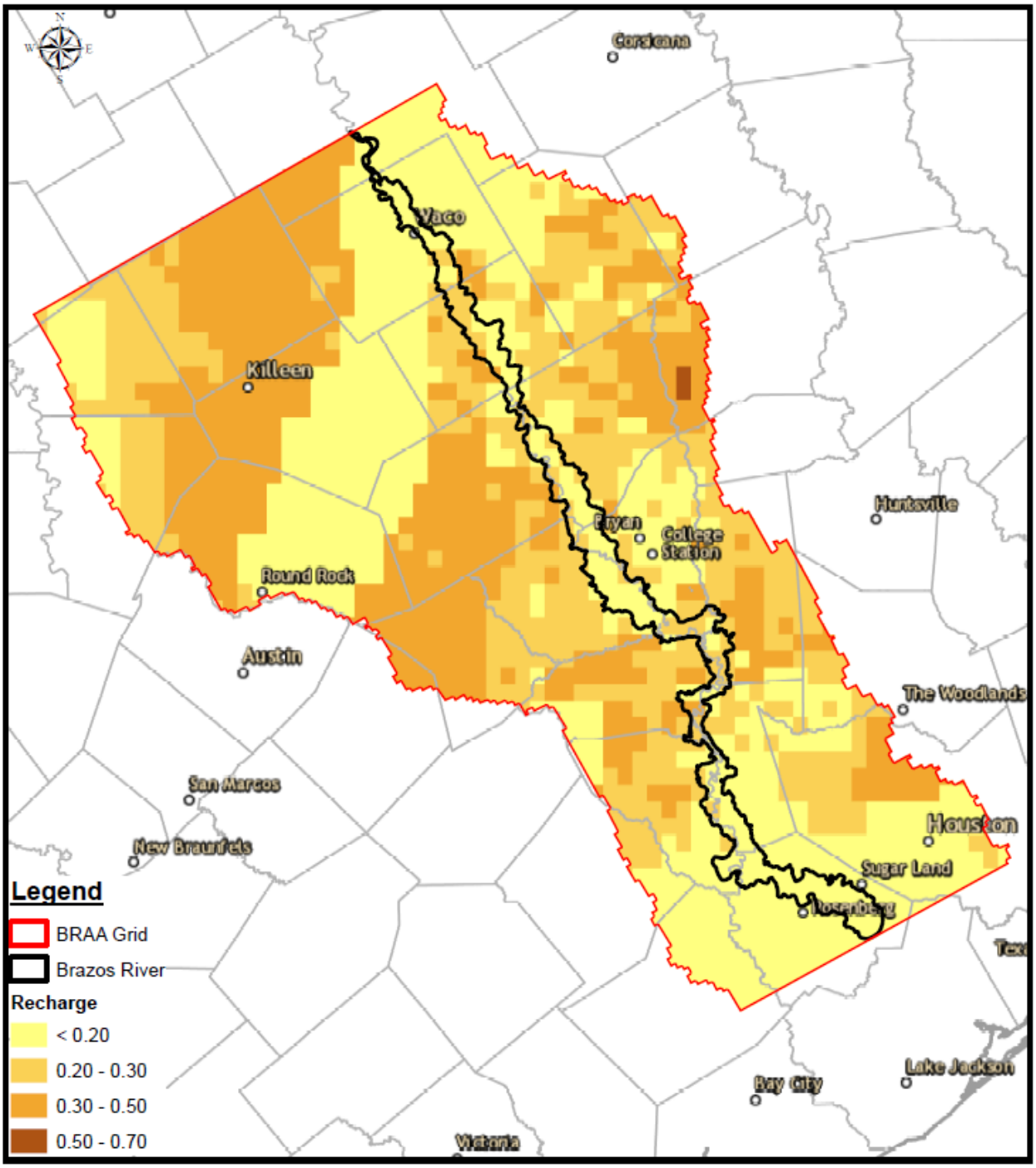

Figure B.5: Monthly average recharge rates in the BRAA (May)

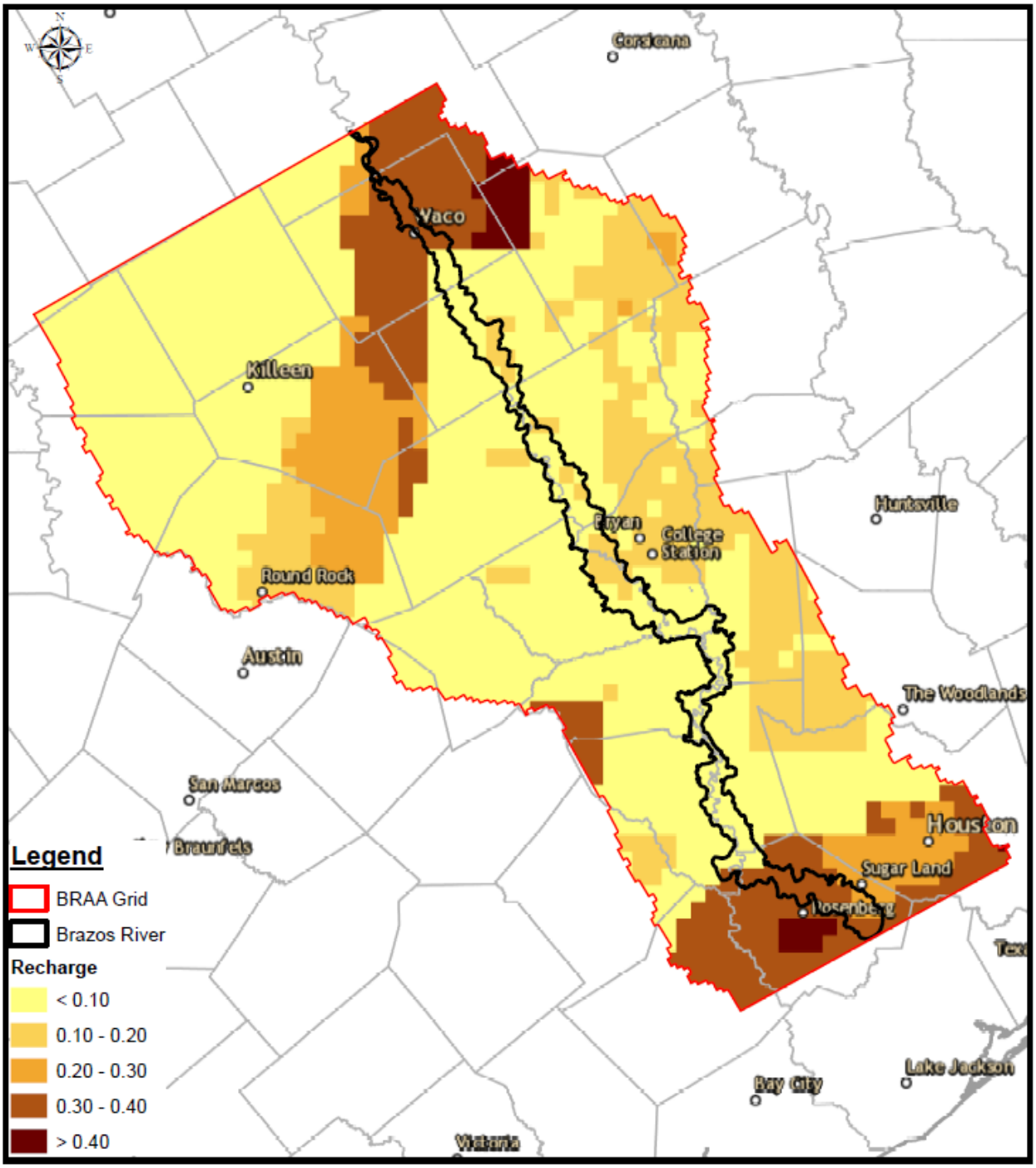

Figure B.6: Monthly average recharge rates in the BRAA (June)

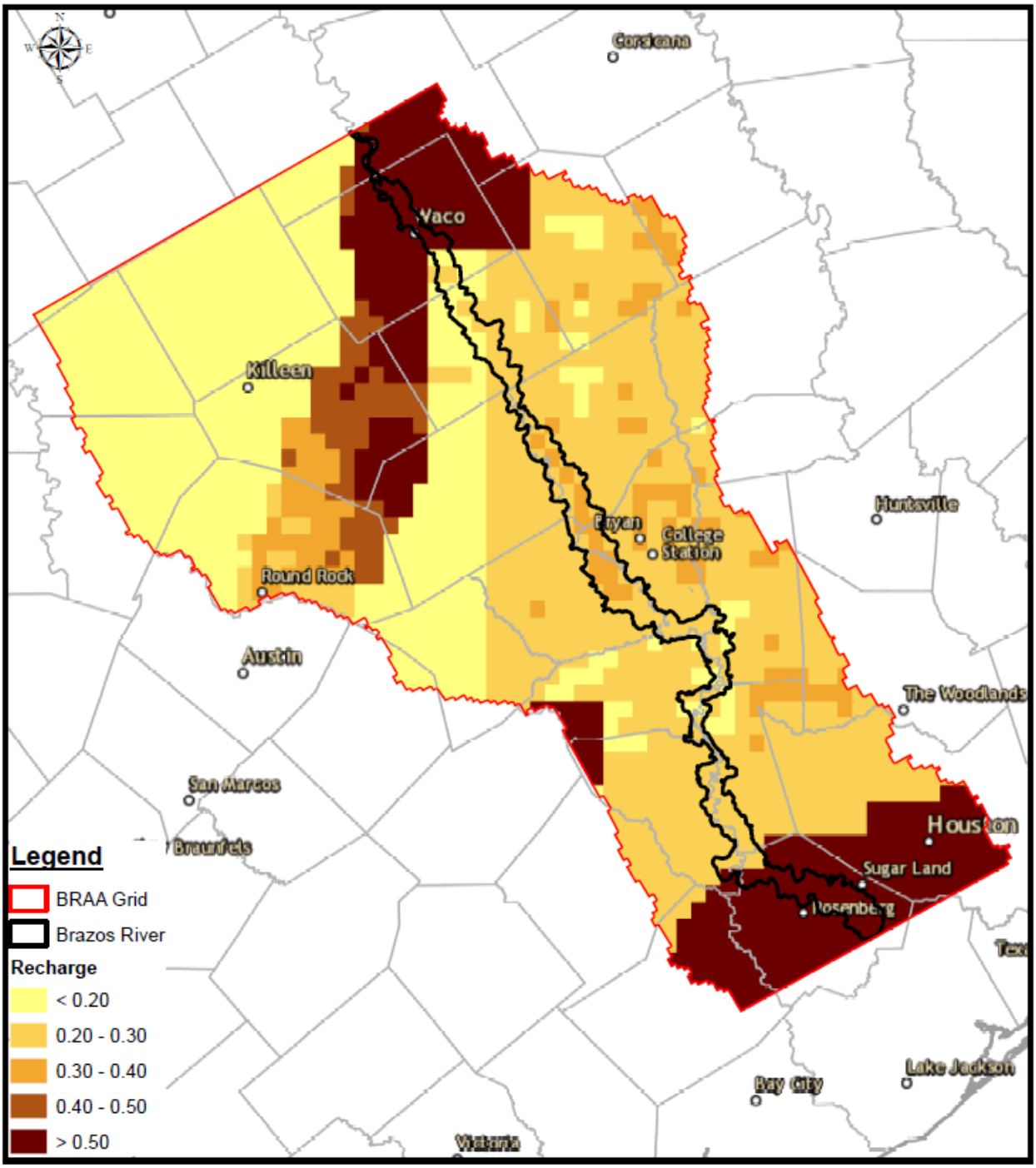

Figure B.7: Monthly average recharge rates in the BRAA (July)

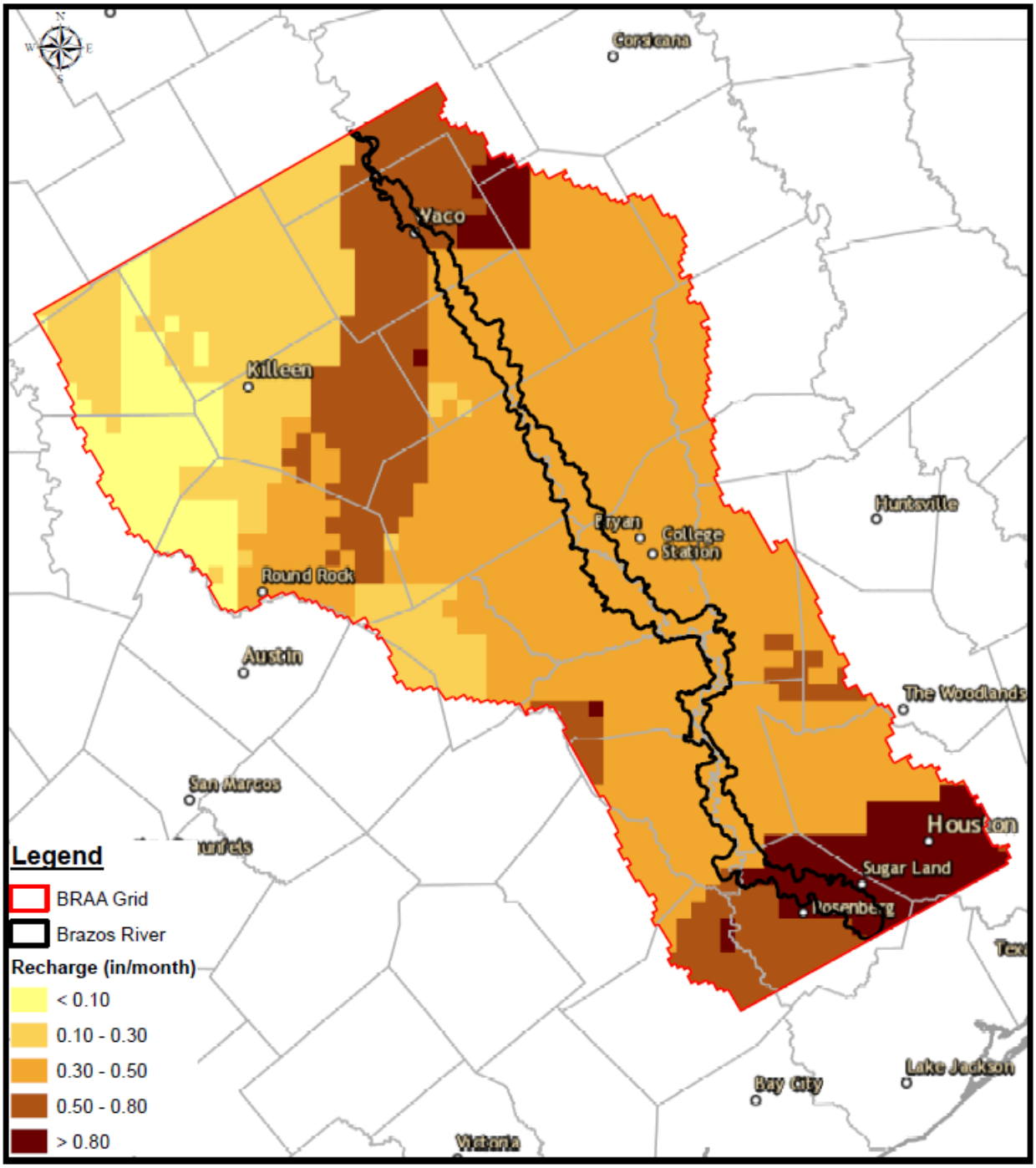

Figure B.8: Monthly average recharge rates in the BRAA (August)

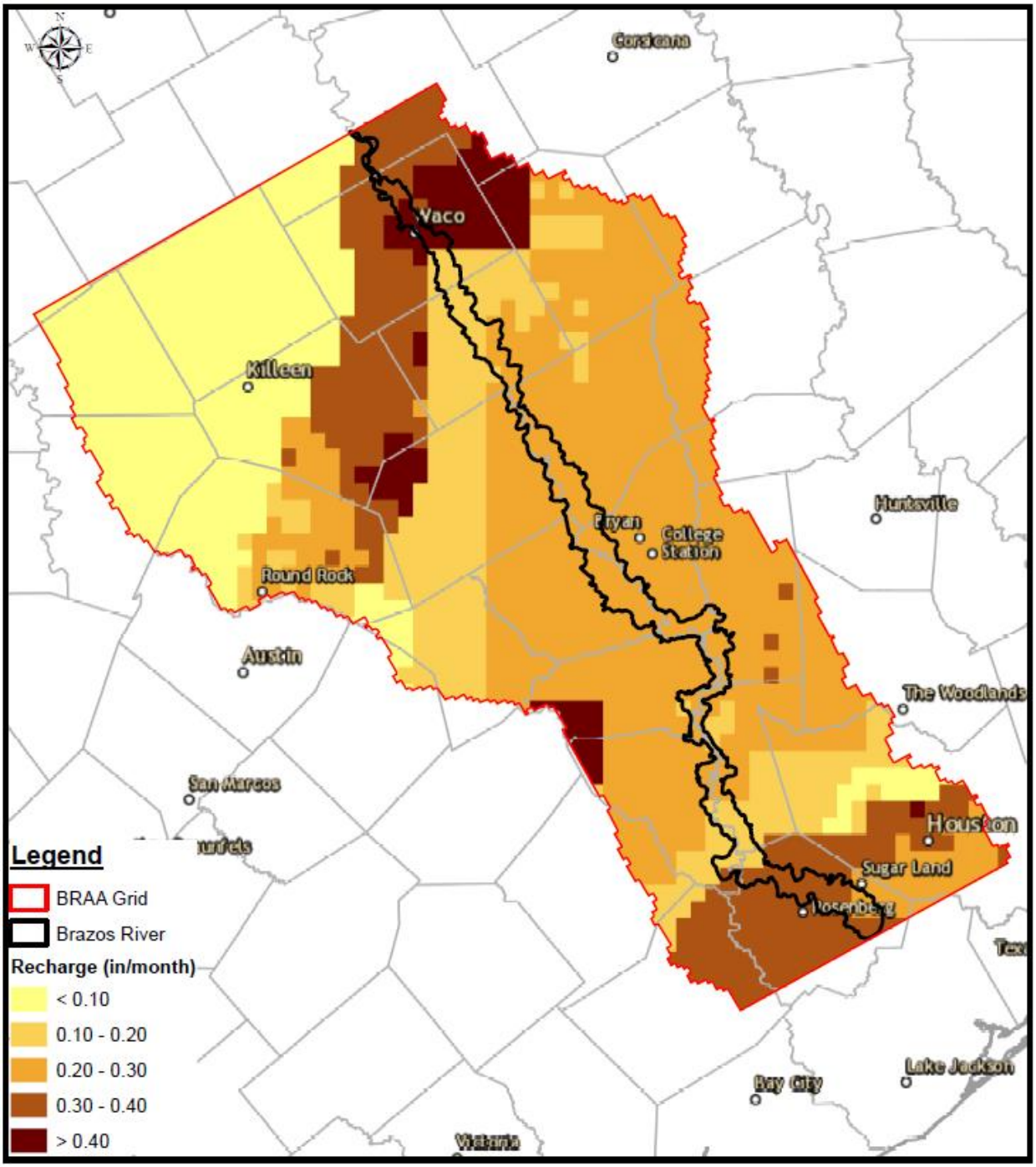

Figure B.9: Monthly average recharge rates in the BRAA (September)

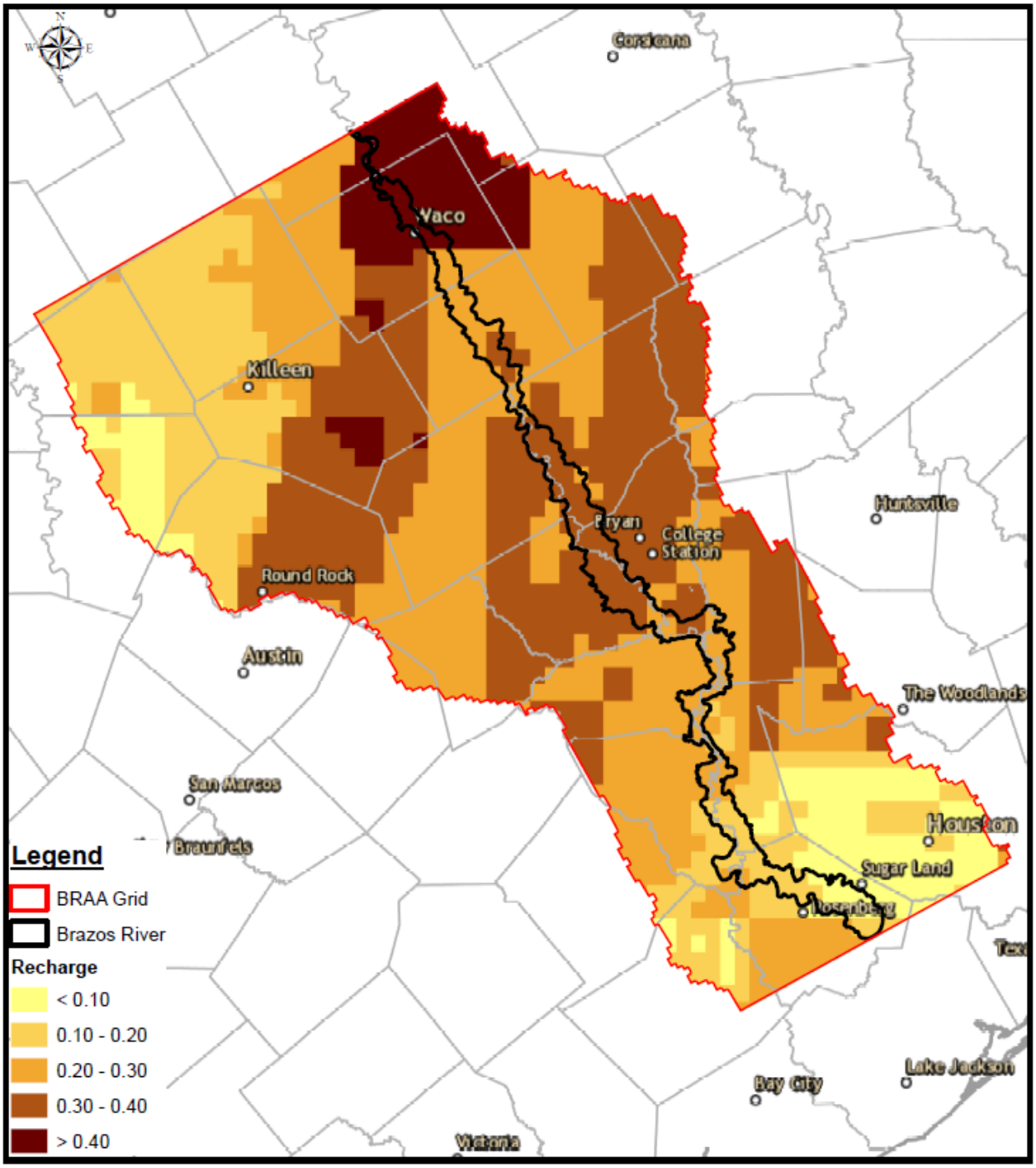

Figure B.10: Monthly average recharge rates in the BRAA (October)

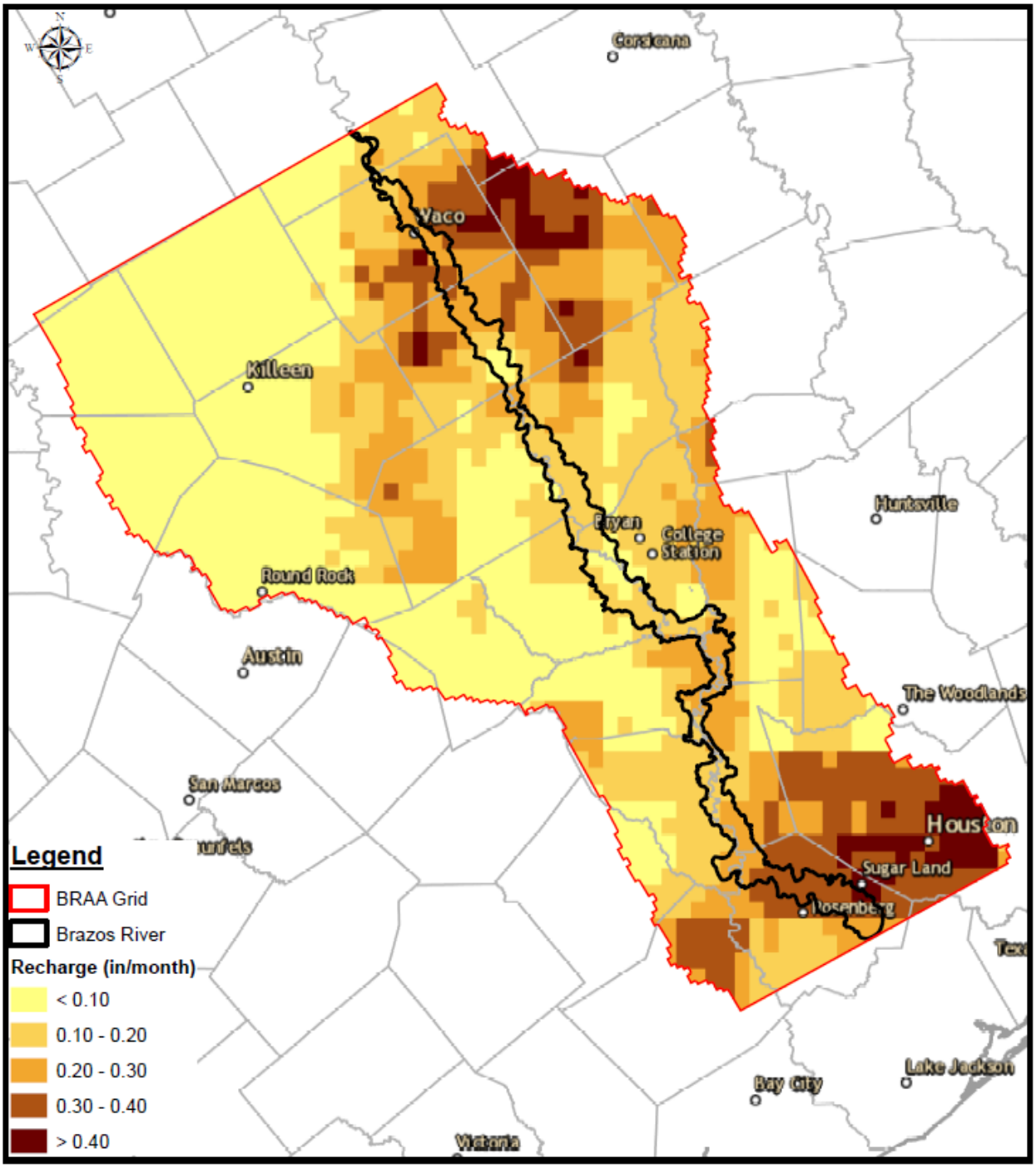

Figure B.11: Monthly average recharge rates in the BRAA (November)

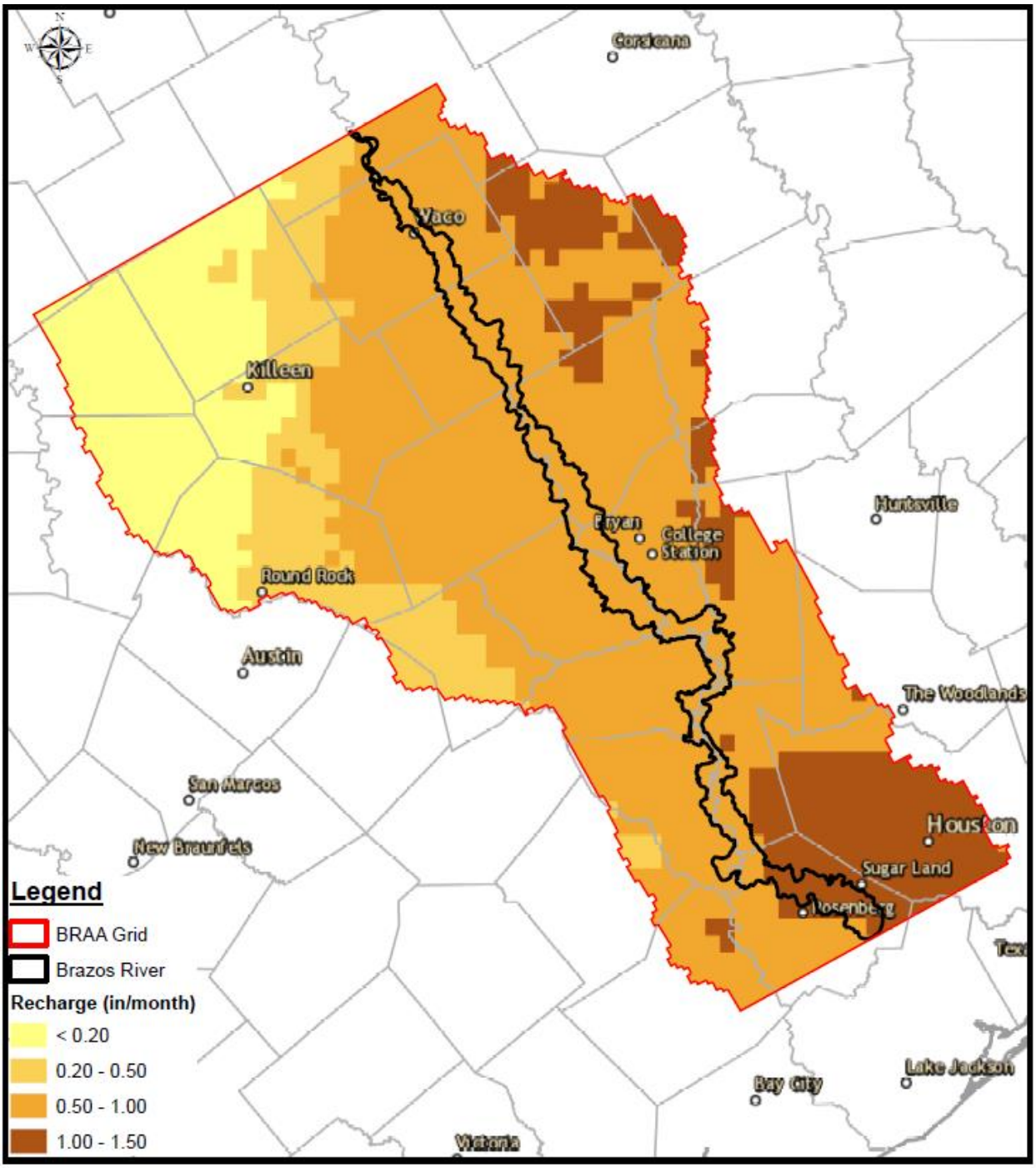

Figure B.12: Monthly average recharge rates in the BRAA (December)

APPENDIX C

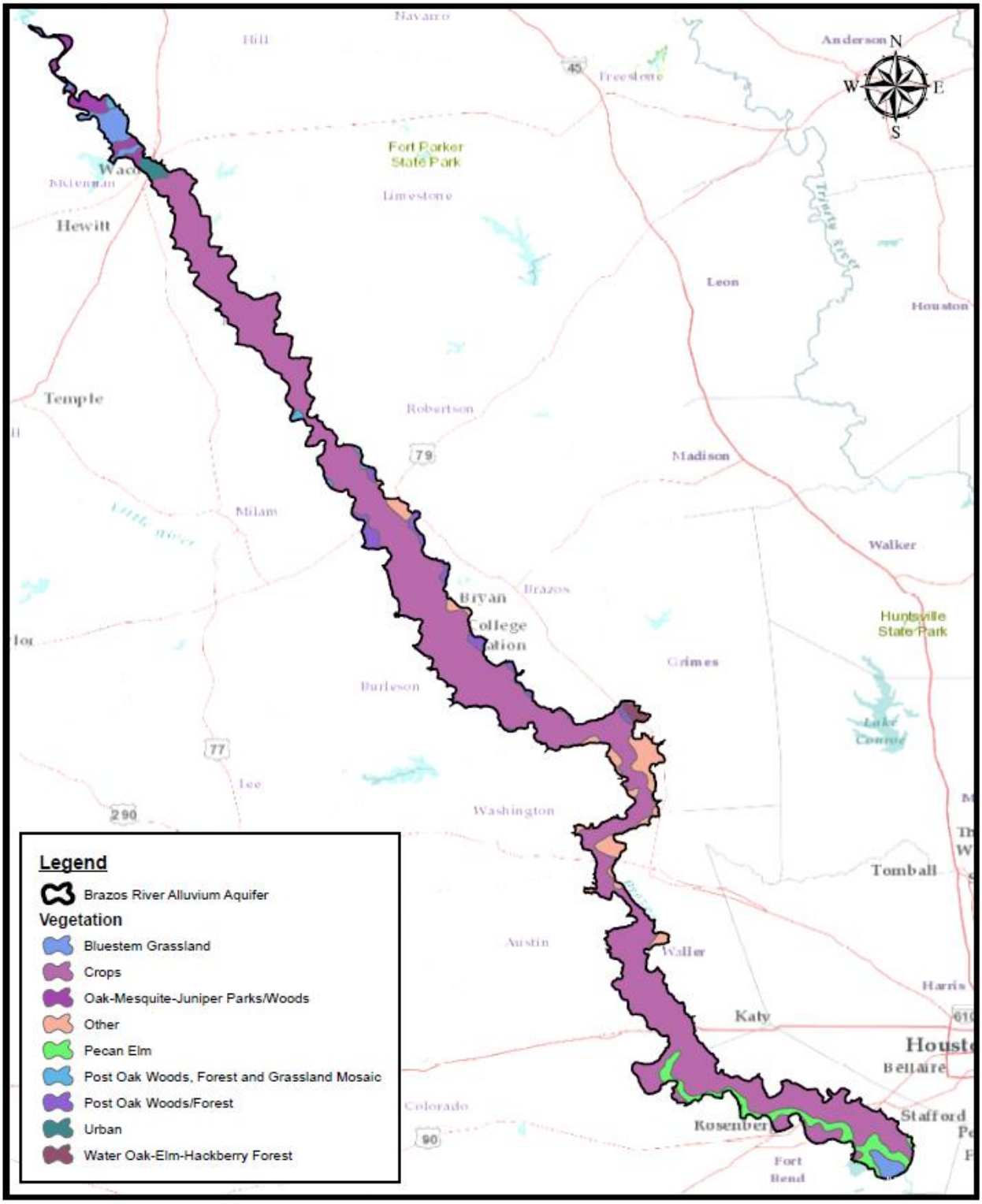

Figure C.1: Vegetation over the BRAA

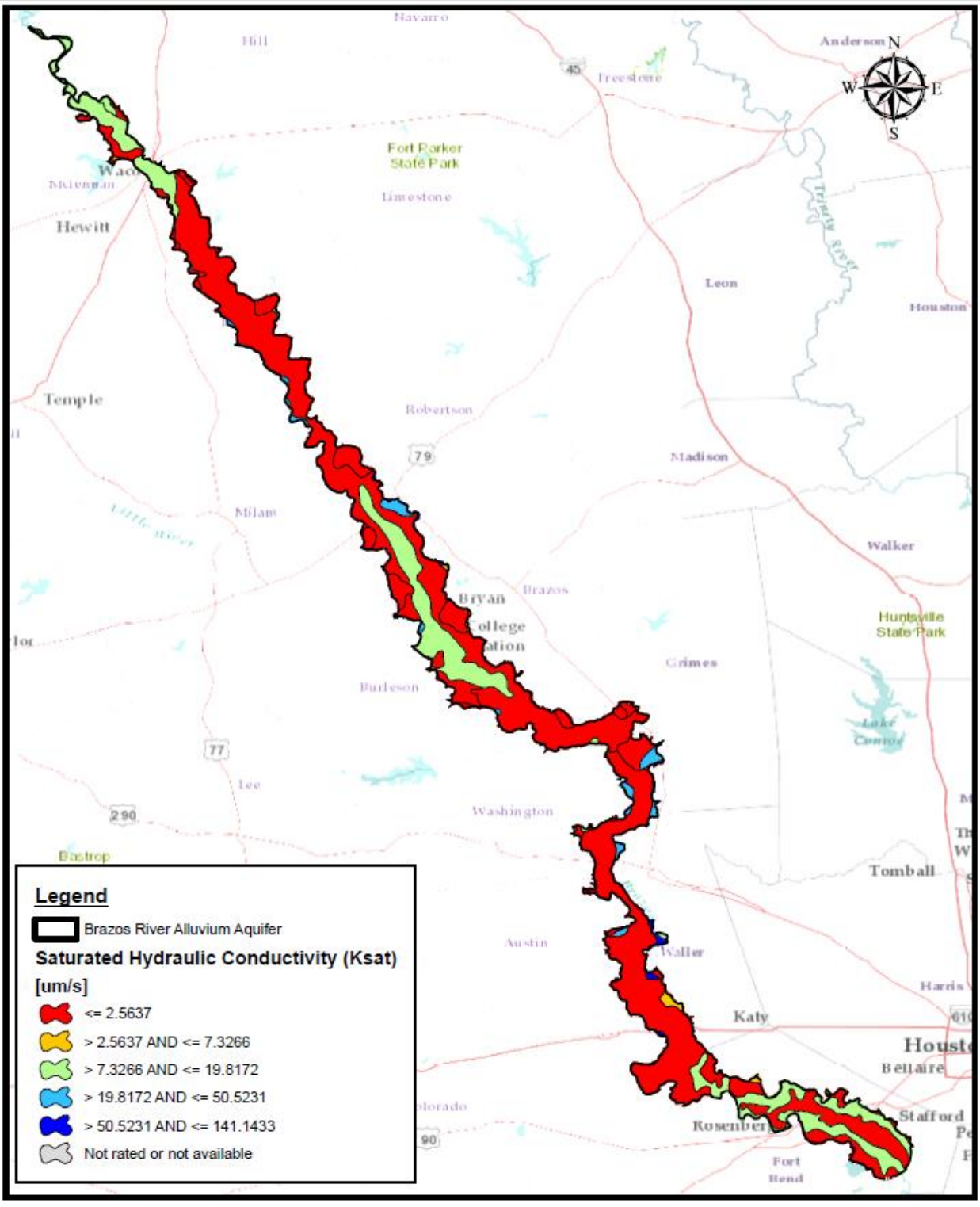

Figure C.2: Saturated hydraulic conductivity over the BRAA

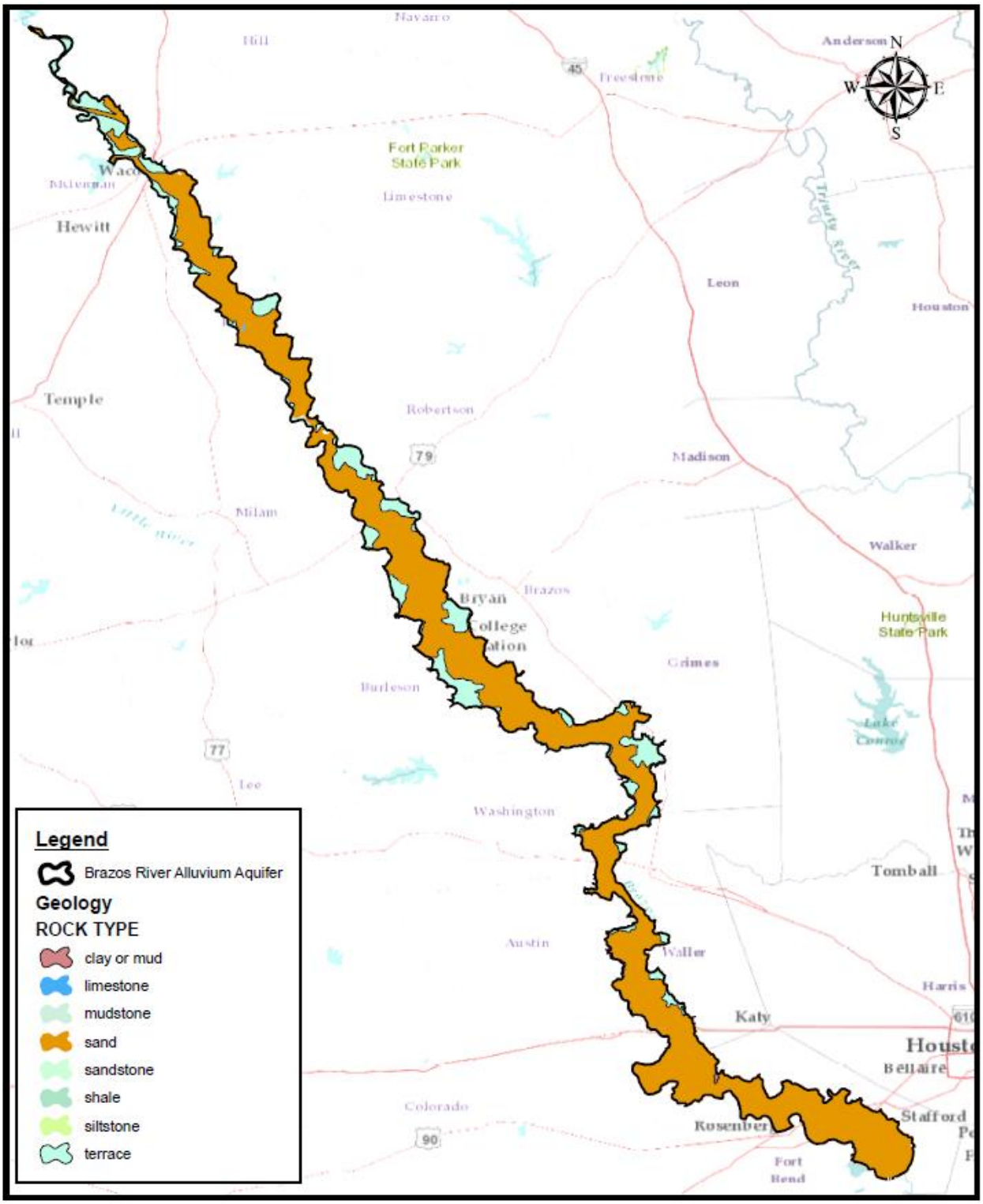

Figure C.3: Geology over the BRAA

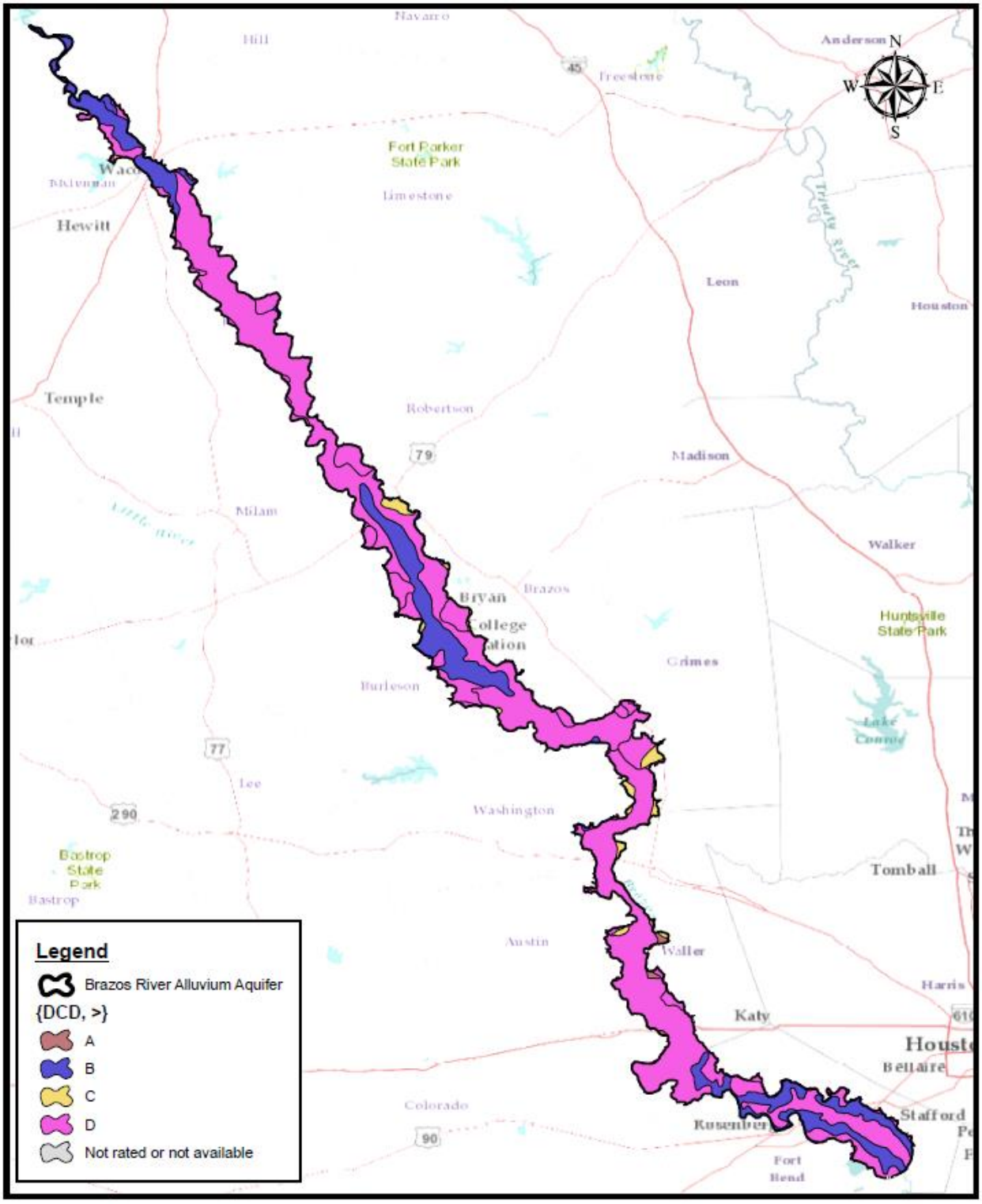

Figure C.4: Hydraulic soil group classification

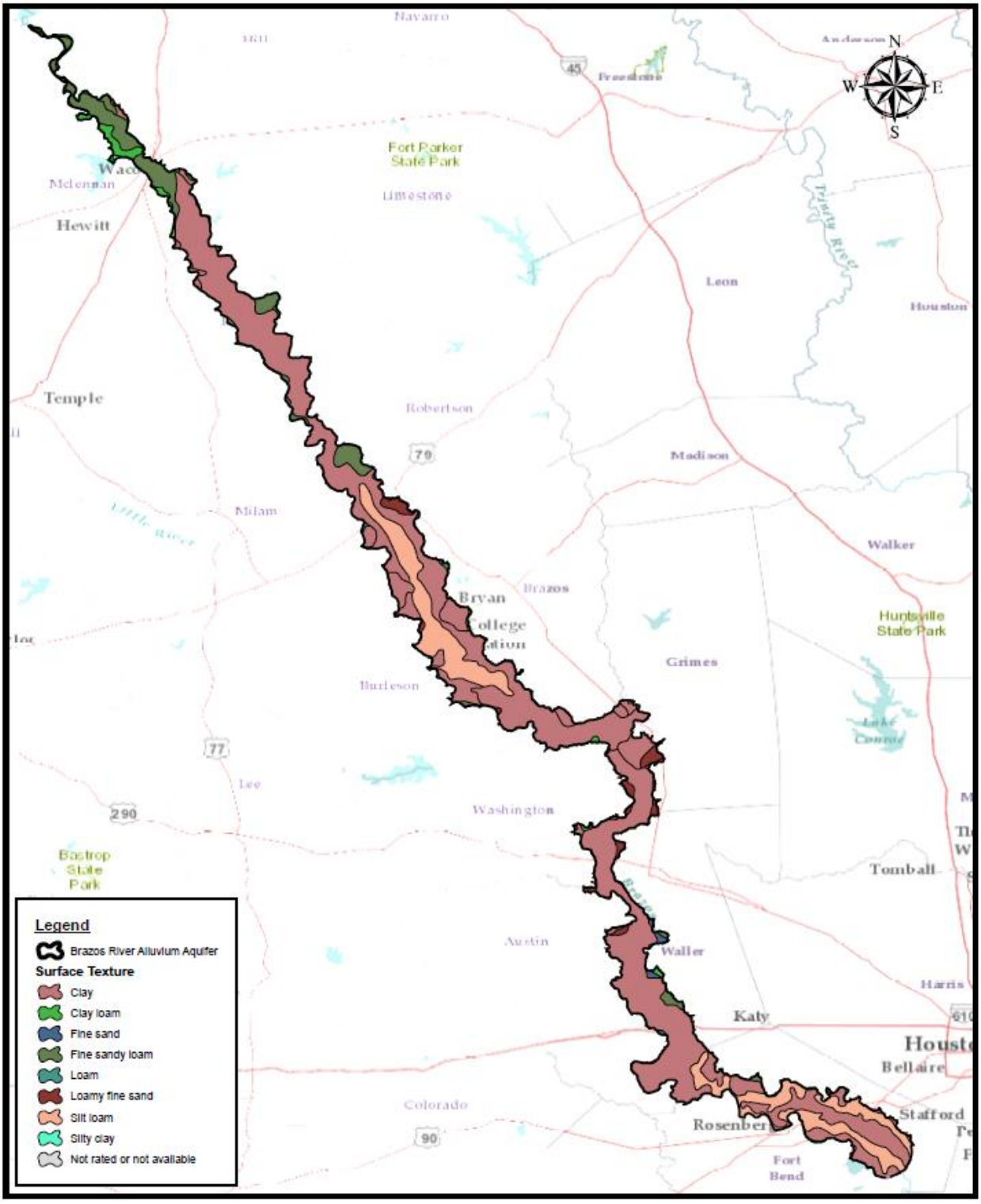

Figure C.5: Soil texture over the BRAA

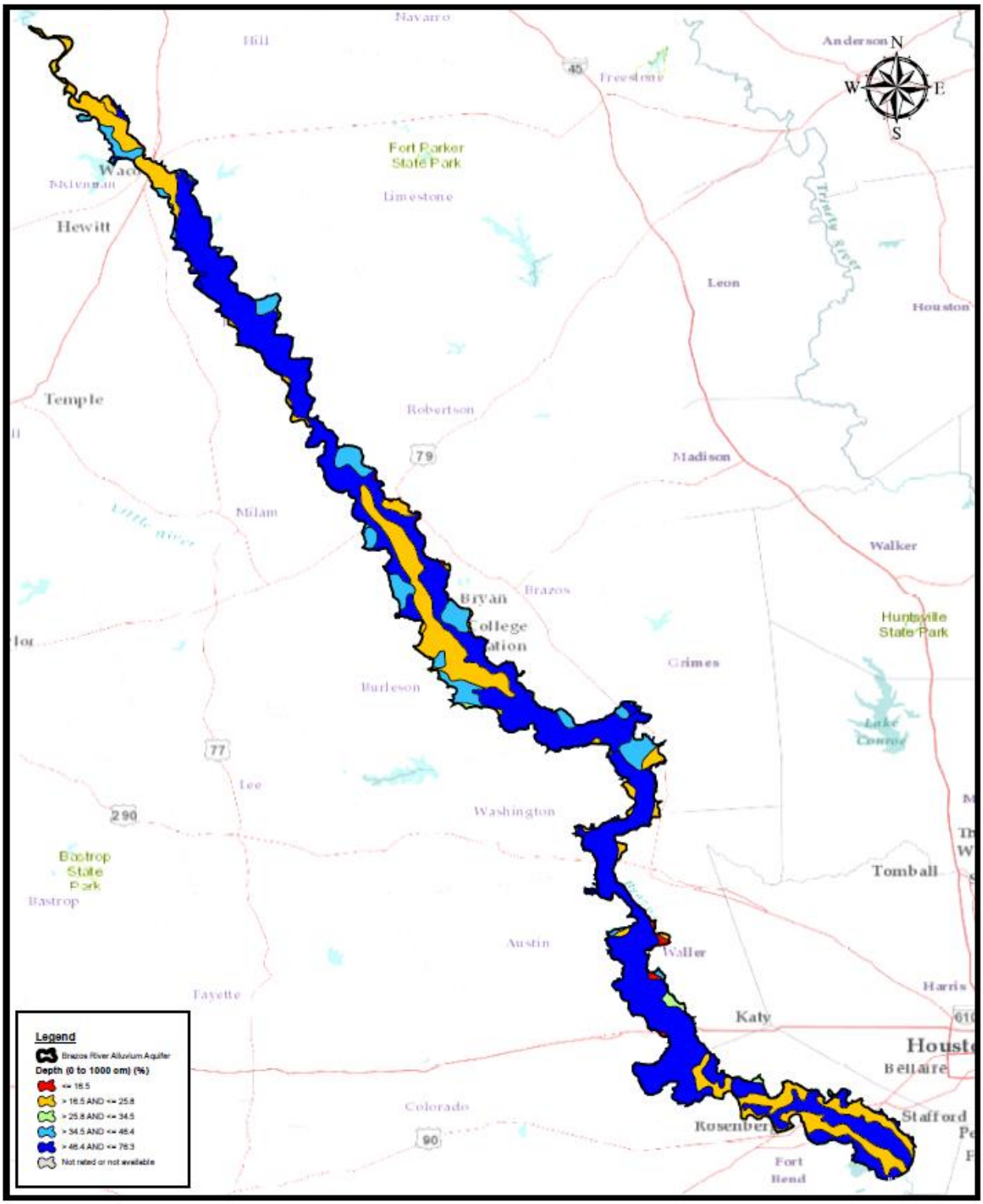

Figure C.6: Percent clay

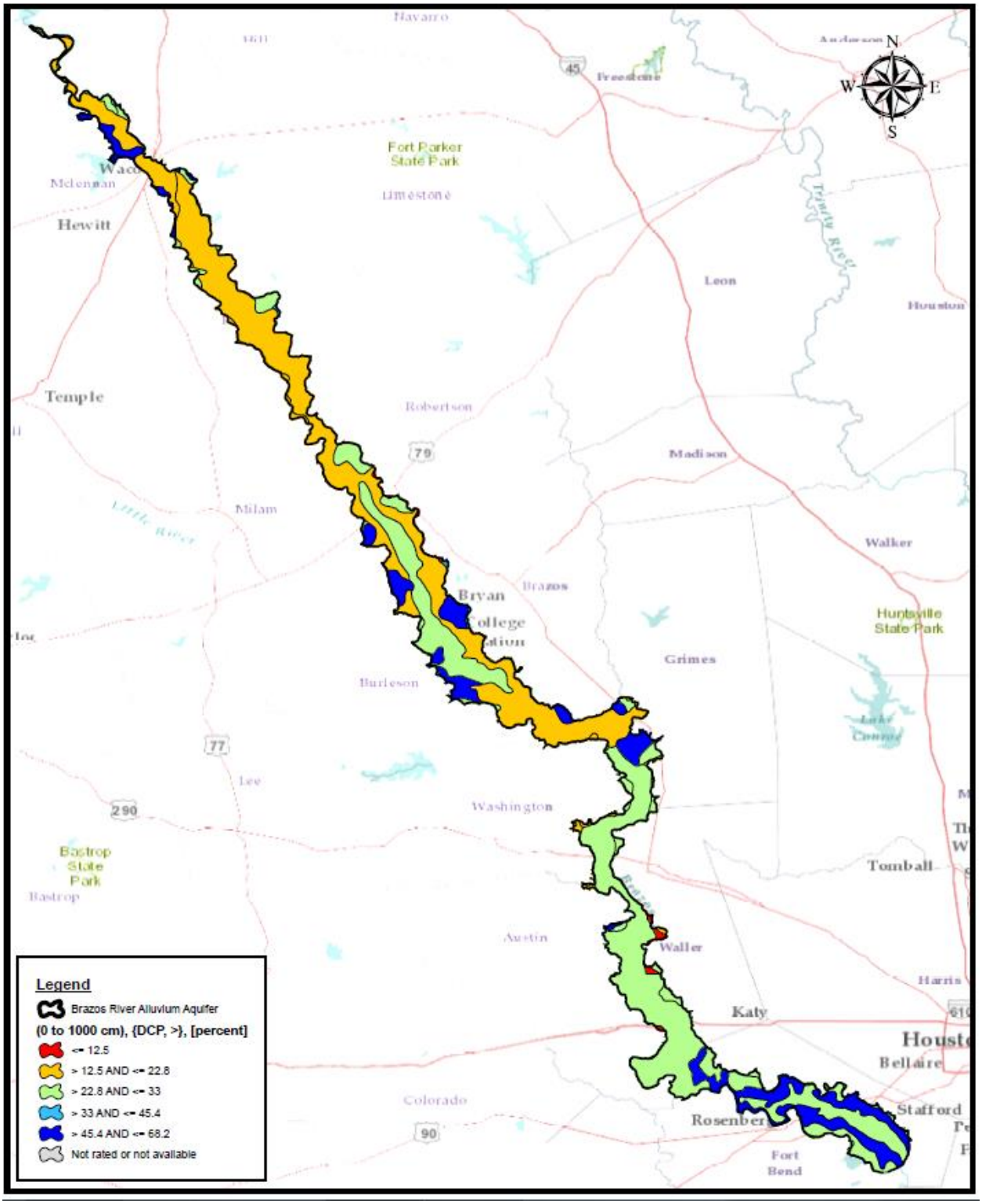

Figure C.7: Percent silt

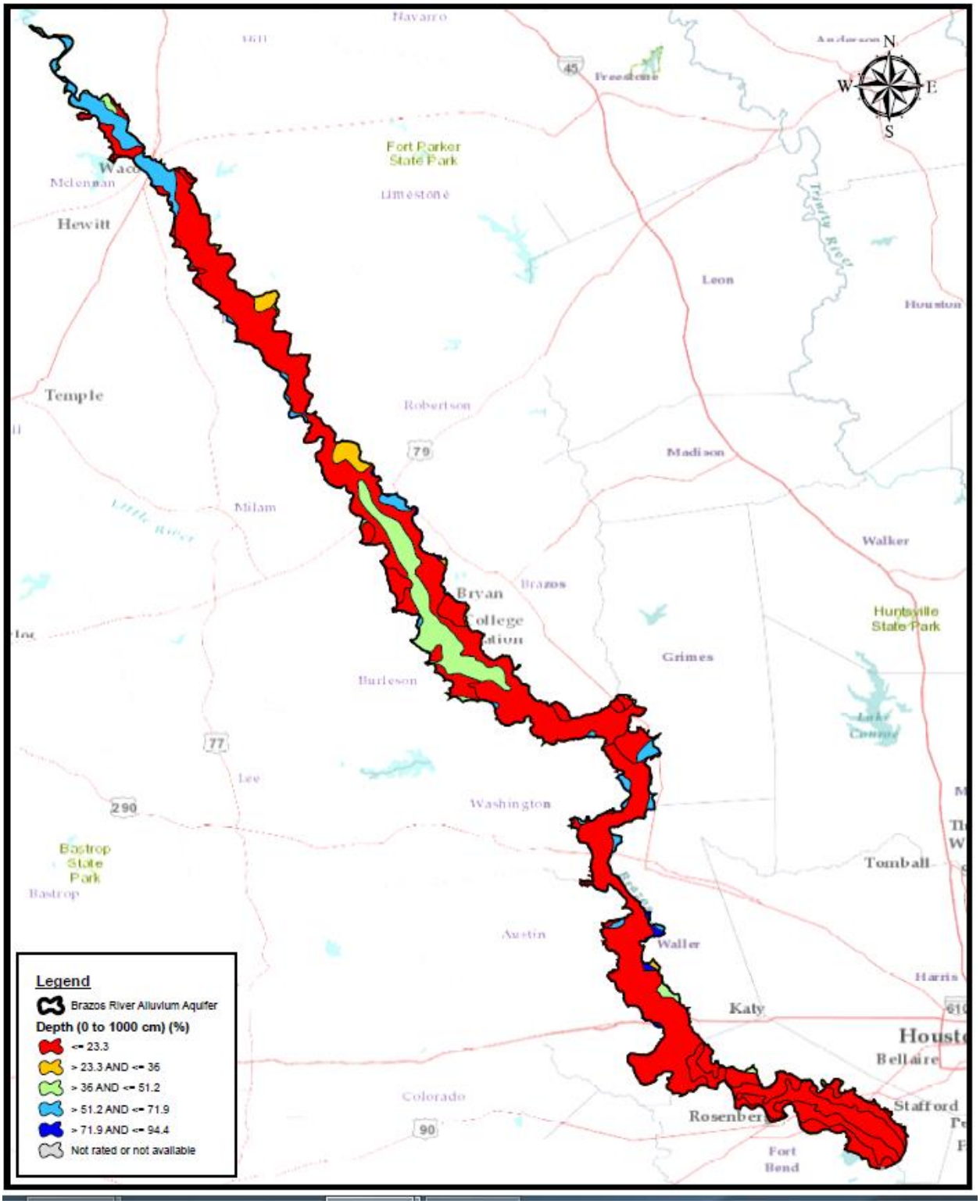

Figure C.8: Percent sand